2016

Synthesis and Characterization of Cyclic Polypeptoids by Organo-Mediated Controlled Zwitterionic Ring-Opening Polymerization and Development of Redox-Responsive Polypeptoid Micelles as Drug Delivery Carriers

Ang Li
Louisiana State University and Agricultural and Mechanical College

SYNTHESIS AND CHARACTERIZATION OF CYCLIC POLYPEPTOIDS BY ORGANO-MEDIATED CONTROLLED ZWITTERIONIC RING-OPENING POLYMERIZATION AND DEVELOPMENT OF REDOX-RESPONSIVE POLYPEPTOID MICELLES AS DRUG DELIVERY CARRIERS

A Dissertation

Submitted to the Graduate Faculty of the
Louisiana State University and
Agricultural and Mechanical College
in partial fulfillment of the
requirements for the degree of
Doctor of Philosophy

in

The Department of Chemistry

by
Ang Li
B.S., Beijing Technology and Business University, 2011
December 2016

Acknowledgments

Firstly, I would like to express my gratefulness to my advisor Prof. Donghui Zhang for the continuous support through my PhD career. I appreciate her patience, enthusiasm, and immense knowledge. She sets an extraordinary example of how a scientist should pursue his profession. With her guidance, I could have exciting discoveries in the research of polypeptoids. Besides my advisor, I would like to thank all my committee members for their inspiring suggestions at all levels of the research project.

I would like to thank all the fellows in my lab for the philosophical conversations, great assistance, and all the pleasant moments we had together.

I want to thank my family for their greatest love through my entire life. I dedicate my deepest love to them.

Table of Contents

List of Acronyms

1,8-ANS ..... 1-Anilinonaphthalene-8-sulfonic acid

ABC ..... Accelerated blood clearance

AcCl ..... Acetyl chloride

AFM ..... Atomic force microscopy

$BnNH_2$ ..... Benzyl amine

BMDCs ..... Bone marrow-derived dendritic cells

Bu-NCA ..... *N*-butyl *N*-carboxyanhydride

c-ATPC ..... Cyclic amylose tris(phenylcarbamate)

CCLMs ..... Core-crosslinked micelles

$CDCl_3$ ..... Deuterated chloroform

CD_2Cl_2 ..... Deuterated methylene chloride

CHCA ..... α-Cyano-4-hydroxycinnamic acid

CL ..... ε-Caprolactone

CL1 ..... 1-Azido-2-[(2-azidoethyl)disulfanyl]ethane cross-linker

CL2 ..... 1,4-diazidobutane cross-linker

CMC ..... critical micelle concentration

CuAAC ..... Copper (I)- mediated alkyne-azido cycloaddition

DBU 1, 8-Diazabicycloundec-7-ene

DCM ..... Dichloromethane

De-NCA ..... *N*-decyl *N*-carboxyanhydride

DLC ..... Drug loading capacity

DLE. ..... Drug loading efficiency

DLS ..... Dynamic light scattering

DMF ..... *N*,*N*-Dimethylformamide

dn/dc ..... The refractive index increment

DOX·HCl ..... Doxorubicin hydrochloride

DP ..... Degree of polymerization

DRI ..... Differential refractive index

DTT ..... DL-Dithiothreitol

E ..... Young's modulus

ELISA ..... The enzyme-linked immunosorbent assay

ESI-MS ..... Electrospray ionization mass spectrometry

Et-NCA ..... *N*-ethyl *N*-carboxyanhydride

G' ..... Storage modulus

GSH ..... Glutathione

HEL229 ..... Human embryonic lung fibroblasts

HEPES ..... (2-hydroxyethyl)-1-piperazineethanesulfonic acid

HepG2 ..... Human hepatoblastoma cells

HLB ..... Hydrophilic and lipophilic balance

ICCLMs ..... Irreversibly core-crosslinked micelles

IDP ..... Initial DOX to polymer mass ratio

k_i.... ..... Initiation rate constant

k_{obs} ..... Observed polymerization rate constant

k_p ..... Propagation rate constant

LCST ..... Lower critical solution temperature

MALDI-TOF MS ..... Matrix-assisted laser desorption ionization time of flight mass spectrometry

MALS ..... Multi-angle light scattering

Me-NCA ..... *N*-methyl *N*-carboxyanhydride

M_n ..... Number average molecuar weight

MRD ..... Multi-drug resistance

MTBD ..... 7-Methyl-1,5,7-triazabicyclo[4.4.0]dec-5-ene

MW ..... Molecular weight

MWCO ..... Molecular weight cut-off

NCLM ..... Non-crosslinked micelles

NHC ..... *N*-heterocyclic carbene

NMR ..... Nuclear Magnetic Resonance

P3HT ..... Poly(3-hexylthiophene)

PBS ..... Phosphate-buffered saline

PCEMA-*b*-PAA ..... Poly(2-cinnamoylethyl methacrylate)-block-poly(acrylic acid)

Pg-NCA ..... *N*-propargyl *N*-carboxyanhydride

PEG ..... Polyethylene glycol

PDI ..... Molecular weight distribution

PLLA ..... Polylactic acid

PMDETA ..... *N*,*N*′,*N*″,*N*″-Pentamethyldiethylenetriamine

PMF ..... Potential of mean force

PMMA ..... Polymethyl methacrylate

PNAG ..... Poly(*N*-allyl glycine)

PNBG ..... Poly (*N*-butyl glycine)

PNDG.....Poly(*N*-decyl glycine)

PNEG.....Poly(*N*-ethyl glycine)

PNMG.....Poly(*N*-methyl glycine)

PNPgG.....Poly(*N*-propargyl glycine)

REP.....Ring-expansion polymerization

REMP.....Ring-expansion metathesis polymerization

R_g.....Radius of gyration

R_h.....Hydrodynamic radius

R-NCA.....*N*-substituted *N*-carboxyanhydride

R-NTA.....*N*-thiocarboxyanhydride

ROP.....Ring-opening polymerization

SANS.....Small-angle neutron scattering

SAXS.....Small angle x-ray scattering

SCM.....Shell-crosslinked micelles

SDD.....Sample-to-detector distance

SEC.....Size exclusion chromatography

TEA.....Triethylamine

THF.....Tetrahydrofuran

TMG.....1,1,3,3-Tetramethylguanidine

VL.....δ-Valerolactone

ZROP.....Zwitterionic ring-opening polymerization

Abstract

Peptoids are peptidomimetic polymers, which have attracted much attention over the past two decades. They have similar building blocks to peptides, and the similarity makes the backbone of peptoids hydrophilic and biocompatible.[1] Two types of peptoid polymers are under development. One is sequence-defined peptoids, which exhibit excellent bioactivities.[2] Another one is polypeptoids. The good biocompatibility and highly tunable side chain substituents allow polypeptoids to be used broadly in future biomedical applications.

Varying polymer architectures, including linear polymers, cyclic polymers, comb-like polymers, and dendrimers can provide distinctive properties to the polymers. Cyclic polymers employ a cyclic architecture and lack chain ends, so their diffusion behaviors, aggregation behaviors, thermal transition behaviors, and crystallization behaviors are very different from the linear analogs. Facile synthetic approaches are required to expand the application of cyclic polymers into a broader scope. In chapter 1, the history of polypeptoids, the synthesis of cyclic polymers, the development of functional polypeptoids, and the cutting-edge biomedical research of polypeptoids were reviewed.

In chapter 2, we reported our most recent work of the polymerization reaction of cyclic polypeptoids using a bicyclic amidine initiator. The study was described from the aspects of molecular weight control, identification of the polymerization, kinetics of the polymerization, and polymer architecture. Zwitterionic ring-opening polymerization of *N*-substituted *N*-carboxyanhydrides (R-NCA) mediated by the bicyclic amidine has been developed and well-defined cyclic polypeptoids can be synthesized.

Pursuit of varying polymer architectures never ends because unique properties can be possibly discovered with the latest developed architecture. Besides cyclic polymers, linear

bottlebrush polymers also attracted much attention due to their distinctive features. In chapter 3, we took one step forward and synthesized the cyclic bottlebrush polypeptoids. We then conducted a systematic study on the characterization of the cyclic bottlebrush polypeptoids and on the solution aggregation behaviors of zwitterionic cyclic polypeptoids with and without long side chains. It was revealed that zwitterionic cyclic polypeptoids tend to form clusters due to dipole-dipole interaction in methanol and even the long side chains cannot prevent this process.

Another important direction of polypeptoid research, the biomedical application, was assessed in chapter 4. Redox-responsive micelles based on amphiphilic diblock copolypeptoids were prepared, and the solution stability, the morphology in dry state, the redox-responsive behaviors, drug release *in vitro*, and cell viability and cell inhibition activity of the micelles were completely studied.

Chapter 1. Introduction to the Polypeptoid Research

1.1 Polypeptoids

1.1.1 History and unique properties

Polypeptoids, also known as poly(*N*-substituted glycine)s, are structural mimics of polypeptides. Despite the backbone similarity to polypeptides, polypeptoids have the substituents connected to the amide nitrogen instead of the backbone carbon, which leads to their achirality and lack of hydrogen bonding along the backbone. As a result, polypeptoids feature enhanced proteolytic stability and thermoprocessability relative to polypeptides. On the contrary to polypeptides whose conformations in solution are determined by their backbone chirality and hydrogen bonding, conformations of polypeptoids only depend on their side chains. With different side chains, polypeptoids can form random coils, polyproline I helix,[3-8] or nanosheets in solution.[9-11] Due to the distinctive properties polypeptoids are good candidates as a class of peptidomimetic materials in the areas of pharmaceutical therapy and biomedical applications (*e.g.* antimicrobial coatings, biosensor fabrication, etc.). Developed as a derivative of polypeptides, the progressed synthetic approaches enabled the production of diverse polypeptoids with much potential to be used predominantly for the future biomedical application.

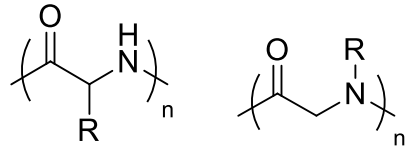

Polypeptides Polypeptoids

In the 1980s, under the revolution of genetic engineering, small biotechnology companies were trying to develop more efficient technologies to facilitate the drug discovery process so that they could expand into the pharmaceutical industry. Peptoids were therefore first produced by a

start-up company- Protos in place of peptides and nucleic acid oligomers due to enhanced pharmacokinetics. Since then sequence-defined peptoids were studied for drug discovery or as binding agents in the pharmaceutical industry.[12]

There is not a distinct boundary between oligomeric peptoids and polypeptoids. Usually peptoids with specific sequences and less than 50 units are considered oligomeric peptoids, and peptoids whose backbone structures contain more than 20 repeating units are considered polypeptoids. The most simple polypeptoid- polysarcosine or poly(*N*-methyl glycine) (PNMG) was synthesized several decades ago through ring-opening polymerization (ROP) of *N*-methyl *N*-carboxyanhydride (Me-NCA) monomers with amine initiators,[13] but it was not unambiguously distinguished from polypeptides by then. The broad and systematic studies of polypeptoids started from recent years when the synthesis of the *N*-substituted *N*-carboxyanhydride (R-NCA) monomers with versatile substituents and the synthesis of corresponding polypeptoids had been developed. Up to date well-defined polypeptoids with controlled chain-length, narrow molecular weight distribution (PDI), and various side chains can be readily synthesized.

The backbone of polypeptoids consisting of tertiary amide bonds is very hydrophilic and has strong dipole-dipole interaction. In order to obtain polypeptoids with wide range of tunability, one has to tailor their side chain substituents. It was found that the thermal and crystallization behaviors[14-17] and other physicochemical properties[18] of polypeptoids are strongly dependent on the substituents.

Luxenhofer *et al.* found that the hydrophilic and lipophilic balance (HLB) of polypeptoids in solution can be tuned by adjusting both the chain length of backbones and side chain substituents.[19] Zuckermann *et al.* demonstrated that the persistence length of charged polypeptoids depends on the specific charge position along the backbone.[20] Solubility of polypeptoids in water

can be tailored by side chains too. When the side chains are short alkyl chains (methyl or ethyl groups) or hydrophilic side chains (methoxy or ethoxy groups) polypeptoids are water-soluble. When the side chains are alkyl chains with four or more carbons polypeptoids become hydrophobic. Polypeptoids also exhibit thermally induced phase transition behaviors in water when the side chains are propyl groups or allyl groups or when they are random copolymers with ethyl and butyl groups as side chains.[1, 21]

1.2 Synthesis of Linear Polypeptoids

1.2.1 Submonomer method

Scheme 1.1. Submonomer method.

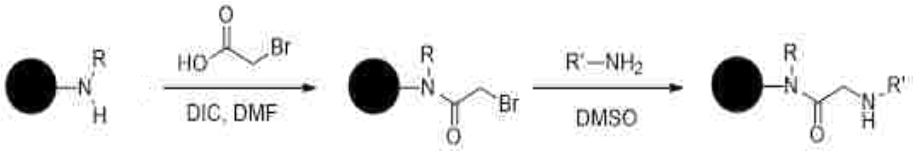

Naturally occurring peptides are able to fold into higher ordered structures and thereby exhibit varying biological activities. In order to mimic the folding behaviors of peptides, the effect of the specific sequences of peptoids must be investigated. Therefore, the precise control over sequences of peptoids is important.[22] Submonomer solid phase synthesis is a broadly used method to synthesize polypeptoids or more accurately sequence-defined peptoids.[23] It is a polymerization that includes two synthetic steps: acylation of the secondary amine in the presence of an acylating agent- carbodiimide and displacement of the halogen with a primary amine. By repeating this synthetic cycle primary amines with varying substituents can be incorporated onto the peptoid chains, resulting in the precise control over the sequence of *N*-substituted polyglycine segments (Scheme 1.1). The method is cost-effective because the amines used in this synthesis are not necessary to be protected and most primary amines with varying substituents are commercially available. As it has already been adapted to robotic synthesizer, it is an attractive method to obtain

sequence-defined peptoids. The main drawback of this method is the limit of the peptoid chain length and the amount of materials that can be produced. So far the longest reported peptoids synthesized by this method only have 50 repeating units.[2] For scientists who need peptoids to be high molecular weight polymers with better thermal and mechanical properties, submonomer method is apparently not an appropriate approach.

1.2.2 Polymerizations of NCA monomers

Polypeptides can be synthesized via the ring opening polymerization of five-membered ring *N*-carboxyanhydride (NCA) monomers.[24] In order to synthesize polypeptoids in such way polymer chemists developed *N*-substituted *N*-carboxyanhydride (R-NCA) monomers. .

Scheme 1.2. Synthesis of R-NCA monomers.

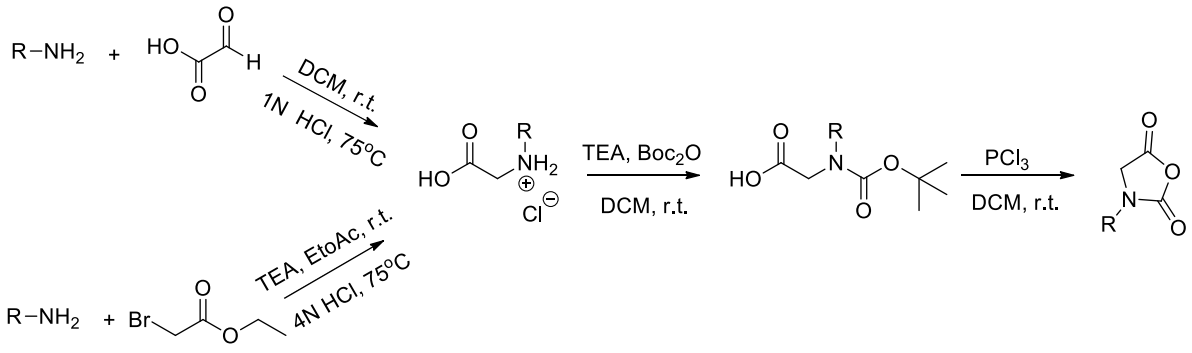

The synthesis of R-NCA usually follows a three-step synthetic pathway (Scheme 1.2). The commercially available primary amine is first reacted with glyoxylic acid or bromoacetate and then acidified with hydrochloric acid to yield the *N*-substituted glycine HCl salt.[25] The HCl salt of the amino acid is then protected by di-tert-butyl dicarbonate (Boc_2O) or benzyl chloroformate.[26] The alkoxy-protected precursor or benzyl formate-protected precursor is finally cyclized with the presence of phosphorus chloride (PCl_3) and purified by sublimation.[27] The cycling agent can also be phosphorus tribromide (PBr_3), thionyl chloride ($SOCl_2$), acyl chloride (AcCl)[21] or acetic anhydride,[26] as long as they can convert the carboxylic acid into a better electrophile (*e.g.* acyl

chloride, acyl bromide or anhydride), which facilitates the ring closure through nucleophilic attack from the carbonyl of the carbamate group. So far R-NCA monomers with alkyl, alkene, alkyne, or benzyl substituents, or short polyethylene glycol chains as substituents have been synthesized (Scheme 1.3).[7, 28, 29] The progress of NCA synthesis facilitates comprehensive investigations of polypeptoids' properties and the development of polypeptoids as novel materials for various applications. One drawback of R-NCA monomers is their high sensitivity towards moisture, which means that R-NCA must be stored and polymerized under a moisture-free condition. The emergence of thio-analogs of R-NCA, *N*-thiocarboxyanhydrides (R-NTAs), is a potential resolution to the limit of polypeptoid synthesis. Due to the substitution of the oxygen with sulfur, the 5-carbonyl becomes less electrophilic, leading to higher stability against moisture (Scheme 1.4). The synthesis and polymerization of *N*-methyl-NTA and *N*-butyl-NTA have been reported.[30, 31]

Scheme 1.3. R-NCA monomers with varying side chain substituents.

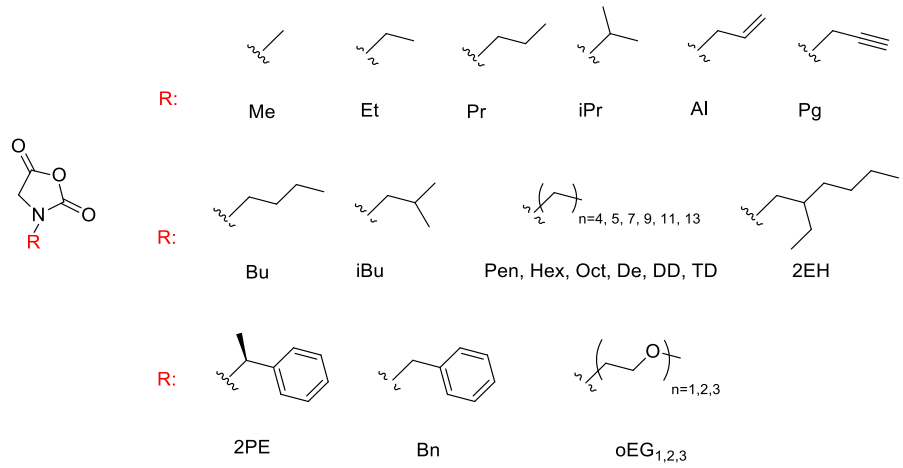

Scheme 1.4. R-NTA monomer.

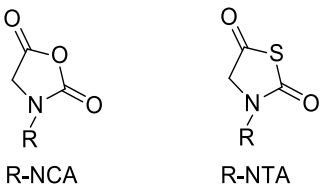

As early as the 1920s, it was demonstrated by Fuchs and Wessely that primary amines can attack the 5 carbonyl of the NCA monomers to trigger the ring-opening polymerizations (ROP).[13] This polymerization was well-developed to study *N*-substitute effect pertaining to polypeptide synthesis, and *N*-methyl NCA (Me-NCA) was one of the mostly used model. [32, 33] As the synthetic routes towards R-NCA monomers became more developed, Me-NCA was then identified as the simplest R-NCA, and the traditional amine-initiated polymerization of NCA, which was used to produce polypeptides, readily became accessible to the synthesis of polypeptoids.[26] Up to date, this is the most popular approach to produce linear polypeptoids with varying side chains, compositions, and properties (Scheme 1.5).

Scheme 1.5. ROP of R-NCA monomers using primary amine as an initiator

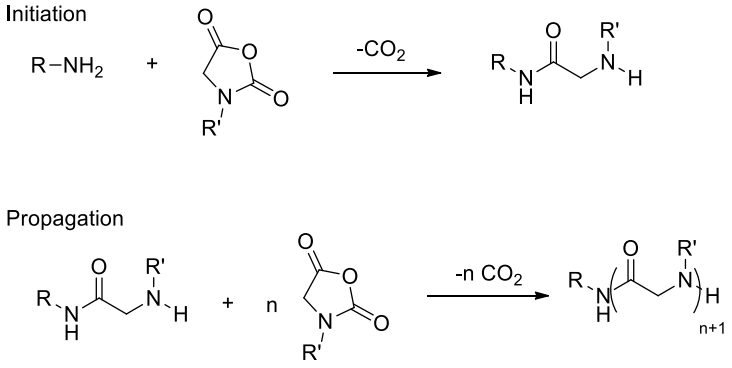

As the initiation of ROP of R-NCA monomers was triggered by nucleophilic attack on the 5 carbonyl, other nucleophilic initiators should also be able to initiate the polymerization. Although primary alcohols have weaker nucleophilicity than primary amines, they were recently demonstrated by Zhang *et al.* that can initiate the ROP of R-NCA monomers in a controlled manner. [34] The polymerization of R-NCA monomers occurs by using an electron-rich primary alcohol initiator with the presence of catalytic amount of 1,1,3,3-tetramethylguanidine (TMG). TMG was used as a promoter that can activate the alcohol initiator via hydrogen bonding interaction (Scheme 1.6). This approach enables a good control over molecular weight (MW) and molecular weight

distribution (PDI) of the resulting polypeptoids. This study indicates that weak nucleophiles can be used to synthesize polypeptoids with the presence of activators, and more combinations of organic nucleophiles and activators are awaiting discovery. New synthetic approaches of polypeptoids employing this combination are possible to provide better control over number average molecular weight (M_n) and higher efficiency, and the resulting polypeptoids with diverse functional end-groups can be expanded into broader applications.

Scheme 1.6. TMG-Promoted ROP of R-NCA with alcohol initiators. (Reprinted with permission from reference[34], copyright (2016) American Chemical Society).

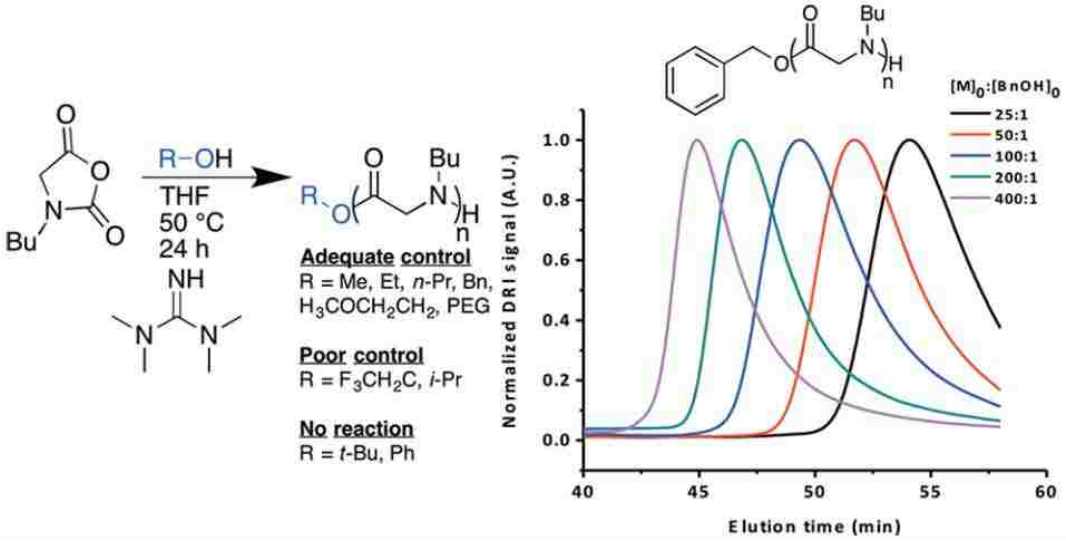

1.3 Cyclic Polypeptoids

1.3.1 Properties and development of cyclic polymers

Cyclic polymers adopt a closed ring structure and do not contain end-group species, which plays an important role in determining the properties of linear polymers. The unique cyclic architecture imparts many distinctive properties to cyclic polymers. It was found that cyclic polymers have lower intrinsic viscosity,[35, 36] higher glass transition and melting temperatures,[14, 37] faster crystallization rates,[38, 39] and wider LCST (lower critical solution temperature) phase transition windows relative to the linear counterparts.[40] Recent studies revealed the influences of

the unique architecture on the aggregation behaviors and mechanical properties of cyclic polymer materials. It was found that both the core and shell of micelles formed by amphiphilic cyclic polymers are more densely packed than those of their linear analogs,[41] and thereby micelles consisting of cyclic polymers possess enhanced stability against salt and thermal changes.[42] Cyclic polystryrene-*b*-polyisoprene was found to adopt micellar microstructures in their crystalline domains, whereas the linear analogs form 2-d hexagonal packing.[43] Cyclic polystyrene-*b*-polybutadiene tends to have smaller domain spacing than linear counterparts,[44] which is in favor of block copolymer lithography by minimizing the characteristic dimensions of nanopatterns.[45] It was reported by Tew *et al.* that the gel network formed by crosslinked cyclic polyoctene exhibits improved mechanical properties than their linear analogs attributed to the extra mesh space created by the cyclic architecture within the gel network.[46] Regarding biomedical applications, it was found that the ring architecture of cyclic polymers facilitates higher gene transfection efficiency than their linear counterparts do presumably due to their more compact conformations and stronger interactions with DNA molecules. [47] In the same study, cyclic polymers also exhibit advantages against branched polymers. It was revealed that cyclic polymers with much smaller molecular weight feature comparable gene transfection efficiency to the branched polymers with higher molecular weight. Given that smaller molecular weight polymers usually lead to less cytotoxicity, cyclic polymers have shown promising potentials for biomedical applications.

1.3.2 Synthesis of cyclic polymers

1.3.2.1 Ring-closure method

To date, several synthetic approaches have been developed to synthesize cyclic polymers. Ring-closure method which cyclizes the linear polymer precursors by using cyclizing agents is a traditional method to synthesize cyclic polymers. For instance, cyclic polyisoprene-*b*-polystyrene-

b-polyisoprene triblock copolymers were obtained by end-to-end cyclization of the linear precursors using a cyclizing agent- 1, 6-diaminohexane at 100 ^{o}C. [48] Synthesis of cyclic polymers through the ring-closure method became popular when copper-mediated cycloaddition was employed as the ring-closure chemistry for unimolecular polymer chains having alkyne and azido groups at chain ends. So far cyclic polymers including polystyrene, [49] polyacrylamide,[40, 50] polylactones,[51] and poly(ethylene imine) have been produced by this method.[47] However, inter-molecular end-to-end reaction is always a competing process during cyclization. Many factors (*e.g.* chain length, chain flexibility, and solution concentration) must be optimized to minimize the competing process, which limits the application of the ring-closure method.[52]

1.3.2.2 Ring-expansion polymerization

Ring-expansion polymerization (REP) is another pathway to obtain cyclic polymers. By using cyclic tin initiators, lactone monomers can be inserted into the cyclic rings through the Sn-O or Sn-S bond to form cyclic polyesters. The polymerization requires extra steps to remove the metallic initiators if the resulting cyclic polyesters are targeted for biological purposes.[53] An analog of REP is the ring-expansion metathesis polymerization (REMP), which is initiated by cyclic ruthenium initiators and then proceeding via insertion of the cyclooctene monomers or their derivatives into the double bonds of the cyclic initiating moieties. Cyclic polyoctenamers and their derivatives have been successfully prepared by this method.[36, 54] Based on the traditional synthetic pathways, recently developed synthetic strategies allow for the synthesis of more complicated cyclic polymers.[55-58]

1.3.2.3 Zwitterionic ring-opening polymerization (ZROP)

Zwitterionic ring opening polymerization (ZROP) is another facile synthetic approach that can produce cyclic polymers by overcoming some of the drawbacks of previously discussed approaches. ZROP entails the formation of a zwitterionic propagating intermediate where the two chain ends are oppositely charged and interact strongly with one another by electrostatic interaction.[59] The zwitterionic intermediate can either react with monomers (by a chain growth mechanism) or with each other (by a step growth mechanism) to elongate the chain or undergo intramolecular chain transfer to yield a mixture of linear and cyclic polymers (via backbiting mechanism). Intramolecular chain transfer that occurs exclusively in an end-to-end fashion will produce macrocyclic polymers cleanly. While the end-to-end macrocyclization is entropically unfavored, high molecular weight cyclic polymers can be cleanly produced by the ZROP method when the interactions between the oppositely charged chain ends of the zwitterionic propagating intermediates overcome the entropic penalties.[59] A distinct advantage of the ZROP method is that the polymerization can be conducted in moderate to high monomer concentration, enabling efficient access to cyclic polymers. This is in contrast to the ring-closure method of linear polymer precursors that typically requires high dilution conditions.

ZROP has recently emerged as a promising strategy to produce high molecular weight cyclic polymers with diverse backbone structures (*e.g.*, polyester[60-63] and polyamide).[64] For example, it was recently reported that isothiourea can mediate the ZROP of lactide to produce cyclic polylactides with relatively high cyclic polymer contents in spite of somewhat slow polymerization rates.[65] $B(C_6F_5)_3$ was used as the electrophilic initiator to mediate the ZROP of glycidyl monomers to yield cyclic polyethers.[66] Several recent studies have shown that *N*-heterocyclic carbenes (NHCs) can initiate and mediate the ZROPs of strained cyclic monomers

(*e.g.*, lactides, caprolactone, and carbosiloxane) to produce high molecular weight macrocyclic polylactides, polylactones, and polycarbosiloxanes with moderate to high efficiency.[60-62, 67] Cyclic gradient polyesters can be obtained by NHC-mediated ZROP of ε-caprolactone (CL) and δ-valerolactone (VL) in a one-pot reaction.[68] We have recently demonstrated that a variety of cyclic poly(*N*-substituted glycine) (*a.k.a.* polypeptoids) with varying *N*-substituents can be obtained by NHC-mediated ZROP of the corresponding R-NCA monomers.[1, 64, 69, 70] The reactions were shown to occur in a controlled manner, producing cyclic polypeptoids with well-defined structure, molecular weight and narrow molecular weight distribution. This is in contrast to early studies on pyridine/tertiary amine/solvent initiated or thermally initiated ZROPs of Me-NCA which only produce low molecular weight cyclic poly(*N*-methyl glycine) (*a.k.a.* polysarcosine).[71-74]

1.3.3 Analysis of cyclic polymers

End-group analysis using the combination of ^{1}H NMR (proton nuclear magnetic resonance) and MALDI-TOF MS (matrix assisted laser desorption ionization-time of flight mass spectrometry) is a common method to detect the cyclic architecture when the end-group and the polymer backbone structures are known. This method is an indirect measurement, and a complementary measurement must be performed to support the architectural confirmation. Size exclusion chromatography (SEC) is widely employed to analyze cyclic polymers. The intrinsic viscosity, radius of gyration, and hydrodynamic volume of cyclic polymers can be measured by a SEC-light scattering-viscometer-DRI (SEC-LS-VIS-DRI) online system. The measurement of linear counterparts as a control group is necessary to suggest the cyclic architecture. This method usually demands large amounts of samples and complicated sample preparations with very limited analytical outcomes besides the architectural information. In contrast, microscopic analysis is able to directly measure the size and the architecture of cyclic polymers in both dry state or solution

phase. It was previously demonstrated that the atomic force microscopy (AFM) can be used to reveal the cyclic backbone architecture.[75-80] When it comes to other physical parameters of cyclic polymers (*e.g.* radius of gyration, persistence length, Kuhn length, etc.) small angle x-ray scattering (SAXS) or small-angle neutron scattering (SANS) are mostly used. Up to date some good examples have shown us that scattering analysis of cyclic polymers is of importance for better understanding the properties of cyclic polymers. Quantitatively analysis of a worm-like chain (c-ATPC) revealed that the helix pitch per residue and the Kuhn segment length of the specific rigid ring are independent of the solvent, which is opposite to the corresponding linear analog, indicating a different local conformation from linear polymers.[81] The absorption of cyclic PEG onto silica particles studied by small angle neutron scattering (SANS) has shown that cyclic PEG has higher absorption on silica nanoparticles than the linear analog does, but the thickness of the *c*-PEG layer decreases as the molecular weight increases, which is very different from the linear PEG.[82] In addition, scattering functions based on various cyclic polymer models have been built, enabling the essential basis for further investigation of cyclic polymers into a broader scope.

1.4 Functional Polypeptoids

In the past few years, more and more functional polypeptoids became available thanks to the progress of synthetic strategies. Functional polypeptoids with alkene and alkyne side chains can be readily synthesized, allowing for post-modifications of polypeptoids for various purposes. Alkene reactions including ozonolysis, alkene metathesis, and thiol-ene click chemistry were carried out to convert the double bond of poly glutamate to other side chains like alcohol, aldehyde, carboxylic acid *et al*.[83] It is possible to functionalize poly(*N*-allyl glycine) (PNAG) via the same method. Schlaad *et al.* demonstrated that post-modification of PNAGs via thiol-ene click chemistry is feasible to connect either 1-thio-*β*-D-glucose tetraacetate or 1-thio-*β*-D-glucose onto

the side chains of polypeptoids to improve the bio-activity of polypeptoids.[84] Poly(*N*-propargyl glycine) (PNPgG) is the most popular model polypeptoid bearing alkyne groups on the side chains. The same research group also demonstrated that several reactions can be performed with the alkyne groups of PNPgG, including thiol-yne radical addition, deprotonation and nucleophilic addition of ethylene oxide, thermally induced cross-linking, and the copper-mediated cycloaddition. [85]

As the progress has been made to produce polypeptoids with well-defined M_n (number average molecular weight) and PDI, polypeptoid nano-rods can be fabricated by seeding primary amines onto various substrates. Garno *et al.* fabricated nano-rods comprising PNAG on a silica surface by in-situ ROP using (3-aminopropyl)triethoxysilane initiators.[86] Adopting this idea, Me-NCA was surface-polymerized on a silica surface pretreated by either photolithography or microcontact method to prepare well-defined surface patterns of polypeptoids in a micro-scale.[87] The precise control over the micro-scale or even nano-scale lithography allows for the evaluation of directional growth of polymers. More importantly it sets a platform for future fabrication of bioelectronics and biosensors made of polypeptoids.

Thermoresponsive hydrogels consisting of A-B-C triblock copolypeptoids, (poly(*N*-allyl glycine)-b-poly(*N*-methyl glycine)-b-poly(*N*-decyl glycine) (PNAG-*b*-PNMG-*b*-PNDG), were prepared by Zhang *et al*. In this material methyl glycine (Me) is used as the hydrophilic segment and decyl glycine (De) is used as the hydrophobic segment. Allyl glycine (Al) is also incorporated because of its thermoresponsive properties. The A-B-C triblock copolymers self-assemble into micelles in solution at room temperature, and undergo sol-gel transition within a wide range of gelation temperatures (26 ^{o}C to 41 ^{o}C) with various polymer compositions. [29] The sol-gel transition behavior is attributed to the thermo-responsive behaviors of the Al segments. When the temperature is increased above the LCST of Al, the original dissolved Al segments become

insoluble in aqueous solution and collapse together to form hydrophobic domains in addition to the original De hydrophobic domains, resulting in the formation of 3-dimentional networks. The resulting gels with a wide range of storage modulus (*G'*) and Young's modulus (*E*) can be tailored by controlling the polymer composition and the solution concentration. The hydrogels are injectable and can be potentially used to encapsulate enzymes without affecting their bioactivities. This is a model platform for the development of drug delivery, tissue engineering and protein storage.

1.5 Cytotoxicity Assessment of Polypeptoids

Peptoids were initially produced as pharmaceutical agents, and it was demonstrated that they have good biocompatibility and protease stability relative to peptides. Since then polymer chemists devoted much effort to expanding the applications of peptoid materials including the optimization of the monomer synthesis and polymerization, post-modification, and the assessment of the physicochemical properties of the polypeptoids. Till now polypeptoids with various side chains, compositions and structures, and physical properties have been produced under controlled manners. Based on the accomplishment of the first-stage study, now scientists can take a step forward to apply polypeptoids as biomaterials for biomedical applications. The bridge that connects the two stages is the evaluation of biological properties of polypeptoids.

A cytotoxicity study is the first step to evaluate the biocompatibility of a biomaterial. Zhang *et al.* investigated the cytotoxicity of cyclic poly [(*N*-ethyl glycine)-*r*-(*N*-butyl glycine)]s [P(NEG-*r*-NBG)]s using the CellTiter Blue cell viability assay. The cyclic polymers were incubated with Human embryonic lung fibroblasts (HEL229in PBS buffers for 24 h at varying concentrations from 0.039 to 5.0 mg mL^{-1}. After 1 day incubation the cell viability was still above 80 % which is on par with the results tested with low molecular polyethylene glycol (PEG).[1] Luxenhofer *et al.*

evaluated cytotoxicity of polypeptoids by incubating $PNMG_{50}$ homo-polypeptoid and block copolypeptoids including poly(*N*-methyl glycine)$_{50}$-*b*-poly(*N*-propyl glycine)$_{43}$ [$PNMG_{50}$-b-$PNPG_{43}$], poly(*N*-methyl glycine)$_{50}$-*b*-poly(*N*-pentyl glycine)$_{10}$ [$PNMG_{50}$-*b*-$PNPenG_{10}$] *et al.* with Human liver carcinoma cells (HepG2) for 24 h in medium. The upper limits of polypeptoid concentrations lied in 2-10 mg/mL depending on the solubility of the polymer in medium and the results indicated minimum cytotoxicity of polypeptoids to HepG2 cells.[19] Ling *et al.* carried out the biocompatibility evaluation of a series of thermoresponsive PNMG-*r*-PNBGs with HepG2 cells for 48 h in 4-(2-hydroxyethyl)-1-piperazineethanesulfonic acid (HEPES) buffer. All samples exhibited minimum toxicity to HepG2 cells when the concentration was as low as 0.1 mg mL^{-1}. By further increasing the concentrations of the samples to 3 mg/mL, the random copolymer whose LCST is way above 37 ^{o}C still showed minimum cytotoxicity as homo-PNMG did, but for those random copolymers whose LCSTs are close or lower than 37 ^{o}C they slightly precipitated out and caused inhibition to the growth of HepG2 cells.[30, 88] So far, homo-PNMG and random or block copolypeptoids exhibit good biocompatibility with cells, but for thermoresponsive polypeptoids the effect of temperature on their cytotoxicity remains to be investigated.

1.6 Drug Delivery Using Polymeric Micelles

1.6.1 History and development of drug delivery systems based on amphiphilic copolymers

When amphiphilic block copolymers are dissolved in an aqueous solution, the hydrophobic segments are surrounded by water molecules, which is called hydrophobic hydration. When the concentration of the polymers reaches the critical micelle concentration (CMC), hydrophobic segments start to get dehydrated and form hydrophobic zones. This entropy-driven process is called micellization. The study of polymeric micelles can date back to the 1960s when the solution properties of micelles comprising Pluronic Polyols were investigated.[89] Early studies of polymeric

micelles were mainly conducted in organic solvents.[90-93] Until the 1990s people started thinking about utilizing the cargo structure of polymeric micelles for small molecule transportations in biomedical applications. Yokoyama *et al.* first developed adriamycin-conjugated polymeric micelles comprising polyethylene glycol- polypropylene glycol- polyethylene glycol (PEO-PPO-PEO) triblock copolymers in aqueous solution and conducted systematic biological studies of this drug delivery system. Their results implied that admin-conjugated micelles have good anti-tumor activity.[94] In their subsequent study the pharmacokinetics of the system was assessed, and it was found that the system has elongated circulation time *in vivo*.[95] Since then polymeric micelles have been widely investigated as nanocarriers for drug delivery applications. The early studies provided adequate evidence that polymeric micelles are capable of enhancing the water solubility of hydrophobic drugs, protecting drugs against degrading enzymes, overcoming multi-drug resistance (MRD), [96, 97] improving accumulation of drugs selectively at the diseased sites, and increasing circulation time of drugs in human body.[98-100]

Conventional polymeric micelles formed by self-assembly of amphiphilic block copolymers via hydrophobic interactions may spontaneously dissociate upon dilution, resulting in pre-leakage during drug delivery. Allen *et al.* found that conventional micelles composed of poly (ethylene glycol)-*b*-poly (caprolactone) are able to maintain their stability *in vivo* even below their CMC presumably due to their relatively stable semicrystalline core, and thereby the pre-leakage issue can be avoided, but the method of preparing such semi-crystalline micellar core is only limited to certain materials.[101] To enhance the *in vivo* stability of the polymeric micelles, crosslinking of the micellar core or shell has been widely adopted. Liu *et al.* prepared several crosslinked nanostructures formed by amphiphilic block copolymers mainly in organic solvents. Based on their previous studies, they reported a newer work in 1997 that poly(2-cinnamoylethyl

methacrylate)-*b*-poly(acrylic acid) (PCEMA-*b*-PAA) was used to construct water-soluble and core-crosslinked micelles (CCLMs) which were shown to be able to maintain the well-defined nanostructures permanently even in dilute conditions.[102] Meanwhile, shell-crosslinked micelles (SCM) based on polystyrene-*b*-poly(4-vinyl pyridine) were also developed by Wooley *et al.* in order to resemble the properties and behaviors of dendrimers in solution.[103] In their subsequent study, SCMs made of poly(caprolactone)-*b*-poly(acrylic acid) were prepared via crosslinking between the diamine crosslinkers and the carboxylic acid side chains. Based on the resulting SCM they further hydrolyzed the core of poly(acrylic acid) to obtain hollow spherical nano-cages, which can be potentially used as nanocarriers with high loadings.[104] Despite of avoiding the stability and pre-leakage issues of conventional polymeric micelles, the permanently crosslinked micelles, which cannot be disintegrated, may be difficult to remove through renal clearance.[105] In order to achieve controlled drug release, stimuli-responsive CCLMs, which can maintain their structures upon dilution and undergo dissociation in response to environmental cues, have been investigated in the last decade.[106, 107]

1.6.2 State of the art of stimuli-responsive core-crosslinked micelles

Nanocarriers based on polymeric micelles that are responsive to light,[108-111] temperature,[112-114] enzymes, pH, and a reductive environment have been developed for controlled drug delivery applications. Among all these triggers, construction of crosslinked micelles responsive to pH or a redox environment has become widely employed. Studies have shown that tumor tissues have reduced pH values and a different redox environment from normal tissues.[115, 116] Controlled drug release is more likely to be accomplished if the pathophysiological characteristics of tumors can be utilized. Preparation of pH responsive micelles usually requires ionic pendants on the backbone of amphiphilic copolymers. When the pH transforms from the

basic to the acidic, the ionic pendants get protonated and the solubility of the polymer segments gets inverted, therefore leading to the rupture of micellar structures and drug release.[117] When it comes to neutral amphiphilic copolymers, another strategy that incorporates redox-responsive covalent bonds into the micellar system is usually adopted. Kataoka *et al.* is one of the groups that developed reduction-responsive CCLMs at the very beginning by aerial oxidation of the thiol-functionalized poly (ethylene glycol)-*b*-poly (lysine) copolymers of the micelles. The reduction-responsive behavior of CCLMs was demonstrated by the release of pre-loaded oligo-nucleotides from the CCLMs under a reductive environment.[118] Since then redox-responsive polymeric micelles have been judiciously designed by incorporating redox responsive units (*e.g.*, disulfide, diselenide[119], thio-ether[120] and acrylboronic ester[121]) either into the polymer backbones, [122, 123] side chains[124, 125] or cross-linkers.[126-128] These micelles were shown to respond to oxidants (*e.g.*, H_2O_2) or reductants (*e.g.*, glutathione (GSH)) that are naturally present in the cellular environment by undergoing morphological changes.

1.6.3 The development of polymers used to construct micelles

Early attempts at the formation of polymeric micelles used various polymers for amphiphilic block segments including polystyrene,[129] polyisoprene,[130] polyethylene oxide, and polydimethylsiloxane.[131] Among these materials, Pluronic, a triblock amphiphilic copolymer (PEO-PPO-PEO), was the most popular one to be used to construct micelles due to its commercial accessibility.[132] In the 1990s, several groups contributed significant effort into comprehensive studies on the properties of micelles formed by Pluronic.[133] Phase behaviors, rheology, and thermodynamics of Pluronic micelles in aqueous solutions were systematically studied, and the results of these studies boosted the fast progress of varying polymeric micelles for biomedical applications in the next 20 years.[134-136] The design of polymeric micelles later on required that the

building blocks of the nanocarriers used *in vivo* are minimally cytotoxic and backbone degradable, allowing for systematic clearance of the materials. The hydrophilic block of Pluronic- polyethylene glycol (PEG) was therefore extensively used with other biodegradable blocks to construct redox responsive micelles due to its commercial accessibility and good biocompatibility (*e.g.* polypeptide-*b*-poly(ethylene glycol) (PEG),[126] poly(ε-caprolactone)-*b*-PEG,[128] polylactide-*b*-PEG,[137] and poly(tyrosine(alkynyl)-OCA)-*b*-PEG[127, 138]). So far PEG is the most widely investigated polymer for various drug delivery systems including several PEGylated micellar or liposomal formulations in advanced clinical studies,[139-142] but studies have shown that PEG can trigger complement activation,[143, 144] and PEGylated liposomes can be cleared rapidly upon repeated injections.[145-148] There is a clear and continued need to develop and investigate new micellar materials for drug delivery applications.

1.6.4 Aggregation of polypeptoids in solutions

In order to use polypeptoids for drug delivery, the first step is to understand the relationship between their structures and their aggregation behaviors in solution. Cyclic and linear $PNMG_{100}$-*b*-$PNDG_{10}$ amphiphilic block copolypeptoids synthesized by sequential polymerizations were found to self-assemble into spherical micelles in MeOH at 1mg·mL^{-1} concentration, and after a few days both of the self-assemblies transformed into micro-scale cylindrical micelles. This morphological transition is tentatively attributed to the gradual crystallization of the decyl segments. Recently, Zuckermann *et al.* synthesized monodisperse amphiphilic diblock copolypeptoids (poly(*N*-decyl glycine)-*b*-poly(*N*-2-(2-(2-methoxyethoxy) ethoxy) ethyl glycine)) with the same hydrophilic and hydrophobic chain lengths. It was found that hollow and multiwalled crystalline nanotubes with diameters ranging from 4.3 to 9.0 nm can be accessed by the self-assembly of the copolypeptoids with varying chain lengths.[149] Another systematic study

into the aggregation behaviors of amphiphilic copolypeptoids in aqueous solution was reported. A series of amphiphilic copolypeptoids (poly(*N*-methyl glycine)-*b*-poly(*N*-propyl/butyl/pentyl glycine)s) with slight differences in their compositions was synthesized. The effects of hydrophilic/lipophilic balance (HLB) on CMC and aggregation behaviors of these copolypeptoids were attempted to be investigated, but several conclusions made in this study remain ambiguous. First, in this study the trend of CMC in micromolar concentration is not proportional to the increase of HLB. Second, the suggestions that higher HLB results in smaller size aggregates and lower HLB results in larger aggregates are not persuasive because the numbers representing the sizes of larger aggregates were obtained from broad size distributions without PDI reported and the example used as smaller aggregates has even bigger aggregates than those so-called larger aggregates. Third, their suggestion that when the hydrophilic fraction= 50 % they may have worm-like micelles composed of polypeptoids formed in aqueous solution was proposed based on only the multi-modal size distributions of polypeptoid aggregates. In order to support this assumption, they did not show any microscopic results besides citing references from other groups focusing on the effect of HLB on the morphology. More work must be completed to efficiently and completely understand the relationship between chemical structures and aggregation behaviors, and micelles comprising polypeptoids with various desired properties can then be easily fabricated.

1.6.5 Polypeptoid used as drug delivery systems

Some recent studies focusing on the construction of drug delivery systems comprising biocompatible polymers have incorporated polypeptoids, more accurately poly(*N*-methyl glycine)-*block*-polypeptide copolymers. Block copolymers, polysarcosine-*b*-polylysine-*ε*-*N*-benzyloxycarbonyl acid benzylester, were synthesized through sequential ring opening polymerizations of NCA monomers. The resulting polymers were able to self-assemble into

micelles that are 28 nm in diameter without drug and 33 nm in diameter with hydrophobic drugs loaded.[150] Block copolymers of poly(*N*-methyl glycine)-*b*-polyglutamic acid (OBn) were synthesized via a similar pathway by using a mannose-terminated primary amine initiator, and then self-assembled into micelles covered by mannose with diameters around 70 nm. The resulting micelles exhibited improved cell uptake when they were incubated with DC 2.4 cells and in bone marrow-derived dendritic cells (BMDCs) which bear mannose-receptors. Targeted drug delivery was already demonstrated possible by using polypeptoid-based micelles.[151] The application of polypeptoids for gene transfer was also demonstrated by the same group. Poly(*N*-methyl glycine)-*b*-polylysine was synthesized and then complexed with DNA. The obtained polyplexes were then incubated with HEK 293T cells and showed up to 50% transfection efficiency.[152] Stimuli-responsive polypeptoid-based micelles were prepared by using a Boc-protected cystamine as the initiator. The disulfide-linked block copolymers were synthesized by the polymerization of one block using the initiator and then the deprotection of the amino group of the cystamine moieties to initiate the polymerization of another block of polymers. The amphiphilic and redox-responsive copolypeptoids can self-assemble into micelles and undergo degradation with the presence of reducing agents like glutathione.[153]

1.6.6 Pharmacokinetics

Block copolymers with PNMG as the hydrophilic segment and poly (lactic acid) (PLLA) as the hydrophobic segment were used to prepare micelles called Lactosome. The pharmacokinetics of Lactosome were studied *in vivo*. The results revealed that Lactosome causes an accelerated blood clearance (ABC) phenomenon in tumor-bearing mice suggested by the production of anti-lactosome IgM and IgG3 related to B-lymphocyte cells. The ABC phenomenon results in the trap of Lactosome in the liver upon multiple dosages. The enzyme-linked

immunosorbent assay (ELISA) study indicated that the epitope moiety is due to PNMG although it was developed intentionally to replace PEG.[154] This ABC issue of Lactosome can be avoided by using (poly(*N*-methyl glycine)$_{s23}$)$_3$-*b*-poly(L-lactic acid)$_{30}$, a A_3B-type polymer, to form micelles. This type of micelles has a more densely packed micellar shell structure which can prevent any penetration through the micellar shells and thereby avoid the interactions with B-cells. However, the win over the ABC phenomenon is at the cost of reduced half-life time of the micelles in the bloodstream, which leads to reduced accumulation of micelles in tumors.[155] Following the same idea, nanosheets which have even more densely packed shell structures were prepared by the same group. Instead of using the same type of copolymer the PLLA was replaced by a helical polypeptide segment, poly (Leu-Aib), whose secondary structure leads to the formation of nanosheets. Although the ability to escape liver is not as good as micelles, this type of nanosheet can also suppress the ABC phenomenon and could accumulate in tumor sites even after multiple dosages.[156]

Thanks to all of these systematic studies, scientists now have deeper insights into aggregation behaviors and biological activities of polypeptoid-based nanoparticles. A remaining problem is that most of the systems investigated are limited to PNMG, but polypeptoids are much more than this. More importantly most of these amphiphilic block copolymers have polypeptides as hydrophobic segments, which are known to exist in solution with helical secondary structures, so the aggregation behaviors and other biological activities of this polypeptoid-polypeptide coil-rod copolymers could be very different from polypeptoid-polypeptoid coil-coil copolymers. Scientists still need to expand the scopes of polypeptoids that can be used for biomedical applications and prepare new amphiphilic block copolypeptoids with unique biological activities for drug delivery. Based on the results of the pharmacokinetics of Lactosome, it seems promising

that the immune system issue caused by polypeptoid-based micelles can be overcome by core-crosslinking or shell-crosslinking to provide densely packed nanostructures without compromising their ability to accumulate in tumor.

Chapter 2. Amidine-Mediated Ring-Opening Polymerization towards Cyclic Polypeptoids

2.1 Introduction

Polypeptoids, also known as poly (*N*-substituted glycine)s, are synthetic mimics of polypeptides. Because of the *N*-substitution, polypeptoids lack main chain chirality and hydrogen bonding interaction, in contrast to polypeptides. This results in polypeptoid having enhanced proteolytic stability relative to polypeptides,[157] thermo-processability[14, 16, 69] and conformational tunability (via side chain structure).[7, 64, 158, 159] Secondary conformations of polypeptoids including random coil, helices, sheet structures have all been reported. [160,4, 11, 161, 162] In addition, polypeptoids have been shown to exhibit minimal cytotoxicity to several cell lines[1, 163, 164] and can degrade under oxidative conditions that mimic the tissue inflammation environment, suggesting the potential uses for *in vivo* biomedical applications.[165]

Cyclic polymers have attracted considerable attention because of their distinctive physical properties as compared to the linear counterparts. The unique topology imparts many interesting properties to cyclic polymers such as lower intrinsic viscosity,[35, 36] higher glass transition and melting temperatures,[14, 37] faster crystallization rates, [166] and wider phase transition windows,[40] relative to the linear counterparts. To date, several synthetic approaches have been developed for the cyclic polymers, including interfacial condensation,[48] ring-expansion metathesis polymerization,[36, 54] end-to-end polymer cyclization,[49, 167] and zwitterionic ring-opening polymerization (ZROP).[60-62, 67]

*This chapter previously appeared as [Ang Li, Lu Lu, Xin Li, LiLin He, Changwoo Do, Jayne C. Garno and Donghui Zhang, Amidine-Mediated Zwitterionic Ring-Opening Polymerization of *N*-Alkyl *N*-Carboxyanhydride: Mechanism, Kinetics and Architecture Elucidation. *macromolecules*, 2016, *49* ,1163–1171.] It is reprinted by permission of American Chemical Society.

The zwitterionic intermediate can either react with monomers (by a chain growth mechanism) or with each other (by a step growth mechanism) to elongate the chain or undergo intramolecular chain transfer to yield a mixture of linear and cyclic polymers (via backbiting mechanism). Intramolecular chain transfer that occurs exclusively in an end-to-end fashion will produce macrocyclic polymers cleanly. While the end-to-end macrocyclization is entropically unfavored, high molecular weight cyclic polymers can be cleanly produced by the ZROP method when the interactions between the oppositely charged chain ends of the zwitterionic propagating intermediates overcome the entropic penalties.[59] A distinct advantage of the ZROP method is that the polymerization can be conducted in moderate to high monomer concentration, enabling efficient access to cyclic polymers. This is in contrast to the end-to-end cyclization strategy of linear polymer precursors that typically require high dilution conditions.

ZROP has recently emerged as a promising strategy to produce high molecular weight cyclic polymers with diverse backbone structures (*e.g.*, polyester[60-62,63] and polyamide)[64]. For example, it was recently reported that isothiourea can mediate the ZROP of lactide to produce cyclic polylactides with relatively high cyclic polymer contents in spite of somewhat slow polymerization rates.[65] $B(C_6F_5)_3$ was used as the electrophilic initiator to mediate the ZROP of glycidyl monomers to yield cyclic polyethers.[66] Several recent studies have shown that *N*-heterocyclic carbenes (NHCs) can initiate and mediate the ZROPs of strained cyclic monomers (*e.g.*, lactides, caprolactone, and carbosiloxane) to produce high molecular weight macrocyclic polylactides, polylactones, and polycarbosiloxanes with moderate to high efficiency.[60-62, 67] Cyclic gradient polyesters can be obtained by NHC-mediated ZROP of ε-caprolactone (CL) and δ-valerolactone (VL) in a one-pot reaction.[68] We have recently demonstrated that a variety of cyclic poly(*N*-substituted glycine) (*a.k.a.* polypeptoids) with varying *N*-substituents can be obtained by

NHC-mediated ZROP of the corresponding R-NCA monomers.[1, 64, 69, 70] The reactions were shown to occur in a controlled manner, producing cyclic polypeptoids with well-defined structure, molecular weight and narrow molecular weight distribution. This is in contrast to early studies on pyridine/tertiary amine/solvent initiated or thermally initiated ZROPs of Me-NCA which only produce low molecular weight cyclic poly(*N*-methyl glycine) (*a.k.a.* polysarcosine).[71-74]

1, 8-diazabicycloundec-7-ene (DBU), a bicyclic amidine, is widely used to catalyze esterification of carboxylic acids[168] and controlled ROPs of lactides, lactones, and cyclic phosphoesters.[169-172] The DBU is commonly considered a strong base with weak nucleophilicity. This view has changed in recent years after DBU was found to be a competent nucleophile that can undergo nucleophilic addition to dimethyl carbonate and chloroformate.[173-176] It was recently demonstrated that DBU can initiate the ZROP of lactide to produce a mixture of cyclic and linear polylactide.[177]

While NHCs can mediate the ZROP of various cyclic substrates, they are air and moisture sensitive. In an effort to identify and characterize alternative organic-initiators that can outperform NHCs in mediating the ZROP of R-NCAs to produce cyclic polypeptoids in a controlled manner and ideally more robust than NHCs, we investigated the DBU as possible initiators for the ZROP of Bu-NCA monomers. Throughout this project, we investigated the polymerization behaviors, polymerization kinetics, and the possible architecture of the resulting polypeptoids obtained from the polymerizations.

2.2 Materials and Methods

2.2.1 Materials

1, 8-Diazabicycloundec-7-ene (DBU) (Sigma-Aldrich) was dried over CaH_2 and purified by distillation before use. All solvents used were purchased from Sigma-Aldrich and purified by passing through alumina columns under argon (Innovative Technology, Inc.) and stored under a nitrogen atmosphere. All other chemicals were purchased from Sigma-Aldrich and used as received. *N*-butyl *N*-carboxyanhydride (Bu-NCA was synthesized by following a reported procedure.[64] Linear poly (*N*-butyl glycine) (PNBG) was synthesized from primary amine-initiated polymerization of Bu-NCA using benzylamine initiators by a reported procedure.[64]

2.2.2 Instrumentation

^{1}H NMR spectra were recorded on a Bruker AV-400 spectrometer and chemical shifts in parts per million were referenced to protio impurities in the deuterated solvent (*e.g.*, $CDCl_3$). Matrix-assisted laser desorption ionization time of flight mass spectra (MALDI-TOF MS) were collected on a Bruker ProFLEX III in the reflective mode. α-Cyano-4-hydroxycinnamic acid (CHCA) was used as matrix.

Size-exclusion chromatography (SEC) analyses were performed using an Agilent 1200 system (Gastorr GT-14 degasser, Agilent 1200 series isocratic pump, and auto sampler) equipped with three Phenomenex 5 μm, 300×7.8 mm columns (100Å, 1000Å and linear), a Wyatt DAWN EOS multi-angle light scattering (MALS) detector (GaAs 30 mW laser at 690 nm) and a Wyatt Optilab rEX differential refractive index (DRI) detector with a 690 nm light source. DMF with 0.1 M LiBr was used as eluent at a 0.5 $mL \cdot min^{-1}$ flow rate. The column and detector operate at room temperature. Wyatt Astra 6.0 was used to process all SEC data. The polymer molecular weight (M_n) and polydispersity index (PDI) were obtained by Zimm-model fit of MALS-DRI data. SEC

samples were prepared by dissolving the polymer (5 mg) in DMF/ 0.1 M LiBr (1 mL) with slight heating followed by filtration through a PTFE syringe filter (pore size = 0.2 μm).

2.2.3 dn/dc Measurement

The refractive index increments (dn/dc) of the synthesized polymers were measured by using the Wyatt's rEX DRI detector and Astra 6.0 software with dn/dc template. A series of polymer solutions in 0.1 M LiBr/DMF whose concentrations ranged from 0.050-3.0 $mg \cdot mL^{-1}$ were injected into the DRI detector. The measured refractive indices were plotted versus concentrations, and the slope from the linear fit of the data is the dn/dc of the polymer. The dn/dc value of the poly (*N*-butyl glycine) obtained from DBU-mediated polymerization of Bu-NCA in DMF/0.1 M LiBr at 25 ℃ and is 0.0797(9) $mL \cdot g^{-1}$. [178]

2.2.4 Representative procedures for the kinetic study

A predetermined amount of DBU stock solution in toluene-d_8 (20 mM each) were added to a toluene-d_8 solution of Bu-NCA (500 μL, 0.075 mmol, 150 mM) at room temperature. The contents were transferred into a resealable J. Young NMR tube. ^{1}H NMR spectra were collected every 3 min at 50 ℃ over the course of four half-lives. Monomer conversion was calculated from the relative integration of the methylene proton resonance of the monomer and polymer respectively. It was determined that by the time the first spectra were taken, approximately 3 - 24 % of the monomer was converted into polymer. Kinetics experiments were repeated at least twice under identical conditions for each set of polymerization conditions.

2.2.5 Representative procedures for DBU-mediated polymerization of Bu-NCA

Inside a glovebox, Bu-NCA (154 mg, 0.98 mmol) was dissolved in THF (2.45 mL) and a predetermined amount of DBU/THF stock solution (381 μL, 9.8×10^{-3} mmol, 40 mM) was added by syringe. The reaction mixture was stirred at 50 ℃ for 16 h under a nitrogen atmosphere and

quenched by precipitating the polymers in an excess of hexane. The white polymers were isolated by centrifugation and decantation, and dried under vacuum (100 mg, 91% yield). ^{1}H NMR of poly (*N*-butyl glycine) (in $CDCl_3$, ppm): 0.91 (C*H*3CH2CH2CH2-), 1.31 (CH3C*H*2CH2CH2-), 1.49 (CH3CH2C*H*2CH2-), 3.37 (CH3CH2CH2C*H*2-), 4.00 (-COC*H*2-).

2.2.6 Representative procedures for convert DBU-PNBG into linear analogs

Inside a glovebox, DBU-$PNBG_{25}$ (1eq., 27 mg, 9.3 μmol) was dissolved in THF (580 μL), into which AcCl (10.6 eq., 7 μL, 99 μmol) was added by a micro-syringe. The reaction solution was stirred at room temperature for 1 h. The solution was then purified by adding the bad solvent, hexane, in an excess amount, and then dried under vacuum to remove excess AcCl to obtain pure AcCl-treated DBU-$PNBG_{25}$.

2.3 Results and Discussion

Scheme 2.1. DBU-mediated ring-opening polymerization of Bu-NCA monomers.

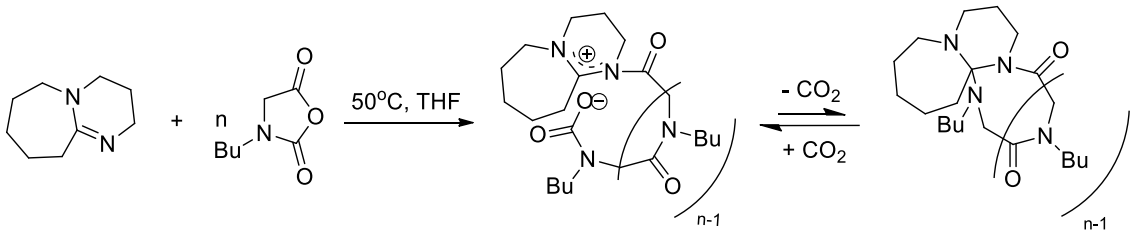

2.3.1 DBU-mediated polymerization of Bu-NCAs

A series of polymerizations of Bu-NCA in the presence of DBU were conducted in 50 ℃ THF with varying initial monomer to DBU feed ratios ($[M]_0$: $[DBU]_0$=25:1 to 400:1) at three different initial monomer concentrations ($[M]_0$= 0.4, 0.8 and 1.6 M). Progression of the polymerization was monitored by ^{1}H NMR spectroscopic analysis of the reaction aliquots taken at different time. All reactions were allowed to reach a complete conversion prior to termination by precipitation of the polymers in hexane.

The isolated polymers were characterized by ^{1}H NMR, MALDI-TOF MS spectroscopy and size-exclusion chromatography coupled to multi-angle light scattering and differential refractive index detectors (SEC-MALS-DRI). ^{1}H NMR analysis revealed the desired PNBG backbone structure and the presence of DBU moieties affixed to the polymer chains, as evidenced by the presence of two methylene groups (f, g) of the DBU moieties at 2.84 and 2.05 ppm respectively (Figure S2.1). MALDI-TOF MS analysis of a low molecular weight polymer revealed the dominant presence of molecular ions that are consistent with the structures of cyclic PNBG polymers bearing one DBU moiety (a,b,c and h, Figure S2.2) and the cyclic zwitterionic PNBG species bearing one DBU moiety and one carbamate end-group (d and e, Figure S2.2) (Scheme 2.1). Minor sets of molecular ions that are consistent with the linear PNBG polymers bearing one carboxylic acid end group and one secondary amino end-group were also present (f and g, Figure S2.2). In addition, some of the cyclic PNBG polymers were co-ionized with methanol (the solvent introduced during the MALDI-TOF MS sample preparation) under the MALDI-TOF MS conditions (Figure S2.2). Similar behaviors have previously been reported for the MS studies of the PNBG polymers obtained from the NHC-mediated ZROP of Bu-NCAs.[179]

SEC-MALS-DRI analysis revealed that PNBGs with predicable M_n values in the 3.5- 32.4 kg·mol^{-1} range can be readily synthesized by controlling the initial monomer to DBU ratios ($[M]_0$= 0.4 M, entry1- 7, Table 2.1). The polymer molecular weight distribution remains relatively narrow (PDI= 1.02-1.03) (Figure 2.1 (A)). The experimental M_n values determined by the SEC analysis agree reasonably well with the theoretical values based on single site initiation by DBU when the initial monomer to initiator ratio ($[M]_0$: $[DBU]_0$) is lower than 150:1. However, when the $[M]_0$: $[DBU]_0$ ratio exceeds 150:1, the experimental M_n values become less than theoretical values, suggesting side reactions in competition with chain propagation. If the DBU initiates the

polymerization by a nucleophilic ring-opening pathway, it is conceivable that intra-molecular macrocyclization or intermolecular head-to-tail chain coupling may occur, resulting in the formation of free DBUs. The liberated DBU can re-initiate the chain growth, resulting in reduced polymer molecular weights.

Table 2.1. DBU-mediated polymerization of Bu-NCA in THF with different initial monomer to initiator ratios ($[M]_0$: $[DBU]_0$) [a]

Entry number	$[M]_0$: $[DBU]_0$	$[M]_0$ [b] (M)	M_n (theor.) [c] (kg·mol^{-1})	Time (h) [a]	M_n (SEC) [d] (kg·mol^{-1})	PDI [d]
1	25:1	0.4	2.9	4	3.5	1.08
2	50:1	0.4	5.8	8	5.9	1.10
3	75:1	0.4	8.6	12	8.4	1.02
4	100:1	0.4	11.4	16	9.7	1.05
5	150:1	0.4	17.1	24	14.1	1.08
6	200:1	0.4	22.7	32	18.4	1.08
7	400:1	0.4	45.4	64	32.4	1.04
8	25:1	0.8	2.9	2	3.8	1.12
9	50:1	0.8	5.7	4	5.7	1.10
10	100:1	0.8	11.4	8	9.5	1.06
11	200:1	0.8	22.7	16	16.6	1.02
12	400:1	0.8	45.4	32	19.3	1.11
13	50:1	1.6	5.7	1	4.6	1.07
14	100:1	1.6	11.4	2	8.5	1.04
15	200:1	1.6	22.7	4	15.2	1.02
16	400:1	1.6	45.4	8	26.5	1.03

[a.] All reactions were conducted in 50 ℃ THF for different duration (1- 64 h) to reach complete conversions; [b] the initial monomer concentration; [c.] the theoretical polymer molecular weight is calculated using the initial monomer to DBU ratio ($[M]_0$: $[I]_0$) assuming a single-site initiation by DBU and complete conversions; [d.] experimental polymer molecular weights were obtained by SEC-MALS-DRI method (DMF/0.1M LiBr, 25 ℃) with a measured dn/dc=0.0797(9) mL·g^{-1}.

Alternatively, residual nucleophilic impurity such as H_2O can also initiate the polymerization, giving rise to reduced polymer M_ns than theoretical values, consistent with the MALDI-TOF MS results suggesting the presence of PNBGs comprised of one carboxylic end-group and one secondary amino end-group in low apparent content. Controlled experiments

showed that while H_2O can initiate the polymerization of Bu-NCA under the standard polymerization conditions (*i.e.*, $[M]_0$: $[H_2O]_0$= 50:1, THF, 50 ℃), the initiation is significantly slower than that by other nucleophilic initiators (*e.g.*, primary amine or DBU). This is supported by the much longer reaction time to reach complete monomer consumption and the significantly higher polymer molecular weight of the resulting PNBG when water is the initiator than when primary amine or DBU are used as initiators. It was also noted that polymerization conducted at higher initial monomer concentration ($[M]_0$= 0.8 or 1.6 M) and initial monomer to initiator ratio ($[M]_0$: $[DBU]_0$= 400:1) (Entry 12 and 16, Table 2.1) yielded PNBG polymers whose M_n deviate more significantly from the theoretical value than that from the lower initial monomer concentration (Entry 7, Table 2.1). The origin for the deviation is presently unclear.

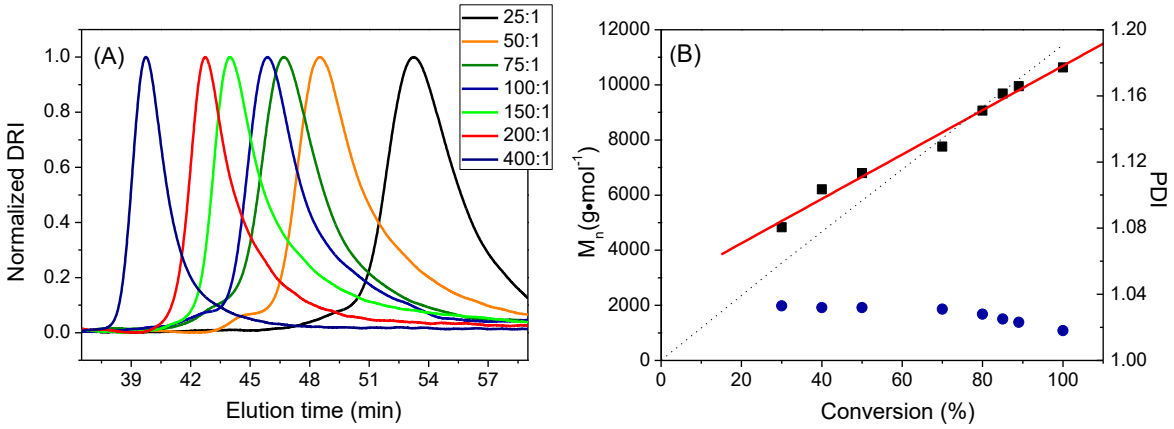

Figure 2.1. (A) Representative normalized SEC chromatograms of PNBG obtained at varying initial monomer to initiator ratios (Entry 1-7, Table 2.1). (B) Plots of experimental M_n (■) and PDI (●) versus conversion of DBU-mediated polymerization of Bu-NCA ($[M]_0$: $[I]_0$= 100:1, $[M]_0$= 0.4 M, 50°C, THF), the linear fit of the M_n versus conversion plot (—) (R^2 = 0.98) and theoretical trend line of a living polymerization (···).

The polymer molecular weight was found to increase linearly with conversion during the DBU-mediated polymerization of Bu-NCA in THF (Figure 2.1 (B)). The polymer molecular weight distribution also remains narrow PDI (PDI= 1.02-1.12) throughout the polymerization. However, the M_n versus conversion plot does not go through the (0,0) origin, suggesting that the

rate of initiation is either comparable to or slower than that of the propagation in the polymerization. ^{1}H NMR analyses of the polymerization reaction mixtures upon reaching quantitative conversion revealed the absence of any free DBU initiators, suggesting that all DBUs ultimately became incorporated into the polymer chains through initiation.

Solvent effect on the M_n and PDI control of the polymerization was investigated by conducting DBU-mediated polymerizations of Bu-NCA with various initial monomer to DBU ratios in a less polar solvent (toluene) and a more polar solvent (DMF) relative to THF. In toluene, the DBU-mediated polymerization of Bu-NCA exhibited a similar level of control over M_n and PDI as those conducted in THF (Table S2.1). By contrast, polymerization of Bu-NCA in DMF under identical conditions produced only low molecular weight PNBGs in the 0.5- 4.3 kg·mol^{-1} albeit with narrow molecular distribution (PDI= 1.04-1.11) (Entry 5-9, Table S2.1). We attributed this to the competitive intramolecular backbiting by transamidation relative to chain propagation in DMF. The liberated DBU can re-initiate chain propagation, leading to high monomer conversion but low polymer molecular weight. This is supported by MALDI-TOF MS analysis of the resulting polymers, which consist of mainly cyclic PNBGs without DBU attached and minor cyclic PNBGs having one DBU moiety attached.

2.3.2 Kinetic study of DBU-mediated polymerization of Bu-NCA

We investigated the polymerization kinetics by conducting the DBU-mediated polymerization of Bu-NCA in toluene-d_8 at 50 ℃ with a constant initial monomer concentration ($[M]_0$= 0.15 M) and varying initial monomer to initiator ratios ($[M]_0$: $[DBU]_0$= 25:1-150:1, Figure 2.2 (A)). The plot of ln($[M]_0$:[M]) versus time for all reactions can be linearly fitted quite well, indicating that the polymerization is first-order dependent on the monomer concentration. The slope of the linear fits afforded the observed polymerization rate constants (k_{obs}) at different DBU

loading. The plot of k_{obs} versus the initial DBU concentration (Figure 2.2 (B)) can also be linearly fitted, indicating that the polymerization is also first-order dependent on the initiator concentration with a second-order propagating rate constant (k_p) of 5.05 ± 0.09 $M^{-1} \cdot min^{-1}$. A close inspection of the ln([M]$_0$: [M]) versus time plots revealed a slightly concaved shape at the initial stage of the reactions, suggesting the initiation rate is either comparable to or slower than the rate of propagation. Thus, the k_p obtained by the above kinetic analysis is somewhat approximate. To determine the relative initiation and propagation rate, a kinetic model that describes a living polymerization with slow initiation relative to propagation was further used to analyze the conversion versus reaction time plot for a selected polymerization ([M]$_0$: [DBU]$_0$ = 150:1, 50 ℃, toluene-d_8).[180] The plot of the concentration of consumed monomers ([M]$_p$) within the initial 25% conversion versus time exhibits good linearity (Figure 2.2 (C)). The model fitting of the kinetic data yields an initiation rate constant (k_i= 3.22 ± 1.29 $M^{-1} \cdot min^{-1}$) that is nearly identical to the propagation rate constant (k_p= 2.38 ± 0.03 $M^{-1} \cdot min^{-1}$). To further validate these rate constants, plot of conversion versus time up to 80 % conversion was also fitted using the kinetic model (Figure 2.2 (D)), which gives the propagation rate constant of k_p = 2.36 ± 0.07 $M^{-1} \cdot min^{-1}$ on par with the k_p obtained by fitting the [M]$_p$ versus time plot in the initial 25% conversion range (Figure 2.2 (B)). As a result, the kinetic study suggests that the DBU-mediated polymerization of Bu-NCA undergoes the initiation event that is comparable in rate relative to propagation. The propagation rate is slightly faster than that of the previously studied ZROP of Bu-NCA using NHC initiators (k_p =1.53 ± 0.10 $M^{-1} \cdot min^{-1}$).[70] The difference in the propagation rate constant in the two systems can be attributed to the difference of counter-ion effect in the zwitterionic propagating intermediates (Scheme 2.1). DBU moieties on the cyclic zwitterionic propagating intermediate is less sterically demanding than the NHC moieties, thereby allowing for slightly faster addition of

the monomer to the zwitterionic chain ends and a faster propagation rate in the former than the latter.

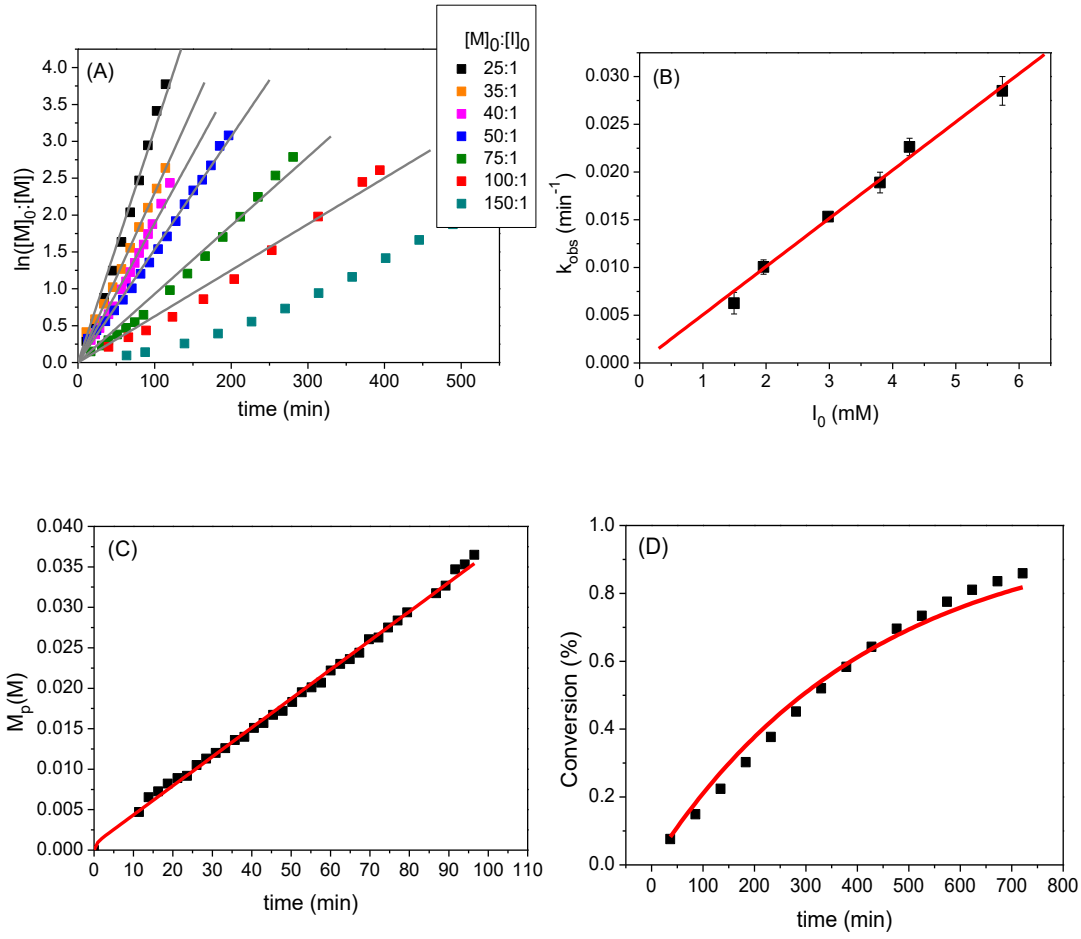

Figure 2.2. (A) Plots of ln([M]$_0$:[M]) versus time for DBU-mediated polymerization of Bu-NCA in toluene-d$_8$ at 50 ºC and the linear fitting of the data (—); (B) plot of observed polymerization rate constants (k_{obs}) versus the initial DBU concentration and the linear fitting of the data (—) (R^2 = 0.998); (C) plot of concentration of polymerized Bu-NCA ([M]$_p$) versus reaction time of DBU-mediated polymerization within the first 25% conversion ([M]$_0$=0.15 M and 50 ℃ in toluene-d$_8$); (D) plot of conversion of DBU-mediated polymerization of Bu-NCA versus reaction time of DBU-mediated polymerization of Bu-NCA up to 80% conversion. The red lines in C and D are the fitting of the data (C: R^2 = 0.997; D: R^2 = 0.983) using a kinetic model describing a living polymerization with slow initiation relative to propagation.

2.3.3 Chain extension experiment

An important feature of controlled polymerization is the living characteristic of the propagating intermediates, allowing for chain extension with additional monomers. Two chain

extension experiments were conducted using two PNBG macroinitiators with different chain length (DP= 25 and 200) prepared by the DBU-mediated polymerization of Bu-NCA. Additional Bu-NCA ($[M]_0$: $[PNBG]_0$=65:1 and 350:1) was introduced into the $PNDG_{25}$ and $PNDG_{200}$ macroinitiators respectively. Both reactions (in 50 ℃ THF) were allowed to reach a complete conversion. SEC analysis of the PNBG polymers after the reaction revealed a single peak with low PDI (Table 2.2) at a shorter elution time relative to the PNBG macroinitiator precursor (Figure S2.3), confirming the success of the chain extension and the living characteristic of the PNBG precursors. While PNBG produced by DBU-mediated polymerization of Bu-NCA can be further enchained, the control of the resulting polymer chain length appears to be dependent on the polymer molecular weight range. For example, chain extension produces PNBG polymers whose molecular weight agrees reasonably well with the theoretical values based on efficient initiation by the PNBG macroinitiators at the low PNBG molecular range (DP < 100, Table 2.2, Entry 1). At the high MW range (DP > 100), the MW of the resulting polymer is substantially lower than the theoretical value after the chain extension, suggesting the presence of competing side reactions.

Table 2.2. Chain extension polymerization from DBU-terminated PNBG macroinitiators[a]

Entry number	Experiment	$[M]_0$:$[I]_0$	M_n (theor.) (kg·mol^{-1})	M_n (SEC) [b] (kg·mol^{-1})	PDI [b]
1	Before Chain Ext.	25	3.0	3.0	1.10
	After Chain Ext.	90	10.2	9.2	1.02
2	Before Chain Ext.	200	22.7	17.2	1.05
	After Chain Ext.	550	62.3	37.4	1.10

[a.] All polymerization reactions were allowed to reach complete conversion; [b.] the measured M_n and PDI were obtained by the SEC-MALS-DRI method (DMF/0.1 M LiBr, 25°C) with a measured dn/dc=0.0797 (9) mL·g^{-1}.

Scheme 2.2. End-group treatment of DBU-PNBG$_{25}$ with AcCl.

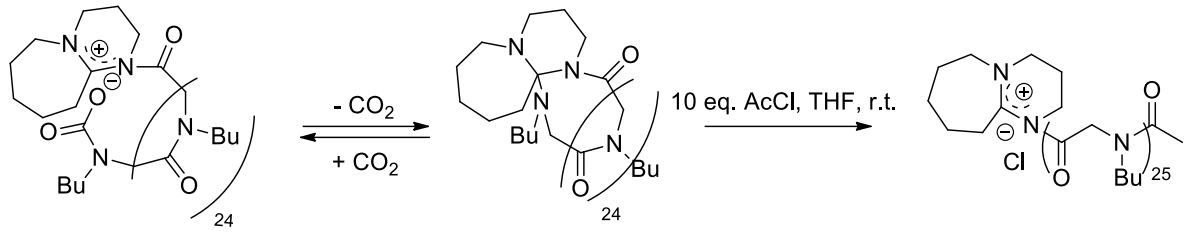

2.3.4 Architecture assessment

It was reported before that NHC-mediated ZROP of Bu-NCA undergoes a spirocyclic/zwitterionic propagating intermediate, so the cyclic polypeptoids can be converted into linear counterparts by end-group treatment using acetyl chloride (AcCl).[181] If DBU-mediated ROP of Bu-NCA monomers follows the similar chain propagating mechanism, it is conceivable that cyclic polypeptoids can also be produced through this pathway, and the linear counterparts of DBU-PNBGs can be obtained by AcCl-treatment as well. To test this hypothesis, a PNBG 25-mer was synthesized by DBU-mediated polymerization of Bu-NCA monomers and then treated with AcCl in excess at room temperature for 1 h in THF (Scheme 2.2). The PNBG sample was then purified by precipitation in hexane (a bad solvent) and dried under vacuum to remove residual AcCl. The ^{1}H NMR analysis of the resulting polymers indicated the successful attachment of acetyl group to the PNBG polymers, evidenced by the appearance of acetyl proton at 2.1 ppm and the downfield shift of methylene protons of the DBU moieties (f) from 2.8 to 3.0 ppm due to the positive charge generated at the adjacent carbon (Figure S2.4). End-group analysis by MALDI-TOF MS (Figure S2.5) also revealed that the major set of mass ions corresponds to the positively charged DBU-PNBGs end-capped with acetyl groups, in agreement with the ^{1}H NMR result. Minor sets of mass ions observed in MALDI-TOF MS spectrum correspond to unreacted DBU-PNBGs and water-initiated DBU-PNBGs end-capped with acetyl groups. M_n values of DBU-PNBG$_{25}$ and AcCl-treated DBU-PNBG$_{25}$ were obtained from MALDI-TOF-MS analysis too. The

M_n of DBU-PNBG$_{25}$ is 2683 g mol^{-1} (PDI= 1.05), which is slightly smaller than the M_n of the sample after AcCl-treatment (2704 g mol^{-1}, PDI= 1.06). SEC analysis of DBU-PNBG and the resulting polymer after AcCl treatment (Figure 2.3) revealed that the latter exhibits a shorter elution time relative to the former, suggesting a larger hydrodynamic volume of the latter than the former sample. This is consistent with the proposed architectural change of cyclic DBU-PNBGs into the linear analogs. The low molecular weight shoulder in the acetyl end-capped PNBGs is attributed to the unreacted DBU-PNBG precursors.

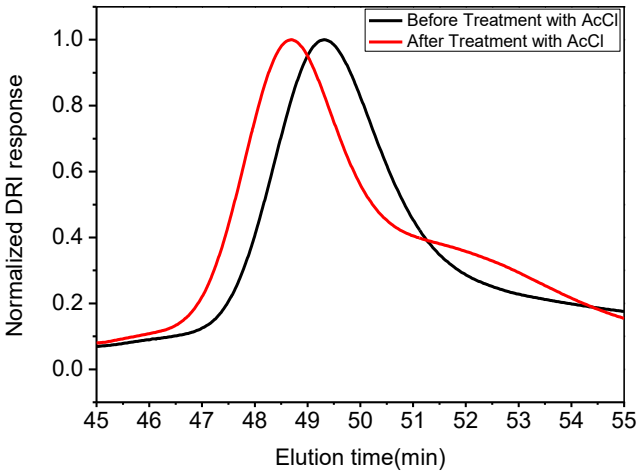

Figure 2.3. SEC chromatograms of DBU-PNBG$_{25}$ and AcCl-treated DBU-PNBG$_{25}$ in 0.01M LiBr/DMF.

2.3.5 Investigation of the initiation event

To gain insights into the initiation step of the DBU-mediated polymerization of R-NCAs, DBU and Bu-NCA in a 1:1 stoichiometric ratio was allowed to react in THF at 50 ℃ for 2 h. ^{1}H NMR analysis revealed the complete disappearance of the reactants. The product was isolated as a brownish solid by precipitation in hexane.

The resulting product was analyzed by ESI-MS (electrospray ionization mass spectrometry) in positive ionization mode. Two molecular species whose mass are consistent with cyclic trimeric or tetrameric *N*-butyl glycine *N*-carboxyanhydride species are observed in the ESI-MS spectrum

(Figure S2.6). This agrees with the kinetic analysis, which revealed an initiation step that is comparable in rate to propagation. This makes isolation of initiating species challenging. Apart from these two species, a third molecular ion consistent with the protonated DBU is also present in the ESI-MS spectrum. The species observed in ESI-MS analysis differ from what was observed in the MALDI-TOF MS analysis of a low molecular PNBG (DP= 25) obtained from DBU-mediated polymerization of Bu-NCA where the major molecular ions are due to the cyclic PNBGs bearing one DBU moiety. The discrepancy may arise from the difference in MS conditions: electrospray ionization can cause elimination of the initiating moieties (*i.e*, DBU in this study) from the cyclic zwitterionic polymeric species as previously demonstrated in the detailed MS studies of cyclic PNBG polymers obtained from NHC-mediated ZROP of Bu-NCAs.[179]

FT-IR (Fourier transform infrared spectroscopy) analysis of the species obtained from the 1:1 molar ratio reaction of DBU and Bu-NCA further confirms the formation of zwitterionic species in the initiation event (Figure S2.7). The peak at 1572 cm^{-1} is due to the carbonyl stretch of the carbamate group at the chain end,[70, 182, 183] which is consistent with the molecular ions observed by the ESI-MS analysis of the reaction mixture. The peak at 1684 cm^{-1} is due to the amide carbonyl group of the PNBG backbone. The amide peak that is immediate adjacent to the cationic DBU moiety is blue-shifted to at 1755 cm^{-1} presumably due to the inductive effect of the cationic DBU moiety. The peak at 1646 cm^{-1} and 1613 cm^{-1} are due to C= N stretching mode of the positively charged DBU-moiety and the unreacted DBU, respectively.[184, 185] As a comparison, the FTIR spectrum of the species obtained from the reaction of benzyl amine ($BnNH_2$) and Bu-NCA in a 1:1 molar ratio exhibits only one carbonyl peak (1680 cm^{-1}) which is due to the amide carbonyl of the linear PBNG backbone, clearly indicating a different initiation and propagation mechanism from that of the DBU-mediated polymerization of Bu-NCA.

It is proposed that DBU initiates the polymerization by nucleophilic ring-opening addition of Bu-NCA at the 5-carbonyl position to form the zwitterionic initiating species **1** (Scheme 2.3). The chain propagation ensues by Bu-NCA monomer addition at the carboxylate end of **1** to form the intermediate species **2**. The carboxylic-carbamic anhydride linkages in **2** is thermally labile and readily undergoes intramolecular decarboxylation to yield **3**, which has been observed spectroscopically in the early studies of small model compounds.[186, 187] Species **3** can undergo decarboxylation to form **4**, which is observed in the MALDI-TOF MS analysis.

Scheme 2.3. Proposed initiation and propagation mechanism of DBU-mediated ZROP of R-NCA monomers.

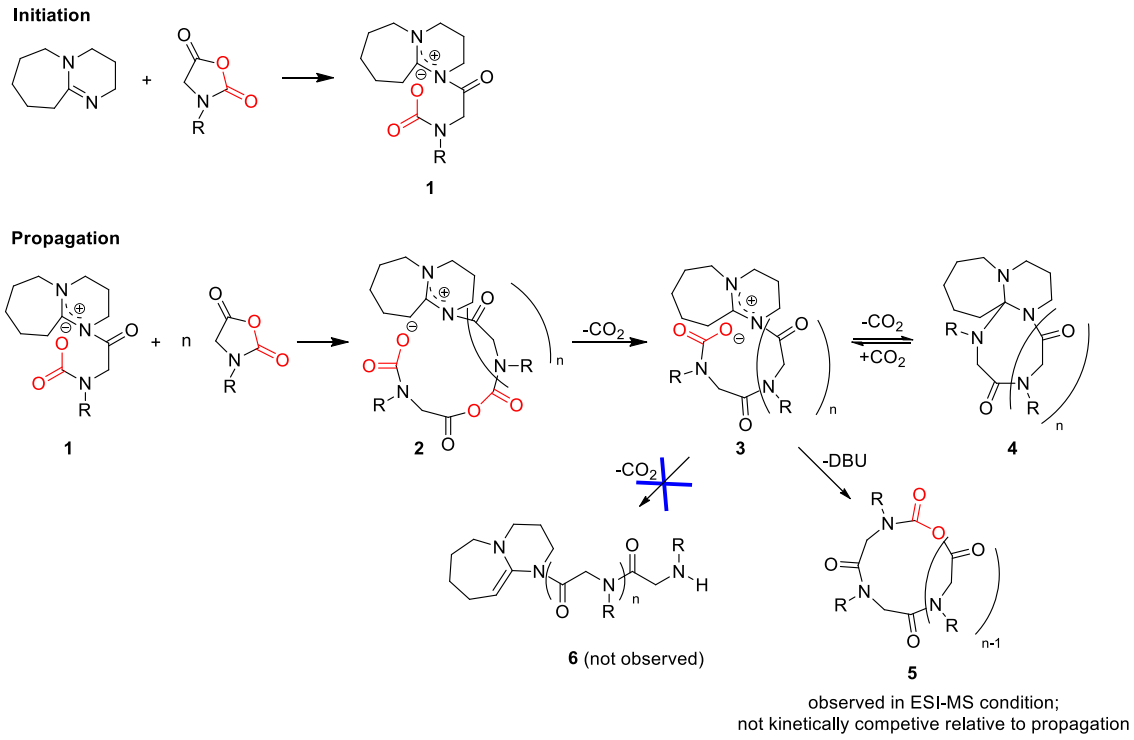

We propose that the decarboxylation is reversible, allowing **4** to regain CO_2 to form **3**, from which monomer addition and chain propagation ensue. This is consistent with the living polymerization characteristics of the DBU-mediated polymerization of Bu-NCA. The formation of species **5** presumably from macrocyclizaion of **3** is supported by the ESI MS analysis. Its

formation is not kinetically competitive relative to monomer addition, thus giving rise to the controlled polymerization behavior. Furthermore, the methylene proton on the cationic DBU end-group that is adjacent to the positively charged carbon is sufficiently acidic to be deprotonated by anionic alkoxide, as shown in a previous study of DBU-mediated zwitterionic polymerization of lactide, resulting in the formation of linear polylactide impurities.[177] In this study, we do not observe the deprotonation of the methylene protons in the DBU end-group based on the ^{1}H NMR analysis of the 1:1 reaction of Bu-NCA and DBU. This is presumably due to the reduced basicity of the anionic carbamate chain end relative to the alkoxide species.

2.4 Conclusions

DBU-mediated ZROPs of Bu-NCAs exhibit characteristics of a controlled polymerization, producing poly (*N*-butyl glycine) with controlled polymer molecular weight (3.5- 32.4 kg·mol^{-1}) and narrow molecular weight distribution (PDI < 1.2). The growing chain ends can be successfully extended with additional monomers, making it useful for the block copolypeptoid synthesis. Kinetic studies revealed that the initiation rate is comparable to the propagation rate in the DBU-mediated ZROP of Bu-NCA, which is slightly faster than previously reported NHC-mediated ZROP. This is presumably due to the steric difference of the DBU versus the NHC moieties in the respective cyclic zwitterionic propagating intermediate. End-group analysis using ^{1}H NMR and MALDI-TOF-MS and SEC analysis of DBU-PNBGs and AcCl-treated DBU-PNBGs suggested the cyclic architecture of DBU-PNBGs. The enhanced robustness and availability of DBU relative to NHCs and the excellent control over the polymerization of R-NCA makes the reported method an attractive route towards well-defined cyclic polypeptoids with tunable ring sizes.

2.5 Supplementary Data

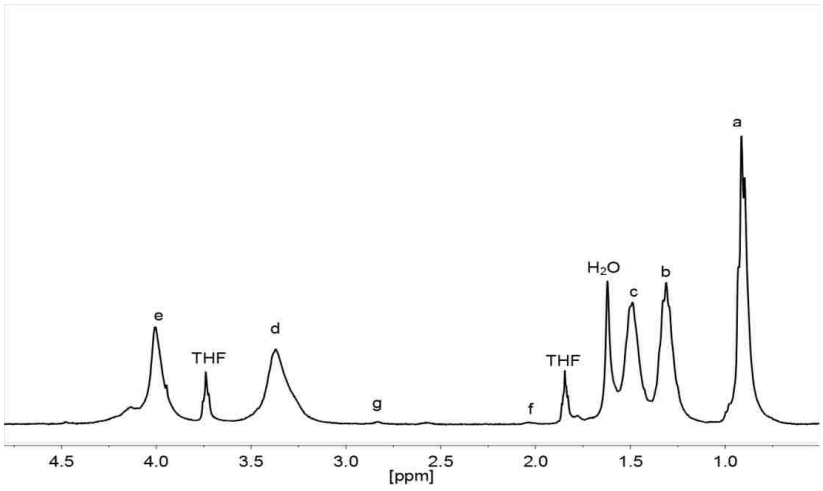

Figure S2.1. A representative ^{1}H NMR spectrum of the low molecular weight poly(*N*-butyl-glycine) in $CDCl_3$ obtained by the DBU-mediated polymerization of Bu-NCA.

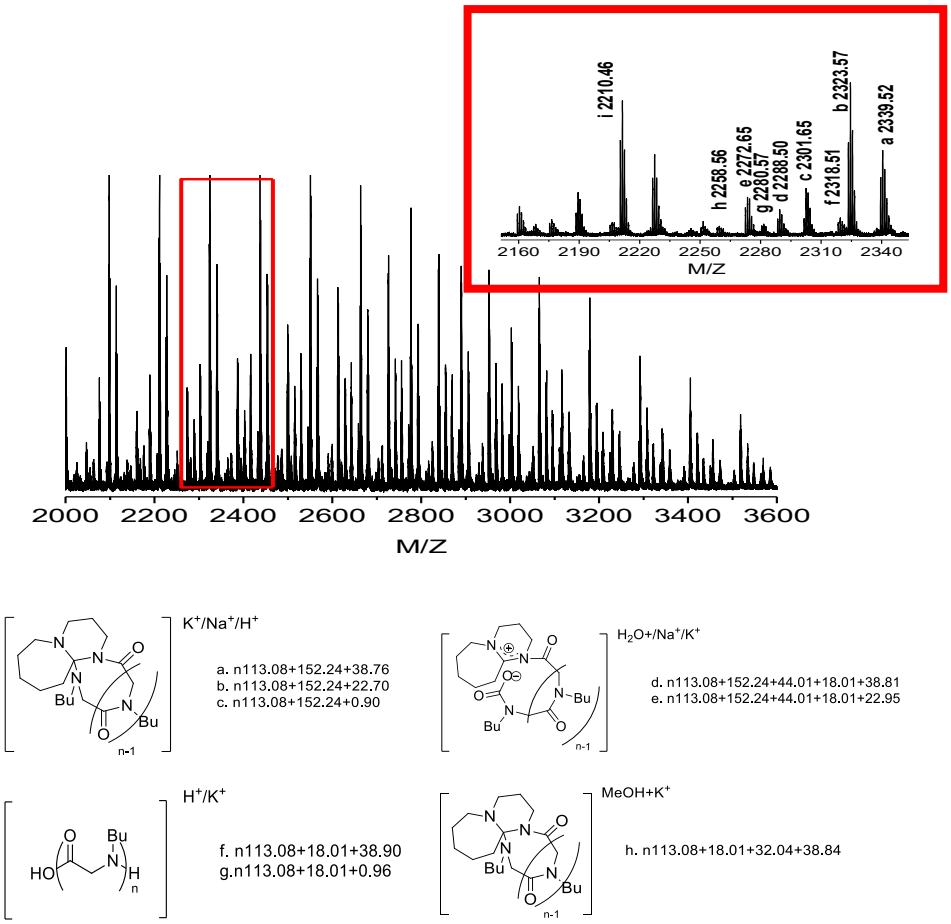

Figure S2.2. A representative MALDI-TOF MS spectrum of low molecular weight PNBG obtained by DBU-mediated polymerization of Bu-NCA in 50 ℃ THF.

Table S2.1. DBU-mediated polymerization of Bu-NCA in different solvents at varying initial monomer to initiator ratios.

Entry	$[M]_0$: $[I]_0$	Solvent	M_n (Theor.) ($kg \cdot mol^{-1}$)	M_n[b] (SEC) ($kg \cdot mol^{-1}$)	PDI[b]
1	50:1	Toluene	5.8	5.7	1.08
2	100:1	Toluene	11.4	9.7	1.01
3	200:1	Toluene	22.7	15.4	1.05
4	400:1	Toluene	45.4	28.4	1.04
5	5:1	DMF	0.7	0.5[c]	1.04[c]
6	10:1	DMF	1.3	1.9	1.06
7	50:1	DMF	5.7	3.0	1.07
8	100:1	DMF	11.4	4.3	1.11
9	200:1	DMF	22.7	3.3	1.04

[a.] All the polymerizations were conducted at 0.4M initial monomer concentration at 50 ℃. All the polymerizations were allowed to reach complete conversion based on ^1H NMR spectroscopy; [b.] M_n values were obtained by SEC-MALS-DRI system in DMF/0.1M LiBr with a measured dn/dc=0.0797(9) $mL \cdot g^{-1}$;[c] M_n and PDI were obtained by ESI-MS analysis.

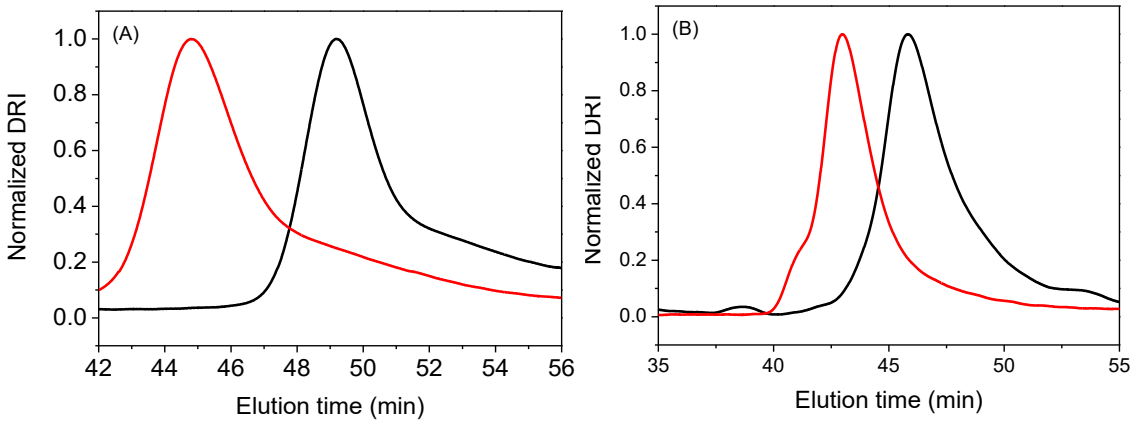

Figure S2.3. SEC chromatograms of PNBG obtained by DBU-mediated polymerization of Bu-NCA and chain-extension experiment in THF at 50 ℃. (A)The PNBG precursor was synthesized with $[M]_0$: $[I]_0$=25:1(—) and the chain-extension experiment was conducted with $[M]_0$: $[I]_0$=65:1(—). (B) The PNBG precursor was synthesized with $[M]_0$: $[I]_0$=200:1(—) and the chain-extension experiment was conducted with $[M]_0$: $[I]_0$=350:1

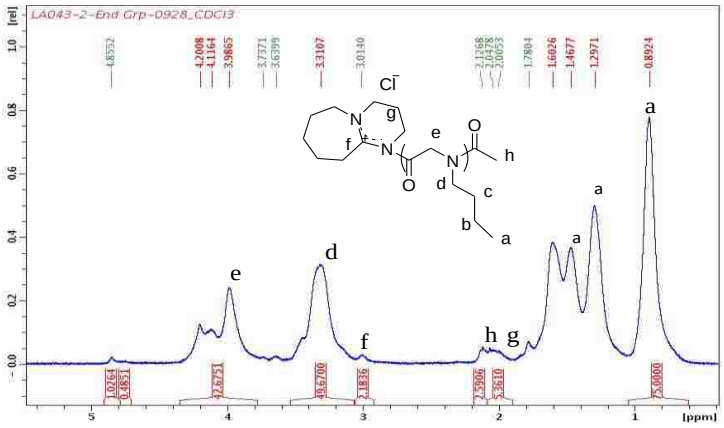

Figure S2.4. A representative ^{1}HNMR spectrum of DBU-PNBG$_{25}$ obtained after AcCl treatment in $CDCl_3$.

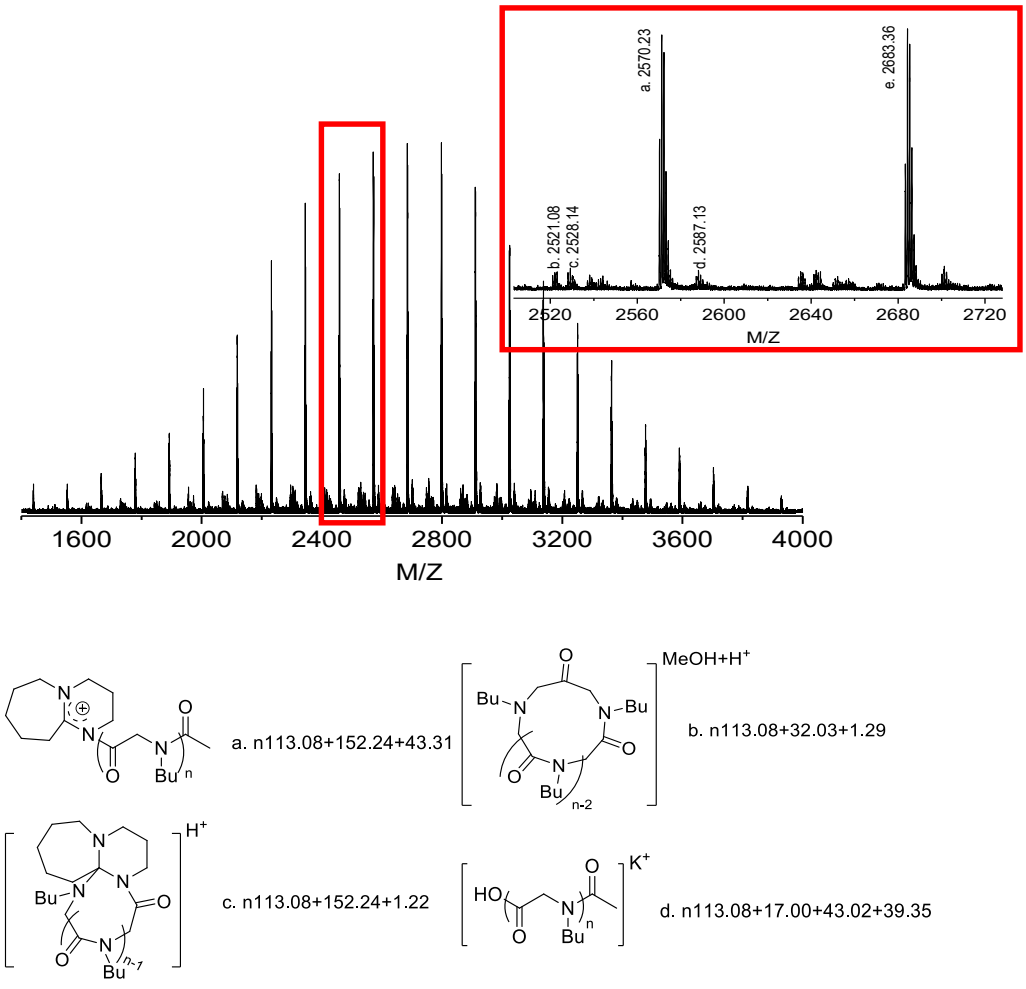

Figure S2.5. A representative MALDI-TOF MS spectrum of AcCl-treated PNBG$_{25}$.

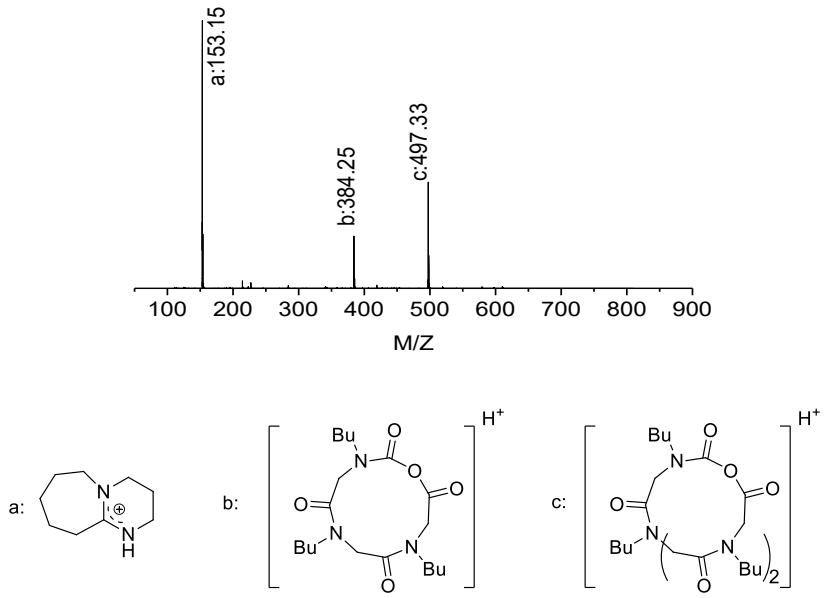

Figure S2.6. A representative ESI-MS spectrum of the product obtained from the reaction of DBU and Bu-NCA in a 1:1 initial molar ratio. The ESI-MS experiment is conducted in positive mode.

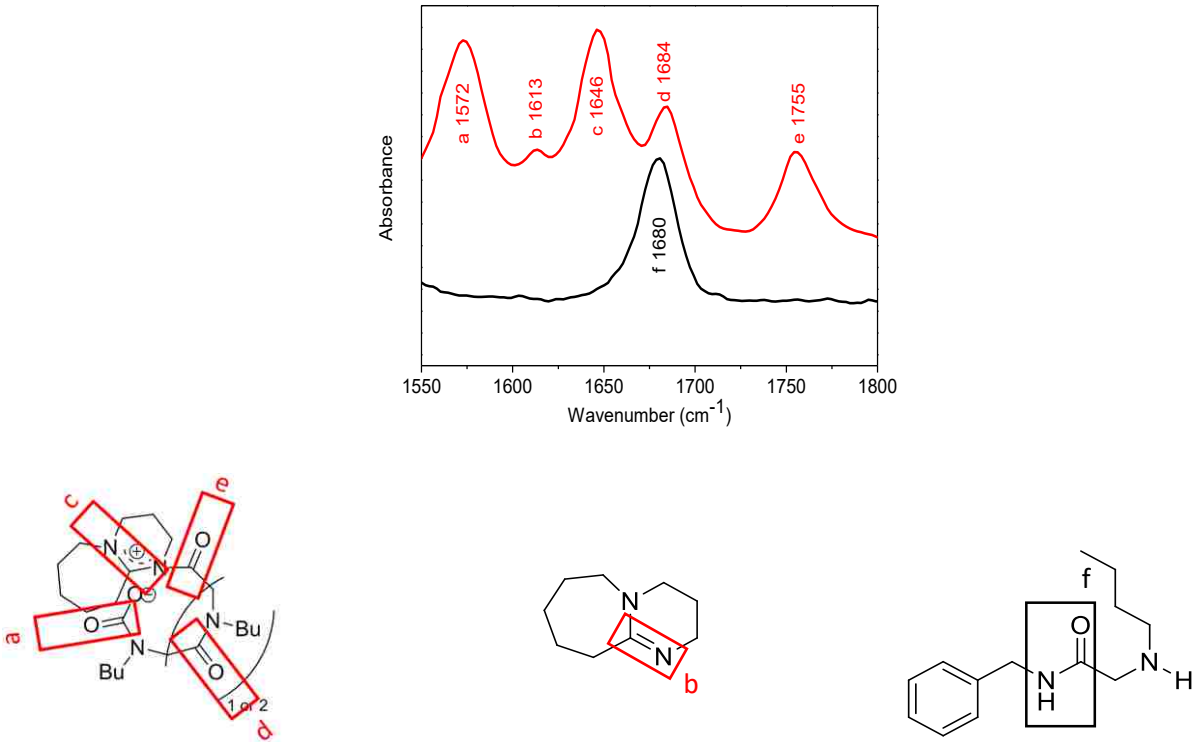

Figure S2.7. Representative FTIR spectra of the product in THF solution obtained from the reaction of Bu-NCA with DBU (—) or $BnNH_2$ (—) in a 1:1 initial molar ratio, respectively.

Chapter 3. Solution Aggregation of Cyclic Polypeptoids Obtained from Amidine-Mediated Zwitterionic Ring-Opening Polymerization

3.1 Introduction

Polypeptoids, also known as poly (*N*-substituted glycine)s, are synthetic mimics of polypeptides. Because of the *N*-substitution, polypeptoids lack main chain chirality and hydrogen bonding interaction, in contrast to polypeptides. The *N*-substitution results in enhanced proteolytic stability,[157] thermo-processability[14, 16, 69] and conformational tunability (via side chain structure) relative to polypeptides,[7, 64, 158, 159] making polypeptoids good candidates for biomedical applications.

Cyclic polymers have attracted considerable attention because of their distinctive physical properties as compared to the linear counterparts. The unique topology imparts many interesting properties to cyclic polymers such as lower intrinsic viscosity,[35, 36] higher glass transition and melting temperatures,[14, 37] faster crystallization rates, [166] and wider phase transition windows,[40] relative to the linear counterparts. Regarding biomedical applications, it was found that the ring architecture of cyclic polymers facilitates higher gene transfection efficiency than their linear counterparts do presumably due to their more compact conformations and stronger interactions with DNA molecules.[47] To date, several synthetic approaches have been developed for the cyclic polymers, including interfacial condensation,[48] ring-expansion metathesis polymerization,[36, 54] end-to-end polymer cyclization,[49, 167] and zwitterionic ring-opening polymerization (ZROP).[60-62, 67] The progressed synthetic approaches allow for the production of more sophisticated ring-structures which may endow the resulting materials with more exciting properties. It was reported recently that eight-shaped amphiphilic copolymers,[55] multi-complex cyclic polymers,[56, 57] and stereocomplex of cyclic syndiotactic Poly(methyl methacrylate) (PMMA) and linear isotactic PMMA [58] can be synthesized.

Polymers with long side chains are usually considered bottlebrush polymers. The unique bottlebrush structure imparts distinctive properties to the polymers. It was demonstrated that linear bottlebrush polymers can be used for water lubrication.[188] The water lubricant can be acquired by absorption of the bottlebrush backbones onto the substrate and the immobilization of large amount of water within the densely packed side chains. When the two substrates are compressed against each other, the inter-chain repulsion and the immobilized solvent lead to the formation of a cushioning layer, and therefore the friction between the two slides can be drastically alleviated. Besides absorbing small molecules, the densely grafted long side chains can also provide stealth properties to the polymer backbones and the grafted small molecules. Grubbs *et al.* synthesized stimuli-responsive linear bottlebrush polymers based on the polynorbornene backbones grafted with long PEG side chains and drug molecules. Cytotoxicity study revealed that upon UV-triggered drug release the cytotoxicity of bottlebrush polymers is similar to that of small drug molecules but much higher than that of the drug-bottlebrush polymer complex without UV-responsive behaviors, indicating excellent stealth properties of the linear bottlebrush polymers.[189] Rzayev *et al.* have demonstrated that linear bottlebrush polymers with amphiphilic side chains can be used to produce tubular nanotubes by first cross-linking the shell of the linearly aligned bottlebrush polymers and then degrading the inner core. [190] In addition to the structural advantages, synthesis of linear bottlebrush polymers is another pathway to access high molecular weight polymers in the condition that the homopolymers with only limited molecular weight can be produced. For example, Thelakkat *et al.* synthesized the linear bottlebrushes (poly(3-hexylthiophene) (P3HT)) that have much higher molecular weight than the traditional homo-P3HT. It was found that the thin films formed by the high molecular weight bottlebrush P3HT have better thermal stability than those formed by the linear counterparts without sacrificing electronic

properties.[191] As to surface patterning bottlebrush polymers have also exhibited the potential to fabricate advanced biosensors because the three dimensional layers formed by vertically immobilized brush polymers allow more small molecules to penetrate through and provide more binding sites than the self-assembled monolayers do, resulting in high sensitivity.[192]

Combination of the two unique architectures into one single molecule results in a new polymer structure- cyclic bottlebrush, which could open a new scope of material science and engineering, and the potential unique properties of this new type of polymers are waiting to be explored. Our group has demonstrated that cyclic bottlebrush polypeptoids can be synthesized by zwitterionic ring-opening polymerization (ZROP) using NHC as an initiator. However, NHCs are air and moisture sensitive, and they used to be the only organo-catalyst to produce cyclic polypeptoids. In an effort to identify and characterize alternative organo-catalysts that can outperform NHCs in mediating the ZROP of R-NCAs to produce cyclic polypeptoids in a controlled manner and ideally more robust than NHCs, we investigated the 1, 8-diazabicycloundec-7-ene (DBU), a bicyclic amidine. DBU is widely used to catalyze esterification of carboxylic acids[193] and controlled ROPs of lactides, lactones, and cyclic phosphoesters. It was recently demonstrated that DBU can initiate the ZROP of lactide to produce a mixture of cyclic and linear polylactides.[177] Our previous study (Chapter 2) suggested that well-defined cyclic polypeptoids can be synthesized by DBU-mediated ZROP of R-NCAs. In this study, cyclic bottlebrush polypeptoids were synthesized through the new pathway with the new initiator.

Analysis of cyclic polymers can be divided into qualitative analysis and quantitative analysis. For cyclic Gaussian chains, their intrinsic viscosity, hydrodynamic radius or radius of gyration have a specific theoretical relationship relative to the linear counterpart. This relationship is called characteristics ratio. For example, it was reported that the ratio of the intrinsic viscosity

of cyclic and linear polystyrene (PS) in the θ conditions is close to 0.65.[194] By measuring the characteristics ratio of the polymers of interests versus the linear polymer analogs under θ conditions, one can determine whether the former polymers have cyclic architectures. When θ conditions are not met, this method provides only qualitative results for the architectural analysis. It was previously demonstrated that the atomic force microscopy (AFM) can be used to verify the polymer backbone architecture including cyclic backbone.[75-80] On the other hand, microscopic analysis and scattering analysis provide accurate dimensions of cyclic polymers. Especially when small angle x-ray scattering (SAXS) or small-angle neutron scattering (SANS) are used for the analysis, physical parameters including radius of gyration, persistence length, Kuhn length, *etc.* can usually be determined. For example, quantitative analysis of a worm-like chain (cyclic amylose tris(phenylcarbamate) (c-ATPC)) was conducted by fitting the Holtzer plots obtained by SAXS measurement using the scattering function of a cylindrical rigid ring. It revealed that the helix pitch per residue and the Kuhn segment length of the rigid rings are independent of the solvent, which is opposite to the linear analog, indicating that rigid cyclic polymers have different local conformation from linear polymers.[81] The SANS study on the absorption of cyclic poly ethylene glycol (PEG) onto silica particles has shown that cyclic PEG has higher absorption on silica nanoparticles than the linear analog does, but the thickness of the cyclic PEG layer decreases as the molecular weight increases, which is very different from the linear PEG.[82] More similar analyses of cyclic polymers have been conducted, and deeper and deeper understanding of cyclic polymers will be obtained through these studies.

A good platform has already been established for the analysis of any type of cyclic polymers. As the synthetic approaches become developed, cyclic bottlebrush polypeptoids can be produced readily in a controlled manner. The densely grafted side chains can rigidify the cyclic

backbone conformation, making microscopic analysis of cyclic polymers possible in both dry state and solution phase. On the other hand, the progressed analytical methods including SAXS or SANS are powerful tools for the characterization of cyclic polymers so that unique properties of the cyclic bottlebrush polypeptoids can be revealed.

The physical properties and solution behaviors of the emerging cyclic bottlebrush polypeptoids were systematically investigated using advanced analytical methods and computational simulation.

3.2 Materials and Methods

3.2.1 Materials

1, 8-Diazabicycloundec-7-ene (DBU) was dried over CaH_2 and purified by distillation before use. All solvents used were purchased from Sigma-Aldrich and purified by passing through alumina columns under argon (Innovative Technology, Inc.) and stored under a nitrogen atmosphere. All other chemicals were purchased from Sigma-Aldrich and used as received. *N*-butyl *N*-carboxyanhydride (Bu-NCA), *N*-propargyl *N*-carboxyanhydride (Pg-NCA), and *N*-methyl *N*-carboxyanhydride (Me-NCA) were synthesized by following reported procedures.[75, 195, 196] All cyclic and linear poly (*N*-methyl glycine) (*c*-PNMG and *l*-PNMG) bearing a DBU initiating moiety as well as the cyclic and linear bottlebrush copolymers bearing poly(*N*-butyl glycine-*r*-*N*-propargyl glycine) backbone and polyethylene glycol (PEG, Mn= 550 $g \cdot mol^{-1}$) and butyl sidechains (in a 6:1 molar ratio) [*c*-P(NBG-*r*-NPgG)-*g*-PEG and *l*-P(NBG-*r*-NPgG)-*g*-PEG] were synthesized and characterized by using previously reported procedures. [195, 197]

3.2.2 Instrumentation

^{1}H NMR spectra were recorded on a Bruker AV-400 spectrometer and chemical shifts in parts per million were referenced to protio impurities in the deuterated solvent (*e.g.*, $CDCl_3$).

Size exclusion chromatography (SEC) analyses were performed using an Agilent 1200 system (Gastorr GT-14 degasser, Agilent 1200 series isocratic pump, and auto sampler) equipped with three Phenomenex 5 μm, 300×7.8 mm columns (100Å, 1000Å and linear), a Wyatt DAWN EOS multi-angle light scattering (MALS) detector (GaAs 30 mW laser at 690 nm) and a Wyatt Optilab rEX differential refractive index (DRI) detector with a 690 nm light source. DMF with 0.1 M LiBr was used as eluent at a 0.5 $mL \cdot min^{-1}$ flow rate. The column and detector operate at room temperature. Wyatt Astra 6.0 was used to process all SEC data. The polymer molecular weight (M_n) and polydispersity index (PDI) were obtained by Zimm-model fit of MALS-DRI data. SEC samples were prepared by dissolving the polymer (5 mg) in DMF/ 0.1 M LiBr (1 mL) with slight heating followed by filtration through a PTFE syringe filter (pore size = 0.2 μm).

3.2.3 AFM sample preparation and experimental procedures

Polymer samples were diluted in chloroform (0.002 $mg \cdot mL^{-1}$) and a 5 μL drop was placed on freshly cleaved mica (0001). The sample was dried and stored in ambient conditions before AFM analysis. A model 5420 scanning probe microscope from Keysight Technologies (Santa Rosa, CA) was used to characterize samples of the cyclic polymers using tapping-mode AFM. Images were acquired using Picoview v1.12. Probes from App Nano (ACTA, Mountain View, CA) were used for tapping-mode AFM studies in ambient conditions. The tip was driven to oscillate at a driving frequency of 315 kHz. Images were processed using Gwyddion, an open source software which is supported by the Czech Metrology Institute.[178]

3.2.4 SANS sample preparation and experimental procedures

The small-angle neutron scattering (SANS) experiments were performed at GP-SANS HFIR[198] and EQ-SANS SNS[199] in Oak Ridge National Laboratory. The scattering profile of the cyclic bottlebrush polymer was measured at GP-SANS using a fixed wavelength at 4.75 Å

combined with the sample-to-detector distance (SDD) at 1 m and 12 m, and the corresponding *Q* range is 0.006 - 0.6 $Å^{-1}$. The scattering profile of the linear bottlebrush polymer was measured at EQ-SANS using the wavelength band of $10.11 < \lambda < 13.2$ Å at SDD = 4 m and $4.24 < \lambda < 7.71$ Å at 1.3 m, with the *Q* range covering 0.005 - 0.5 $Å^{-1}$. The polymers were directly dissolved in deuterated methanol at 1wt% concentration at room temperature. The solution samples were loaded into 1 mm thick banjo cells for measurements and the transmissions of all the samples are larger than 0.9. The scattering intensities were scaled to absolute values on the basis of standard sample measurements (Al-4 and Porsil B).

3.2.5 Cryo-Transmission electron microscopy

Sample preparation for Cryo-TEM was carried out on FEI Vitrobot. The bottlebrush copolymer was dissolved in methanol (7mg/ml) and then passed through a 0.45um filter. 12ul of the solution was applied to a 300-mesh lacey carbon grid. Excess liquid was blotted by filter papers for 2 seconds to form a thin film prior to vitrification in liquid ethane. The sample was then loaded to a cryo specimen holder and imaged on S1032_FEI G2 F30 Tecnai TEM operated at 100kV.

3.2.6 Dynamic light scattering (DLS)

DLS was conducted on a Brookhaven Instrument (90 Plus PALS) whose laser wavelength is 640 nm. DLS data was collected by BIC particle solutions software (version 3.1) and analyzed using CONTIN method. Lognormal median diameters which were reported as effective diameters and averaged size distributions were obtained from triplicate measurements. DBU-initiated PNMGs (targeted DP= 100) and DBU-initiated bottlebrush polypeptoids (targeted DP= 100) and their relevant linear analogs obtained by AcCl-treatment were dissolved in MeOH (6.0- 6.3 mg/mL) and then filtered through hydrophilic filters (0.1 μm) into clean cuvettes before DLS measurement.

3.2.7 Representative procedures for the synthesis of the cyclic bottlebrush polypeptoids

In a glovebox, *N*-propargyl NCA (50 mg, 0.36 mmol) and *N*-butyl NCA (13 mg, 0.07 mmol) were dissolved in anhydrous THF (510 μL THF). A stock solution of DBU in THF (24 uL, 2.25 μmol, 95.2 mM) was added to the reaction flask. The flask was sealed and stirred at 50 ^{o}C for 2 d. The polymerization was terminated by adding cold hexane (8 mL). The precipitated polymer was isolated by decantation and dried under vacuum (36 mg, 83% yield). ^{1}H NMR (in $CDCl_3$, ppm): 0.91 (C*H*3CH2CH2CH2-), 1.31 (CH3C*H*2CH2CH2-), 1.50 (CH3CH2C*H*2CH2-), 2.38 (C*H*CCH2-), 3.39 (CH3CH2CH2C*H*2N-), 4.64- 3.90 (-COC*H*2N-).

Inside a glovebox, the previously synthesized D-PNBG$_{41}$-*r*-PNPgG$_{177}$ (15.6 mg, $[propargyl]_0$ = 0.13 mmol) and PEG-N_3 (105 mg, 0.18 mmol, M_n = 550 g mol^{-1}, PDI = 1.05, $[N_3]_0$: $[propargyl]_0$ = 1.4:1) were both dissolved in CH_2Cl_2 (910 μL). A measured volume of CH_2Cl_2 stock solution containing CuBr/PMDETA (175 μL, 0.043 mmol, 247 mM, $[Cu]_0$: $[PMDETA]_0$: $[propargyl]_0$ = 33:33:100) was added to the solution which was then stirred at 40 ^{o}C for 3 h. The reaction mixture was then passed through a silica column. The solvent of the filtrate was then pumped off under vacuum to yield the cyclic bottlebrush polymers. (36 mg, 40% yield, grafting density: 81%). ^{1}H NMR (in $CDCl_3$, ppm): 3.63 (-CH2C*H*2O-), 3.88 (-NC*H*2CH2O-), 4.55 (-CC*H*2N-, -NC*H*2CO-), 7.97 (-NC*H*C-).

3.2.8 Representative procedures for the synthesis of the cyclic PNMG bearing a DBU initiating moiety (*D*-PNMG)

In a glovebox, Me-NCA (33 mg, 0.29 mmol) was dissolved in anhydrous acetonitrile (700 μL). A stock solution of DBU in THF (30 μL, 2.9 μmol, 95.2 mM) was added to the reaction flask. The flask was sealed and stirred at room temperature for 16 h. The polymerization was terminated by adding hexanes (8 mL). The precipitated polymer was isolated by decantation and dried under vacuum (18 mg, 86% yield). ^{1}H NMR (in $CDCl_3$, ppm): 1.06- 0.76 (C*H*3CH2-), 1.58-1.21 (-

CH2C*H*2CH2-, CH3C*H*2-), 2.62- 2.25 (-CC*H*), 3.51-3.20 (-CH2C*H*2N-), 4.64- 3.90 (-CC*H*2N-, -NC*H*2CO-, -NC*H*2CO-).

3.2.9 Representative procedures for the synthesis of the linear PNMG bearing a DBU initiating moiety (*D*-PNMG-Ac)

In a glovebox, the cyclic PNMG bearing a DBU initiating moiety (10 mg, 87 μmol) was dissolved in anhydrous THF (250 μL). A THF stock solution of acetyl chloride (AcCl) (156 μL, 0.14 μmol, 0.9 M) was added to the reaction flask. The flask was sealed and stirred at room temperature for 16 h. The volatiles were removed under vacuum to yield the final polymer product (10 mg, 100 % yield).

3.2.10 Computations

Computational studies were carried out on the linear and the cyclic counterpart of the $PNMG_{100}$ polypeptoid in methanol solvent. In the cyclic case, the two ends are represented by oppositely charged groups, namely $-O^-$ and $-NH_3^+$ whereas in the linear case the end groups are –OH and $-NH_3^+$. While these are not the end groups in the actual peptoids, they carry the appropriate charge and hence present a reasonable representation of the relevant end group interactions.

3.2.10.1 Molecular dynamics (MD) simulations

The initial configuration of each of the two types of peptoid oligomers were generated by connecting 100 monomers with methyl side chains. The OPLSAA force field parameters for the Lennard-Jones and intramolecular interactions were used along with the partial charges determined from electronic structure calculations for the peptoids.[200, 201] The same dihedral parameters that are used in the peptide case for the planarity of the amide bond was used here. The OPLS based force-field has previously been used successfully to model peptoids.[202] *l*-$PNMG_{100}$ with a chloride counter anion and *c*-$PNMG_{100}$ were each solvated, using the packmol program,[203] in a periodic cubic box of length 100 Å consisting of the same number (11500) of methanol (represented using

the united atom OPLS force-field)[200] molecules in each case. The system was equilibrated for 10 ns, with a 1 fs timestep, in the canonical (NVT) ensemble at a temperature of 300 K using a Nose-Hoover thermostat. Production runs of 40 ns each were then carried out for each peptoid system.

3.2.10.2 Umbrella sampling (US) simulations

Umbrella sampling along with the weighted histogram analysis method (WHAM) was used to determine the free energy profile or potential of mean force (PMF) of bringing the center of mass of one *c*-PNMG$_{100}$ monomer to the center of mass of another *c*-PNMG$_{100}$ monomer in methanol solution.[204, 205] The simulation box was generated by replicating the previous C-PNMG$_{100}$ system along the x-axis. A total of sixteen umbrella sampling windows ranging from an inter-polymer distance of 50 Å to 22 Å were carried out, each with a ten nanosecond equilibration run followed by a 40 ns production run. A harmonic force constant of 3.0 kcal/mol was used for the 22 and 23 Å windows and 2.0 kcal/mol for the remaining windows. All simulations, both canonical and umbrella sampling, were carried using the LAMMPS package.[206]

3.3 Results and Discussion

Our group has demonstrated that cyclic bottlebrush polypeptoids can be synthesized via first NHC-mediated ZROP of NCA monomers and subsequent side chain conjugation with PEG (M_n= 550 g·mol^{-1}, PEG550). However, NHC is moisture-sensitive and expensive. DBU which is moisture-stable and commercially available was developed as a candidate of NHC. Because our previous study has suggested that cyclic polypeptoids can be produced by DBU-mediated ZROP of R-NCA monomers in a controlled manner, polypeptoid backbones of the cyclic bottlebrushes for this study were synthesized using DBU as the initiator. Hydrodynamic volume and end-group structures of cyclic polypeptoids were analyzed before in order to obtain the architectural information, but the request for further important physical parameters cannot be satisfied. In this

study SANS analysis was performed on both cyclic bottlebrush polypeptoids and cyclic poly(*N*-methyl glycine)s (*c*-PNMGs) in MeOH to investigate their physical parameters and solution behaviors. Compared to cyclic polypeptoids with simple side chains, the densely grafted side chains of cyclic bottlebrush polypeptoids may rigidify the backbone conformation, so quantitative analysis was conducted to probe the dimensions of cyclic bottlebrush polypeptoids in both dry state and solution phase by a combination of AFM, TEM, and SANS methods.

3.3.1 Synthesis of cyclic bottlebrush polypeptoids

A series of cyclic random copolypeptoids was synthesized by DBU-mediated ZROP of a mixture of Pg-NCA monomers and Bu-NCA monomers in THF (Scheme 3.1). The targeted composition of the resulting poly (*N*-propargyl glycine)-*r*-poly (*N*-butyl glycine)s [P(NPgG-*r*-NBG)s has the molar ratio of Pg segment and Bu segment equal to 6:1, and the targeted repeating units are 105, 210, 315, and 420. The choice of a random copolypeptoid backbone is based on our previous observation that the poly(*N*-propargyl glycine) homopolymers (PNPgG) have strong tendency to aggregate in solution,[75] and the incorporation of Bu segments onto the polypeptoid backbone spaces out Pg segments, so P(NPgG-r-NBG) copolypeptoids can afford higher PEG grafting efficiency.

Scheme 3.1. A representative synthetic approach of cyclic P(NPgG-*r*-NBG)

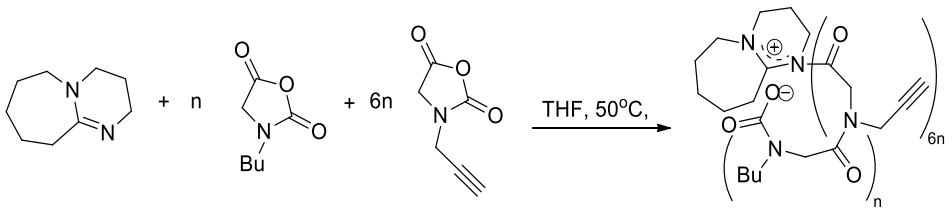

The percent yield of each random copolypeptoid is from 80% to 90%.[1]H NMR spectra of all the random copolymers showed characteristic peaks a, b and c corresponding to the methylene and methyl protons of the butyl side chains. Characteristic peak h relevant to the alkyne protons

of the propargyl side chains was also observed (Figure S3.1). End-group analysis using ^{1}H NMR revealed that the actual compositions of each random copolypeptoid are DBU-P(NBG$_{22}$-*r*-NPgG$_{118}$) [*D*-P(NBG$_{22}$-*r*-NPgG$_{118}$)], DBU-P(NBG$_{34}$-*r*-NPgG$_{190}$) [*D*-P(NBG$_{34}$-*r*-NPgG$_{190}$)], DBU-P(NBG$_{73}$-*r*-NPgG$_{302}$) [*D*-P(NBG$_{73}$-*r*-NPgG$_{302}$)], and DBU-P(NBG$_{91}$-*r*-NPgG$_{389}$) [*D*-P(NBG$_{91}$-*r*-NPgG$_{389}$)], respectively. Among all the random copolypeptoids, the one with targeted DP= 210 is large enough to be probed by microscopic analysis and short enough to be synthesized effectively, so another batch of DBU-initiated copolypeptoids (targeted DP= 210) was synthesized and used as a model sample for atomic force microscopic analysis (AFM) and Kratky plot analysis. The sample's actual composition determined by ^{1}H NMR is DBU-P(NBG$_{41}$-*r*-NPgG$_{177}$) [*D*-P(NBG$_{41}$-*r*-NPgG$_{177}$)] which is slightly different from the first batch. The SEC traces of all the random copolypeptoids have shoulders of varying intensity at low elution time, indicating the existence of high molecular weight species. We tentatively attribute them to the aggregates of the random copolypeptoids.[75] The poly(*N*-propargyl glycine)s have strong tendency to aggregate in solution. Despite of the large aggregates and broad molecular weight distribution, the SEC traces of random copolypeptoids shift to high molecular weight as the targeted DP increases (Figure S3.2 (A)). The random copolypeptoids were then reacted with N_3-terminated PEG550 via Copper (I)-mediated alkyne-azido cycloaddition (CuAAC) click chemistry to yield cyclic bottlebrush polypeptoids with the same repeating units and compositions to their precursors (Scheme 3.2).

The CuAAC click chemistry was performed in DCM at 40 ^{o}C for 2 h. Excess PEG550 and CuBr catalysts were removed by passing the crude reaction solution through a silica-gel packed mini column to yield the pure cyclic bottlebrush polypeptoids (Percent Yield= 40 to 60 %).

Scheme 3.2. Synthesis of cyclic bottlebrush polypeptoids via CuAAC click chemistry.

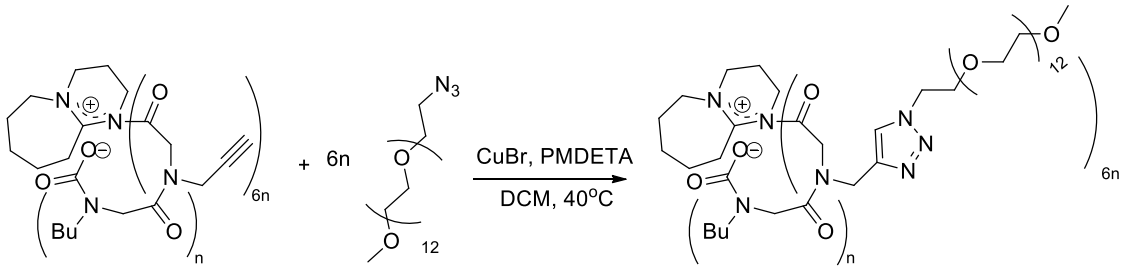

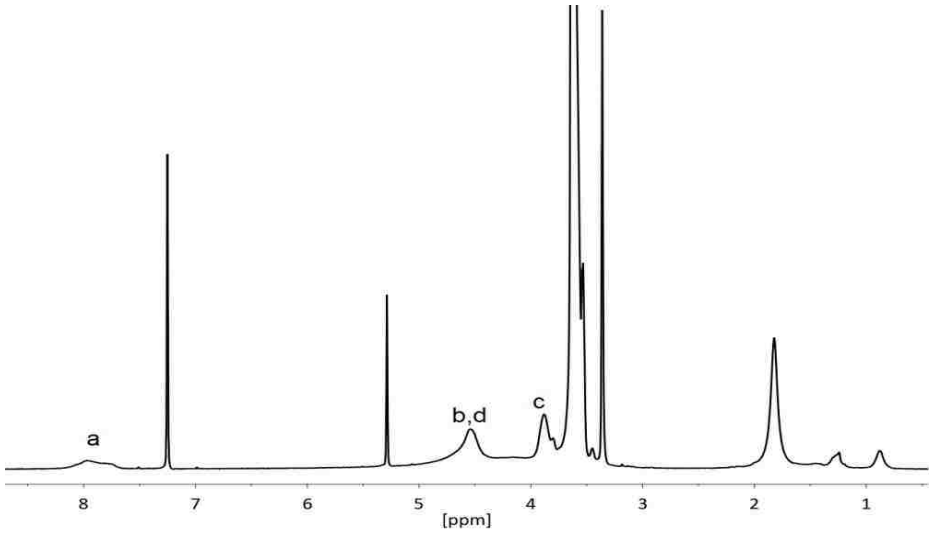

Figure 3.1. A representative ^{1}H NMR spectrum of the cyclic bottlebrush polymer DBU-P(NBG$_{41}$-*r*-NPgG$_{177}$)-*g*-(PEG550)$_{177}$.

100% grafting efficiency was observed by ^{1}H NMR spectra of all cyclic bottlebrush polypeptoids based on the disappearance of the alkyne peak at 2.3 ppm and the appearance of the triazole peak at 8.0 ppm (Figure 3.1). SEC analysis of the model random copolypeptoids [*D*-P(NBG$_{41}$-*r*-NPgG$_{177}$)] and the corresponding bottlebrush polypeptoids [*D*-P(NBG$_{41}$-*r*-NPgG$_{177}$)-g-(PEG550)$_{177}$] revealed a larger hydrodynamic volume after grafting with PEG550 (Figure 3.2). These combined results confirmed the successful synthesis of cyclic bottlebrush polypeptoids.

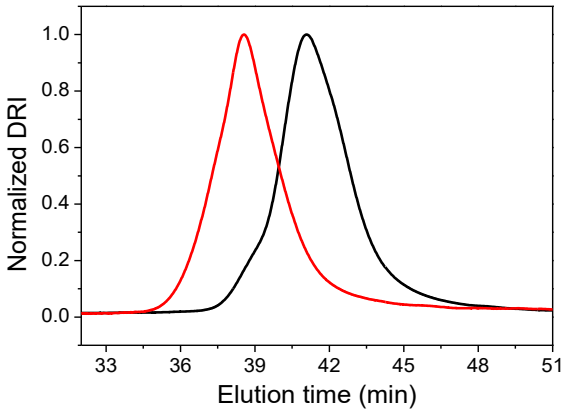

Figure 3.2. SEC chromatograms of DBU-P(NBG$_{41}$-*r*-NPgG$_{177}$)-*g*-(PEG550)$_{177}$ (—) and the DBU-P(NBG$_{41}$-*r*-NPgG$_{177}$) precursor (—).

Two linear analogs of each cyclic bottlebrush polypeptoids were synthesized. Linear analog 1 bottlebrush polypeptoids were prepared by treating the cyclic bottlebrush polypeptoids with excess amount of AcCl in DCM. Our previous study has shown that cyclic polypeptoids can be converted to linear counterparts by AcCl-treatment. Representative SEC traces of linear analog 1 polypeptoids are shown in Figure S3.3. Linear analog 2 bottlebrush polypeptoids were prepared by first ROP of a mixture of Pg-NCA monomers and Bu-NCA monomers using $BnNH_2$ as the initiator and subsequent side chain conjugation with PEG550. As the role of AcCl is only for end-capping the zwitterionic polypeptoids, the chain length and the composition of cyclic bottlebrush polypeptoids are not affected by the AcCl-treatment. The same characterizations of cyclic bottlebrush polypeptoids including ^{1}H NMR and SEC analysis were performed on linear analog 2 bottlebrush polypeptoids. The actual composition of the linear analog 2 determined by end-group analysis of ^{1}H NMR is *Bn*-P(NBG$_{33}$-*r*-NPgG$_{184}$)-*g*-(PEG550)$_{184}$.

In order to investigate the effects of the brush-like side chains on the properties of cyclic polypeptoids, a series of cyclic poly (*N*-methyl glycine)s (*D*-PNMG), the simplest polypeptoids with only methyl group as the side chains, was synthesized through DBU-mediated ZROP of Me-

NCA monomers (Scheme 3.3). The targeted DPs of *D*-PNMGs are 100, 200, 300, and 400, respectively. Formation of white precipitates to some extent during the polymerization in acetonitrile was observed, which might result in further aggregation. Especially for the polymerization with targeted DP= 400, it took the longest time to reach complete conversion, so it may have formed the largest aggregates. SEC analysis is consistent with our observations (Figure S3.2 (B)). It revealed that the SEC traces of *D*-PNMGs (targeted DP= 100 to 300) are single peaks with aggregates to some extent. The SEC trace of *D*-PNMGs (targeted DP= 400) has bi-modal distribution. The elution times of *D*-PNMGs are in the right sequence with respect to their targeted DP values.

Scheme 3.3. Synthesis of *D*-PNMG and the corresponding linear analog 1.

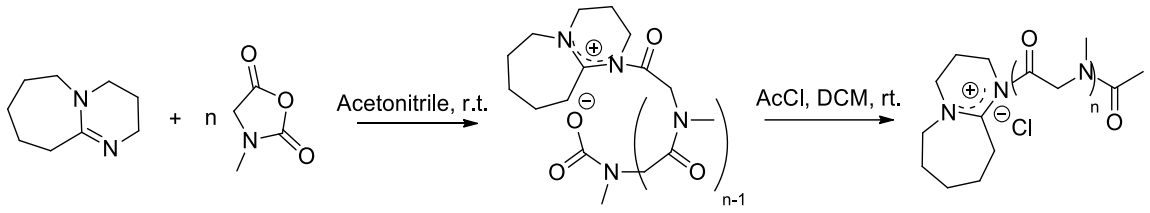

Table 3.1. The degree of polymerization (DP) values of cyclic polypeptoids

Targeted DP	*D*-PNMGs		Targeted DP	*D*-P(NBG-*r*-NPgG)-*g*-PEG cyclic bottlebrush polypeptoids	
	DP (SEC) [a]	PDI (SEC) [c]		DP (NMR) [b]	PDI (SEC) [c]
100	124	1.01	105	140	1.03
200	188	1.01	210	224	1.15
300	241	1.02	310	375	1.12
400	412	1.01	420	480	1.13

[a] DP was determined by SEC analysis using dn/dc = 0.0991 mL g^{-1} in 0.1 LiBr/DMF. [b.] DP was determined from end-group analysis using ^{1}H NMR. [c.] PDI is determined from SEC analysis.

Actual M_n values of *D*-PNMGs were obtained by SEC analysis with dn/dc= 0.0991 mL g^{-1}. Actual DP of each *D*-PNMG was then calculated based on the M_n of one single repeating unit. The DP results of both cyclic bottlebrush polypeptoids and cyclic PNMGs are summarized in table 3.1. The linear analog 1 PNMGs were obtained by AcCl-treatment of *D*-PNMGs (Scheme 3.3). The representative SEC traces of *D*-PNMG (targeted DP= 100) and linear analog 1 PNMG can be found in Figure S3.3. Linear analog 2 PNMGs were prepared by using $BnNH_2$ as the initiator to polymerize Me-NCA monomers. Targeted DPs of linear analog 2 PNMGs (*Bn*-PNMG) are 200 and 400, respectively, and SEC analysis revealed that the actual DPs of the *Bn*-PNMGs are 216 (PDI= 1.01) and 439 (PDI= 1.01), respectively.

3.3.2 AFM analysis

A dilute DCM solution of the cyclic bottlebrush polypeptoids (*D*-P(NBG_{41}-*r*-$NPgG_{177}$)-*g*-$(PEG550)_{177}$) was dried on a mica substrate under ambient conditions. The bottlebrush polypeptoids were characterized by taping-mode AFM. Samples of the cyclic bottlebrush polymers exhibited toroid structures with a relatively uniform distribution across the flat mica substrate (Figure 3.3). The diameter and width of the rings measured 61 ± 11 nm and 23 ± 9 nm, respectively (Figure S3.4). The dimensions measured with AFM are larger than the theoretically estimated diameter (d = 25 nm) and width (l = 9 nm) assuming a fully extended backbone and side chain structures. The discrepancy can be attributed to the effect of AFM tip-sample convolution.[207] For comparison, AFM analyses of the linear analog 1 and the linear analog 2 were also conducted.

Samples of the linear analog 1 bottlebrush polypeptoids (*D*-P(NBG_{41}-*r*-$NPgG_{177}$)-*g*-$(PEG550)_{177}$- Ac) exhibited mostly rod-like structures across the mica substrate with the lengths in the range from 200 nm to 500 nm (Figure 3.4 (A)), which are much longer than the estimated chain length, indicating aggregates of linear bottlebrush polypeptoids were formed.

Similarly, samples of the linear analog 2 bottlebrush polypeptoids (*Bn*-P(NBG$_{33}$-*r*-NPgG$_{184}$)-*g*-(PEG550)$_{184}$) were observed exclusively as rod-like structures with an average length and width of 208 ± 100 nm and 41 ± 12 nm, respectively (Figure 3.4 (B)). The theoretically estimated length and width of the linear analog 2 bottlebrush polypeptoid should be 78 nm and 9 nm, assuming a fully stretched polymer backbone and sidechains. This suggests that the rod structures are also likely the aggregates of the linear analog 2 bottlebrush polypeptoids. There is no toroid structures observed in any of the AFM images of the two linear analogs.

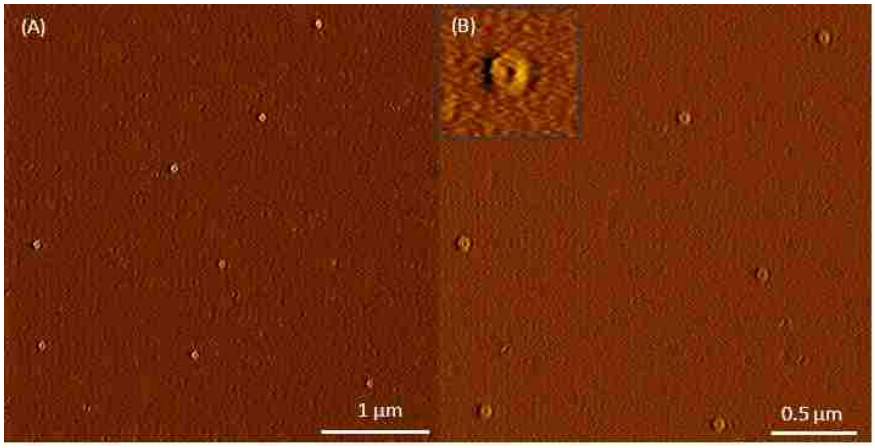

Figure 3.3. Toroid-shape structures of cyclic bottlebrush polypeptoids (*D*-P(NBG$_{41}$-*r*-NPgG$_{177}$)-*g*-(PEG550)$_{177}$) viewed in representative AFM amplitude images. (A) 4 × 4 µm^2, (B) 2.5 × 2.5 µm^2.

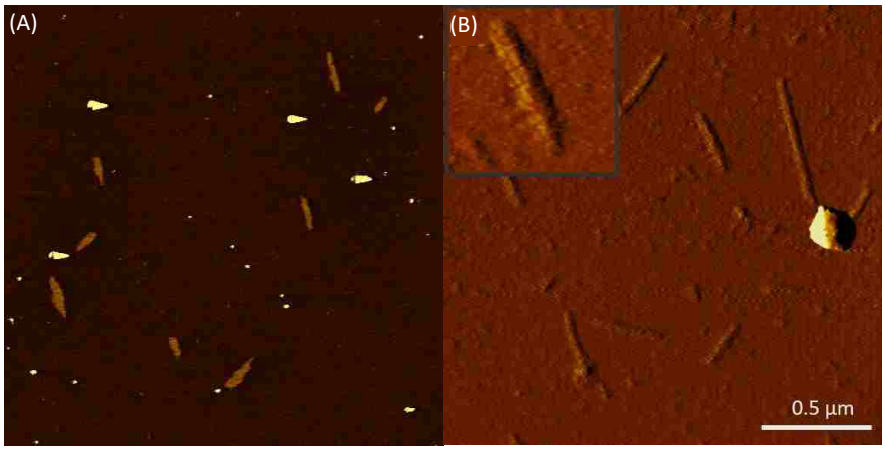

Figure 3.4. Linear bottlebrush polypeptoids viewed in representative AFM images. (A) *D*-P(NBG$_{41}$-*r*-NPgG$_{177}$)-*g*-(PEG550)$_{177}$-Ac, (B) *Bn*-P(NBG$_{33}$-*r*-NPgG$_{184}$)-*g*-(PEG550)$_{184}$.

3.3.3 Kratky plots

To further verify the cyclic architecture in solution, small angle neutron scattering (SANS) was conducted on dilute solutions of the cyclic and linear bottlebrush polypeptoid ensembles respectively in MeOH. The concentration of the solutions was kept in dilute regime (1 wt%) to ensure that the scattering data reflects the intramolecular conformation without interference from intermolecular interaction. To obtain the Kratky plots, the incoherent background, determined by fitting the high Q region of the scattering profile using a power function plus a constant, is subtracted from the original I(Q) before multiplying the square of momentum transfer (Q). The cyclic architecture can be identified by the pronounced peak at Q= 0.06 $Å^{-1}$ in the Kratky plot (red circle, Figure 3.5), which is attributed to the strong intramolecular correlation of the cyclic bottlebrush backbones.[208] Theoretically, the strong intramolecular correlation can also result from a dendrimer or a hyperbranched molecular architecture rather than a cyclic molecular architecture, so it is not possible to identify the cyclic architecture by only analyzing the Kratky plot of the cyclic bottlebrush polypeptoids. In order to exclude the possibility that the pronounced peak is due to other molecular architectures with strong intramolecular correlation, the linear analog 1 bottlebrush polypeptoids were analyzed by Kratky plot as well. For the specific zwitterionic cyclic polypeptoid backbones, it was shown that they can be converted into linear polymers after end-group treatment with AcCl, and thereby the intramolecular correlation of the linear analog 1 bottlebrush polypeptoids should be much reduced than that of the cyclic precursors. On the other hand, after end-group treatment, the dendrimer-like polymers or the hyperbranched polymers should still maintain the original architecture without compromising the intramolecular correlation. Kratky plot analysis revealed that the peak of the linear analog 1 bottlebrush polypeptoids is lower than the peak of their precursors (blue circle, Figure 3.5), which is consistent with our assumption

that the cyclic bottlebrush polypeptoids are present in the solution. The linear analog 2 bottlebrush polypeptoids have the least pronounced peak in Kratky plot (black circle, Figure 3.5). Considering that the side chain is PEG with M_n= 550 g mol^{-1}, the small bump in the Kratky plot of the linear analog 2 may be attributed to the weak intramolecular correlation of the PEG side chains. The peak of the linear analog 1 is higher than that of the linear analog 2. This implies an incomplete architectural conversion from cyclic bottlebrush polypeptoids to the linear analogs after AcCl-treatment, which is consistent with the results from our previous architecture study in Chapter 2. The peak of the linear analog 1 is attributed to the intramolecular correlation of the cyclic architecture of the residual cyclic bottlebrush polypeptoids and the PEG side chains.

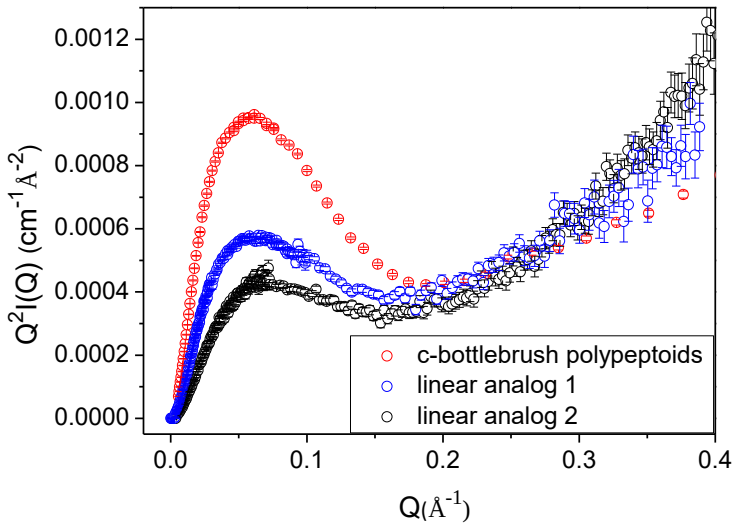

Figure 3.5. Kratky plots of cyclic bottlebrush polypeptoids [*D*-P(NBG$_{41}$-*r*-NPgG$_{177}$)-*g*-(PEG550)$_{177}$] (red circle: ○), the linear analog 1 [*D*-P(NBG$_{41}$-*r*-NPgG$_{177}$)-*g*-(PEG550)$_{177}$-Ac] (blue circle: ○), the linear analog 2 [*Bn*-P(NBG$_{33}$-*r*-NPgG$_{184}$)-*g*-(PEG550)$_{184}$] (black circle: ○).

3.3.4 Guinier analysis

Model-free Guinier analysis on the SANS profiles was performed for all the samples including cyclic bottlebrush polypeptoids, the linear analog 1 bottlebrush polypeptoids, the linear analog 2 bottlebrush polypeptoids, cyclic PNMGs, the linear analog 1 PNMGs, and the linear

analog 2 PNMGs. Their radii of gyration (R_g) were obtained by Guinier plot analysis, and all Guinier plots are shown in Figure (S3.5-S3.9). The Q range was selected with the criteria of $R_gQ_{max}<1$. The size of a cyclic polymer is expected to be smaller than its linear analog having the same contour length, resulting in a characteristic ratio ($R_{g,c}/R_{g,l}$) in the 0.5 (θ condition)- 0.72 range, due to their intrinsic topological difference.[209] Hence, it can be expected that R_g of the linear analog 1 polypeptoids and the linear analog 2 polypeptoids should be larger than the cyclic polypeptoids. However, in contradiction, the radii of gyration of the cyclic bottlebrush polypeptoids and the cyclic PNMGs are larger than their respective linear analog 1 polypeptoids (*D*-bottlebrush polypeptoid-Acs and *D*-PNMG-Acs) and linear analog 2 polypeptoids (*Bn*-bottlebrush polypeptoids and *Bn*-PNMGs) at all the characterized DP values (Figure 3.6). This suggested that the cyclic polypeptoids may not behave as individually solubilized molecules in solution and have formed small clusters, resulting in larger effective R_gs relative to their linear counterparts. As the cyclic polypeptoids contain oppositely charged chain ends, it is anticipated that the dipole-dipole interaction may provide the driving force for the cluster formation. By contrast, the linear analog 1 molecules only bear a positively charged chain end with a chloride counter-ion, and the linear analog 2 molecules have neutral chain ends. The absence of dipole-dipole interaction may preclude the cluster formation in solution for the linear polymers.

The effects of brush side chains on the properties of polypeptoids were further studied by fitting the measured SANS profiles of *D*-PNMGs and cyclic bottlebrush polypeptoids (both targeted DP= 100) with the model of cyclic ideal chains,[210] to obtain the structural information such as Kuhn length and the cross sectional radius. Two plots of cyclic PNMG and cyclic bottlebrush polypeptoid are shown in Figure 3.7, respectively.

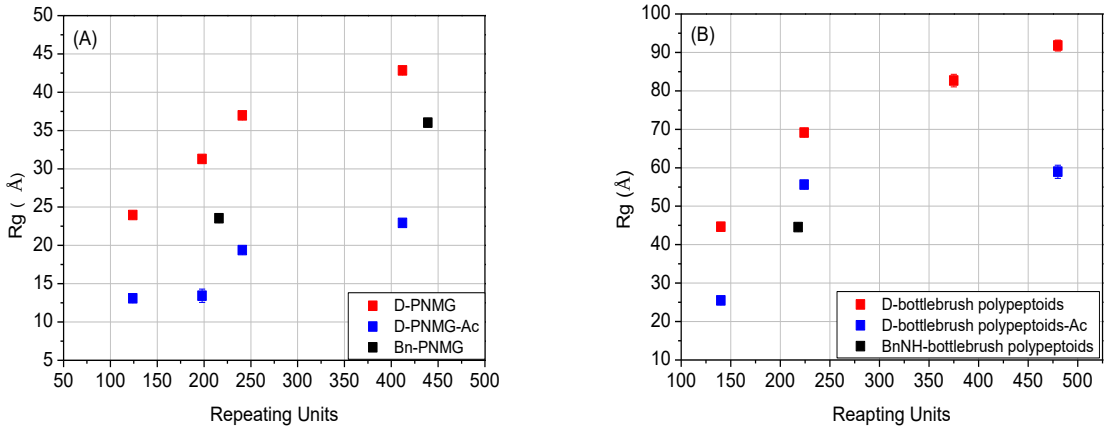

Figure 3.6. Plots of R_g vs. DP for *D*-PNMGs and their linear analogs (A) and *D*-bottlebrush polypeptoids and their linear analogs (B).

In the data fitting, the contour lengths were fixed based on the DP values characterized by SEC for *D*-PNMG (DP= 124, contour length= 518.3 Å) and NMR spectroscopy for the cyclic bottlebrush polypeptoid (DP= 140, contour length= 511 Å). The fitted Kuhn length is 5.9 Å and the cross sectional radius is 1.5 Å for the *D*-PNMGs, and 18.7 Å and 9.5 Å for the cyclic bottlebrush polypeptoids, respectively. The results are consistent with the observation for bottlebrush polymers that the attachment of brush side chains onto polymer backbones rigidifies the backbone conformation and largely increases the chain stiffness and cross-sectional radius. The results suggested that the cyclic bottlebrush polypeptoids may exist in methanol as a cyclic cylindrical chain with high stiffness. However, it can be seen that for both models, the model fittings deviate from the experimental data points, indicating that the system is not composed of cyclic ideal chains. Given the results of Guinier plot analysis of both cyclic polypeptoids and the linear analogs, the deviations could be due to cluster formation in solution. One can also note that the model fitting of *D*-PNMGs has more deviation at low q than the cyclic bottlebrush polypeptoids does, and this could be due to the solvent quality or large aggregation of molecules.

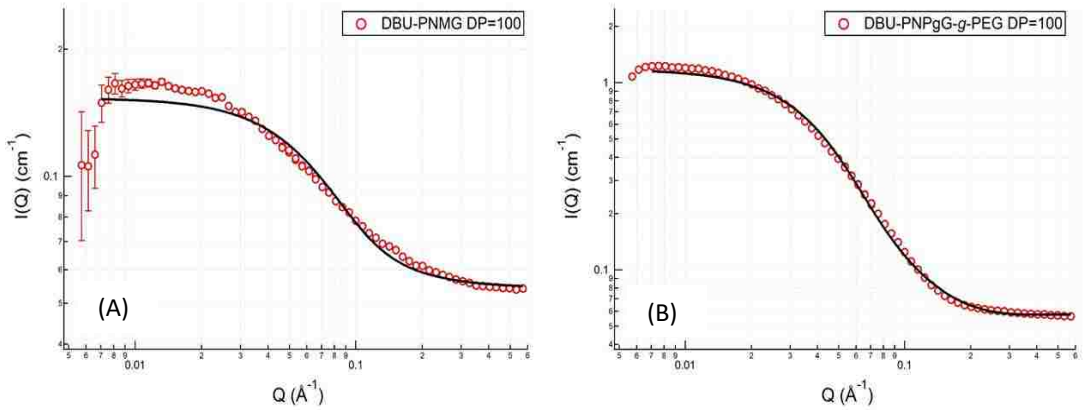

Figure 3.7. Representative SANS profiles of *D*-PNMGs (A) and cyclic bottlebrush polypeptoids (B) (both targeted DP= 100). The black solid line is the data fitting using cyclic Gaussian chain model.

3.3.5 DLS analysis

Size distributions of cyclic bottlebrush polypeptoids and *D*-PNMG (both targeted DP= 100) and their corresponding linear analog 1 polypeptoids were analyzed using dynamic light scattering (DLS) in MeOH (Figure 3.8). It was revealed that the hydrodynamic radius (R_h) of *D*-PNMGs in MeOH is 25.0 ± 0.5 Å (PDI= 0.14) and the R_h of the relevant linear analog 1 is 21.9 ± 0.1 Å (PDI= 0.12). The R_h of cyclic bottlebrush polypeptoids is 49.7 ± 0.3 Å (PDI= 0.11) and the R_h of its linear analog 1 is 44.1 ± 0.1 Å (PDI= 0.14). Both *D*-PNMGs and cyclic bottlebrush polypeptoids have larger sizes than their corresponding linear analog 1 polypeptoids, and the size of cyclic bottlebrush polypeptoids is much larger than that of *D*-PNMGs attributed to the incorporation of brush side chains. Shape factor ($\rho = R_g/R_h$) is usually used to estimate the shape of polymer chains in solution. When the theoretical value of ρ is 0.778, it indicates the presence of homogeneous hard spheres. When the value is between 0.778 and 0.816, it represents the presence of random-coil chains. The shape of ellipsoids is reflected when the ρ value lies in the range of 0.875 to 0.987.[211] The ρ values of the cyclic polypeptoids and their linear analog 1 polypeptoids were analyzed. It was found that the ρ value of cyclic bottlebrush polypeptoids is 0.897 and the ρ value of *D*-PNMGs is 0.956.

Although the size of cyclic bottlebrush polypeptoids is much larger than *D*-PNMGs in solution, it is suggested by their shape factors that both of them may adopt an ellipsoid shape in solution. In contrast, the ρ values of the linear analog 1 of the cyclic bottlebrush and the linear analog 1 of *D*-PNMGs are 0.576 and 0.594, respectively, indicating that the linear polypeptoids may adopt a random coil shape in solution. The different shapes in solution for the cyclic polypeptoids and the corresponding linear analogs could be due to the conformational differences of the polymer backbones or cluster formation of cyclic polypeptoids.

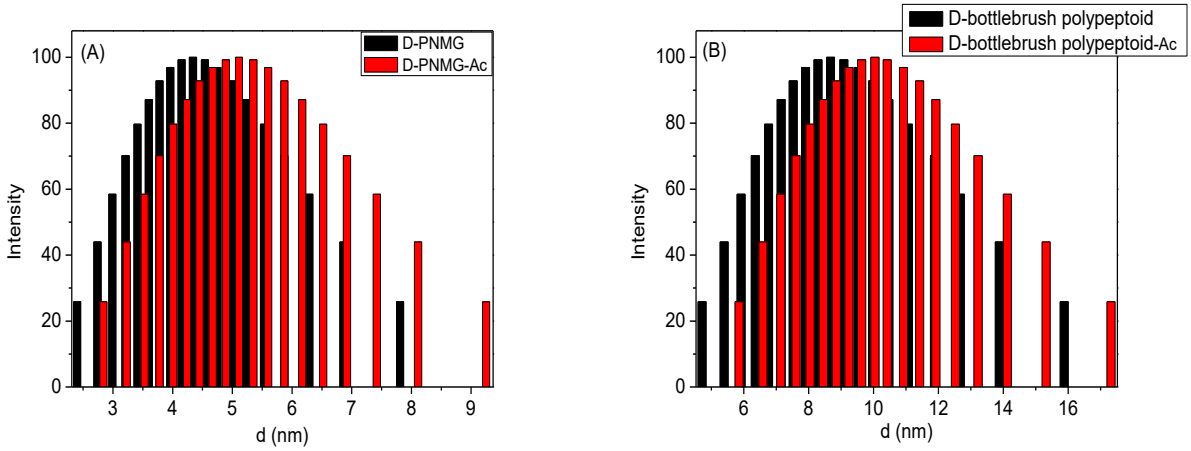

Figure 3.8. Size distribution of *D*-PNMGs (targeted DP= 100) and their linear analog 1 (A) and cyclic bottlebrush polypeptoids (targeted DP= 100) and their linear analog 1 (B) based on dynamic light scattering.

3.3.6 Cryo-Transmission electron microscopic results

To verify the formation of small clusters of cyclic polymers, we measured the cyclic P(NBG-*r*-NPgG)-*g*-PEG bottlebrush copolymer (targeted DP= 400) using cryo-TEM. Due to the resolution limit of cryo-TEM, we selected the largest cyclic bottlebrush polypeptoids for direct imaging in vitrified methanol. A representative cryo-TEM image is shown in Figure S3.10 (A). The presence of these small clusters can explain the abnormal variation of the particle sizes (R_g) in Figure 3.6. The mean size of these small clusters (12.2 $\pm$ 2.8 Å) (Figure S3.10 (B)) is in the

same length scale of a single polymer chain. Thus, their features in SANS profiles cannot be separated from each other. The measured SANS profile is actually the average of the profiles of all species including single molecules, dimers, trimers, and oligomers, weighted by their scattering power. Therefore, it is not surprising that there is a large deviation between the model fitting using the cyclic Gaussian chain model and the experimental SANS data, as the model only describes the structure of a single polymer chain. The cluster structures observed in the dilute methanol solution of the cyclic bottlebrush polypeptoids (targeted DP= 400) are expected to present for those with lesser DP values and also for the cyclic PNMGs, since they have similar chemical composition and the SANS measurements show the same trend in the R_g variation for all DP values and both types of cyclic polypeptoids.

3.3.7 Computational study

In the effort to investigate the driving force for cluster formation, our collaborator conducted computational study. Given the fact that the peripheral volume due to PEG side chains cannot effectively restrain the process, the simplest zwitterionic cyclic PNMG (DP= 100) and its linear counterpart were used for the computational simulation whose results should apply to the case of cyclic bottlebrush polypeptoids too. Our collaborator simulated the process of dimer formation for the cyclic polymers using the free energy profile, also called the potential of mean force (PMF), as a function of the distance of mass centers. Using umbrella sampling, we obtained the PMF of two cyclic PNMG polymers with DP=100 in methanol solution, as shown in Figure 3.9 (A). At a separation of about 24 Å there is a free energy minimum of around 0.5 kcal/mol, indicating an attractive region. However, the statistical error of the overall PMF is comparable to the energy barrier, and the depth of the relative free energy is of the order of k_BT, so both the formation and dissociation of dimers can rapidly occur, indicating an equilibrium of the reversible

process. In terms of the PFM simulation, monomers, dimers, and oligomers should exist in solution, which is consistent with our experimental results (Figure S3.10 (A)). On the other hand, the PMF of the linear counterpart suggests that the linear polymer is unlikely to aggregate in dilute solution (Figure 3.9 (B)).

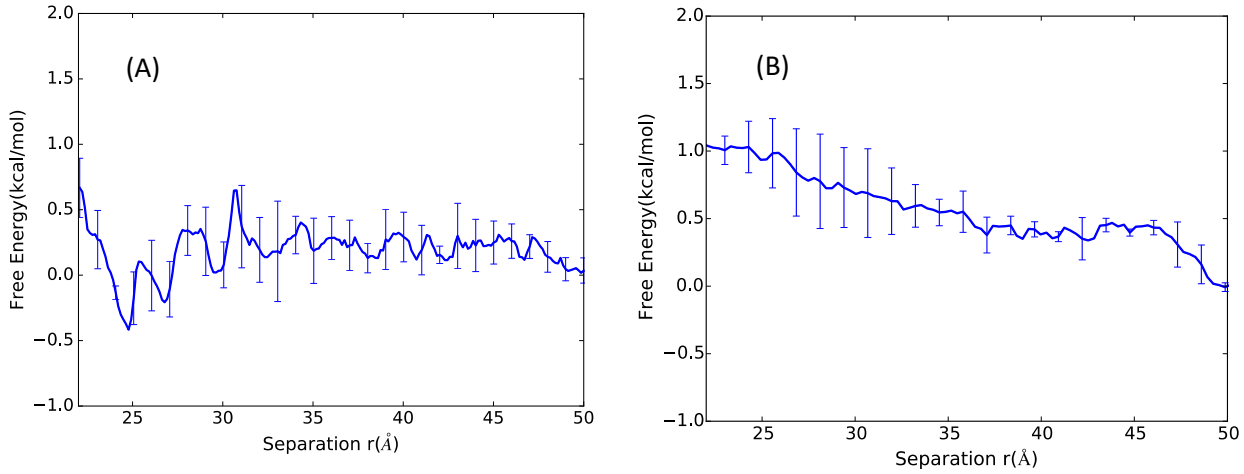

Figure 3.9. The free energy profile as a function of the mass center separation between (A) two *c*-PNMG polymer chains (DP= 100) and (B) two *l*-PNMG polymer chains (DP=100).

We defined one building block of the cyclic PNMG backbone as "coordinated" to solvent molecules if there is at least one oxygen atom of methanol is located within the first solvation layer of the carbonyl oxygen of the building block. The percentage of the coordinated building blocks in the whole polymer chain indicates the level of solvation of the cyclic PNMG chain. Then the coordination percentage as a function of distance of mass centers during dimerization was simulated, as shown in Figure 3.10. The coordination percentage gradually decreases as the two polymers are approaching to each other because solvent molecules keep getting excluded from the first solvation shell. A plateau is reached when their mass centers get into the range from 25 Å to 35 Å, where the solvent molecules located in the first solvation shells of the two polymers are rearranged in order to minimize the free energy. Until the distance of their mass centers reaches r= 25 Å, the first solvation shell between the two PNMG polymers starts to get fully excluded and

the coordination percentage reaches its minimum value. It is worth noting that even at the shortest mass center distance, more than half of the building blocks in the dimerized PNMGs are still exposed to the surrounding solvent molecules, so it is reasonable that the coordination percentage is reducing from 80.5% to 67.5%. This study illustrated the process of dimerization as a result of solvophobic interaction.

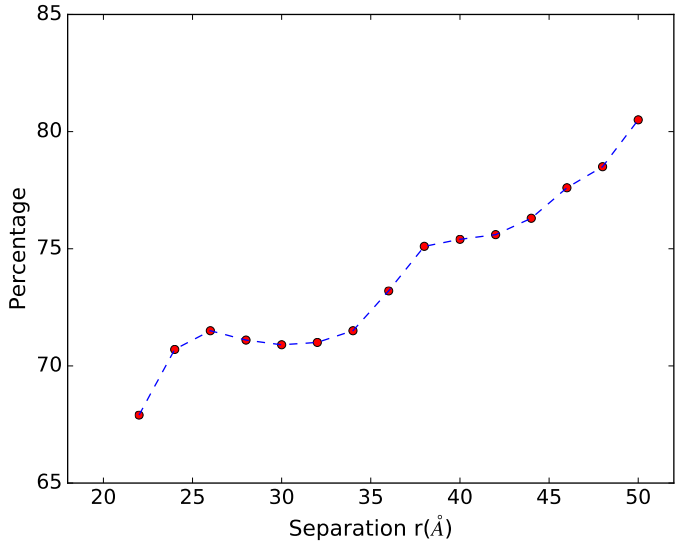

Figure 3.10. The percentage of O atoms on the polymer backbones that are coordinated to methanol as a function of mass center distance of the two *c*-PNMG monomers (DP= 100).

It has been demonstrated by the coordination percentage simulation that the solvophobic interaction is one attractive force for cluster formation. It is also conceivable that the dipole-dipole interaction plays a role during dimerization according to our pervious study that DBU-initiated polypeptoids are zwitterions. To further study the mechanism of dimerization and the interplay between these forces, we calculated the probability distribution of dipole-dipole interaction as a function of dipole-dipole distance at different distances of mass centers between the two PNMG polymers, presented in Figure 3.11. It was revealed by the study that as the two polymers are approaching to each other from 36 Å to 28 Å, the probability distribution of dipole-dipole interaction is shifting to the smaller dipole-dipole distance, indicating the orientation of the dipoles

towards each other. Dipole-dipole interaction is suggested the dominant driving force for this region. As the two polymers are approaching even closer to 24 Å, the orientations of the dipoles are rotating opposite to each, evidenced by the probability distribution shifting to a longer dipole-dipole distance. Solvophobic interaction is suggested the dominant driving force for this region. Although solvophobic interaction tends to drive the two cyclic polymers to get closer, the dipoles have strong preference to be solvated, which counteracts the dominant driving force and prevents the formation of larger aggregates.

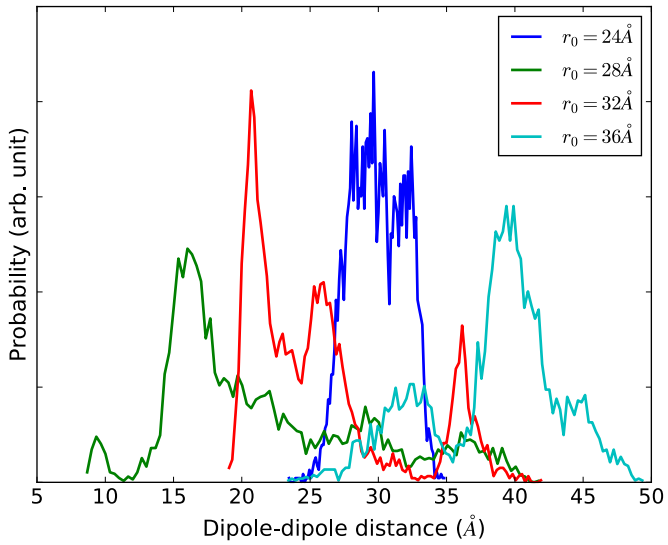

Figure 3.11. Dipole-dipole distance distribution as a function of the distance between mass centers of the two *c*-PNMG monomers (DP= 100). The curves are normalized to have unit area.

3.4 Conclusions

Cyclic bottlebrush polypeptoids with various compositions were synthesized by first DBU-mediated ZROP of Pg-NCA monomers and Bu-NCA monomers and subsequent conjugation with PEG550 chains. AFM analysis revealed toroid structures of cyclic bottlebrush polypeptoids in dry state which are different from the rod-like structures formed by the linear analogs. Kratky plot analysis further suggested that the strong intramolecular correlation of the cyclic bottlebrush

polypeptoids is due to the cyclic backbone conformation in solution. Guinier plot analysis revealed that the R_g values of both cyclic bottlebrush polypeptoids and cyclic PNMGs are larger than their corresponding linear analog 1 polypeptoids, indicating cluster formation of cyclic polypeptoids in MeOH. Clusters were observed by cryo-TEM images of cyclic bottlebrush polypeptoids (targeted DP= 420). DLS analysis showed that R_hs of both cyclic bottlebrush polypeptoids (targeted DP= 100) and cyclic PNMGs (targeted DP= 100) are larger than their linear analog 1 polypeptoids, which is consistent with Guinier plot analysis. The shape factor indicates that cyclic polypeptoid backbones may adopt an ellipsoid shape in solution. Computational study revealed that the cluster formation is driven by both dipole-dipole interaction and solvophobic interaction but counteracted by dipole solvation, with different interaction dominating at different inter-polymer distances. The solution aggregation behaviors of zwitterionic cyclic polypeptoids both with and without long side chains were systematically studied for the first time. The results indicate that the aggregation behaviors of the zwitterionic cyclic polypeptoids are not affected by the backbone chain length (targeted DP= 100 to 400) or the side chains (PEG, M_n= 550 g·mol^{-1}) but strongly dependent on the ion pairs at the polymer chain ends.

3.5 Supplementary Data

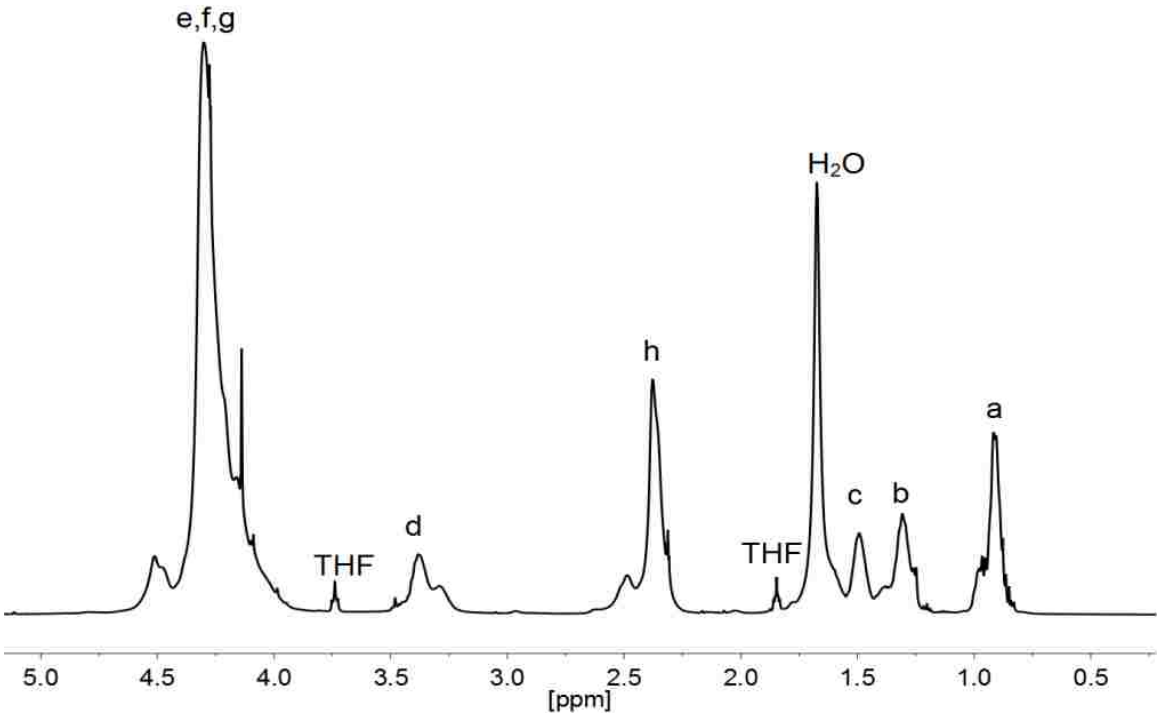

Figure S3.1. A representative ^{1}H NMR spectrum of DBU-P(NBG$_{41}$-*r*-NPgG$_{177}$) obtained by DBU-mediated polymerization of Bu-NCA and Pg-NCA in THF at 50 ℃.

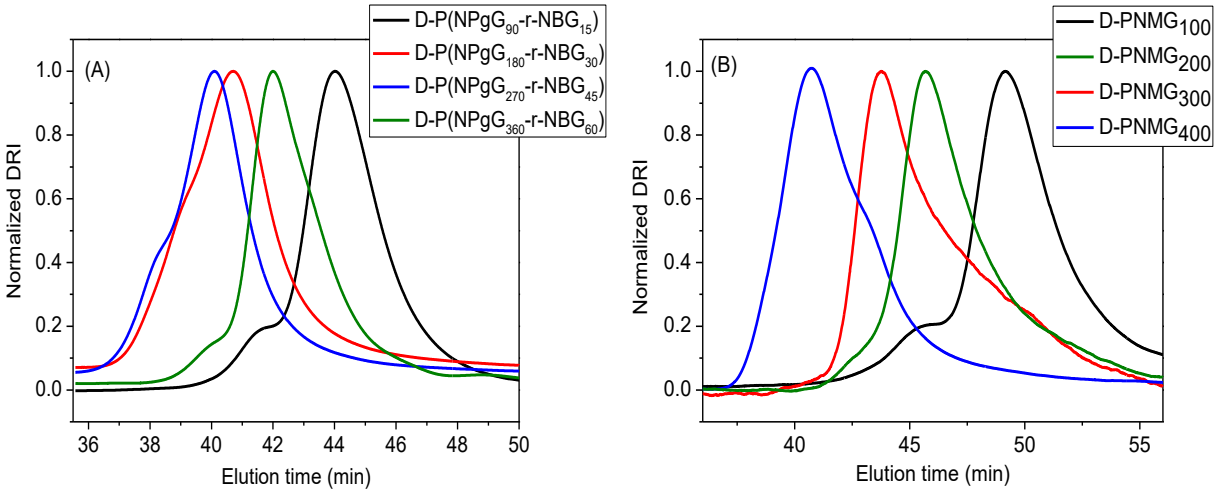

Figure S3.2**.** Normalized SEC traces of *D*-P(NPgG-r-NBG) with varying compositions (A) and *D*-PNMG with varying compositions (B).

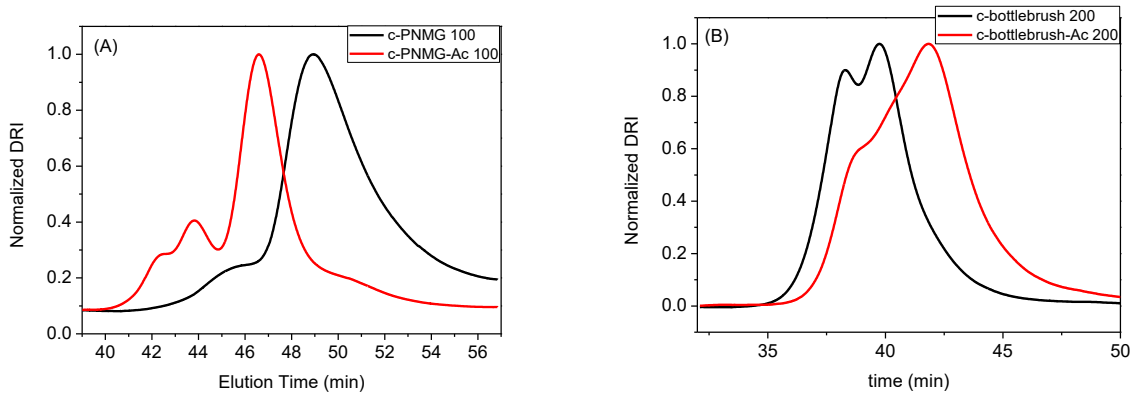

Figure S3.3. Representative normalized SEC traces of *c*-bottlebrush polypeptoids with targeted DP= 210 and the linear analog 1 (A) and *c*-PNMGs targeted DP= 100 and the linear analog 1 (B).

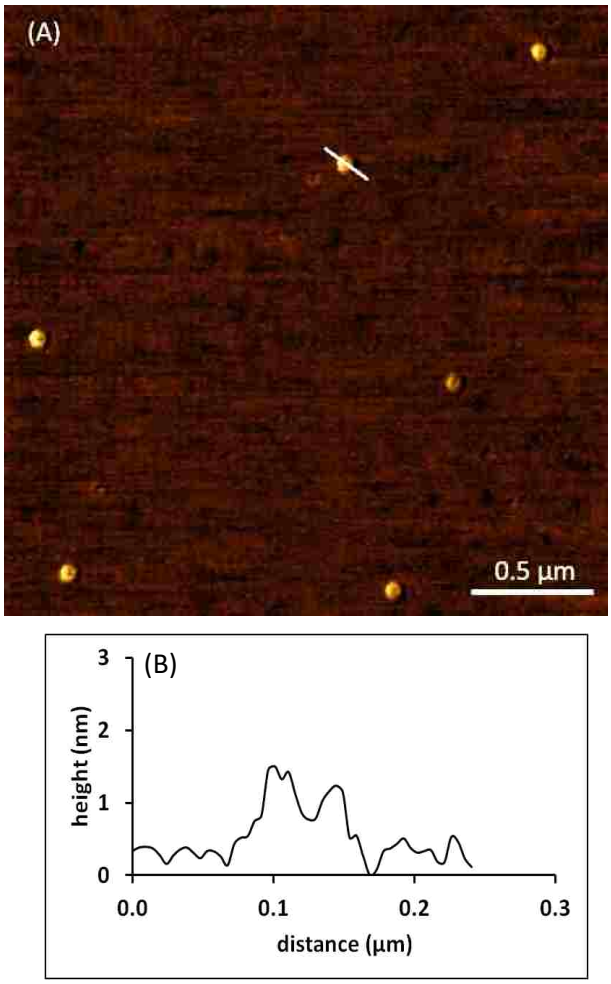

Figure S3.4. (A) A representative AFM image of the cyclic bottlebrush polymer DBU-P(NBG$_{41}$-*r*-NPgG$_{177}$)-*g*-(PEG550)$_{177}$ and (B) cross-section of the toroid-shape structure under the white line in (A).

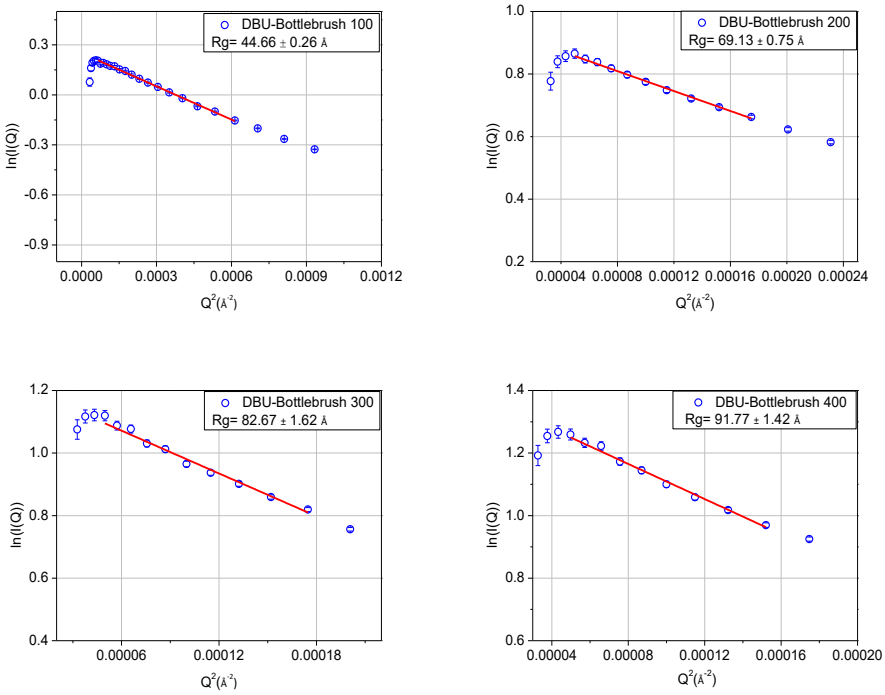

Figure S3.5. Guinier plots of *D*-bottlebrush polypeptoids with varying compositions.

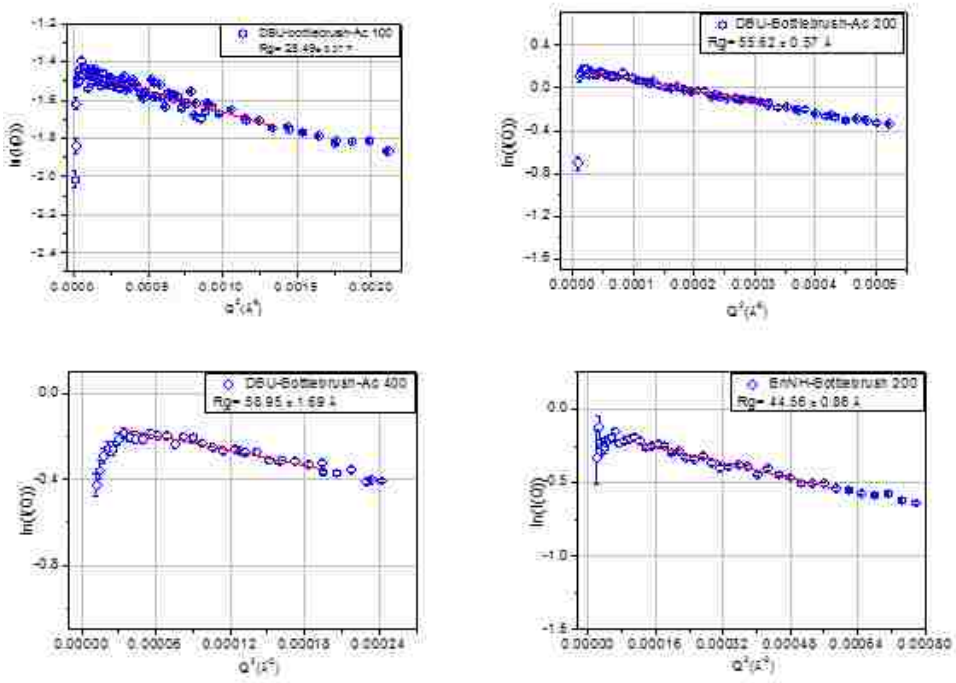

Figure S3.6. Guinier plots of linear analog 1 bottlebrush polypeptoids and linear analog 2 bottlebrush polypeptoids with varying compositions.

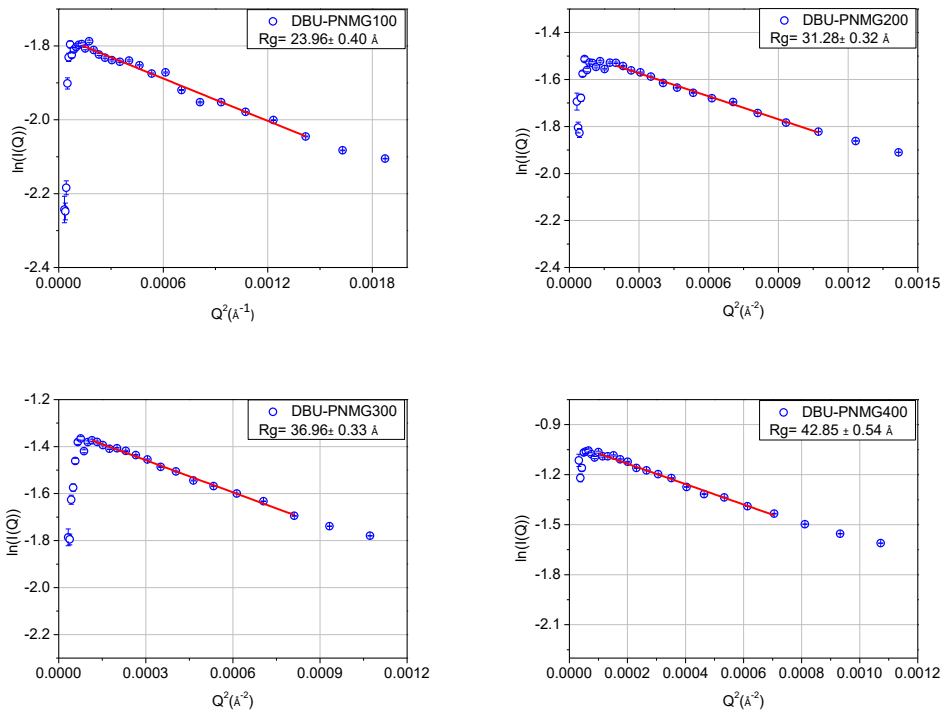

Figure S3.7. Guinier plots of DBU-PNMGs with varying chain lengths.

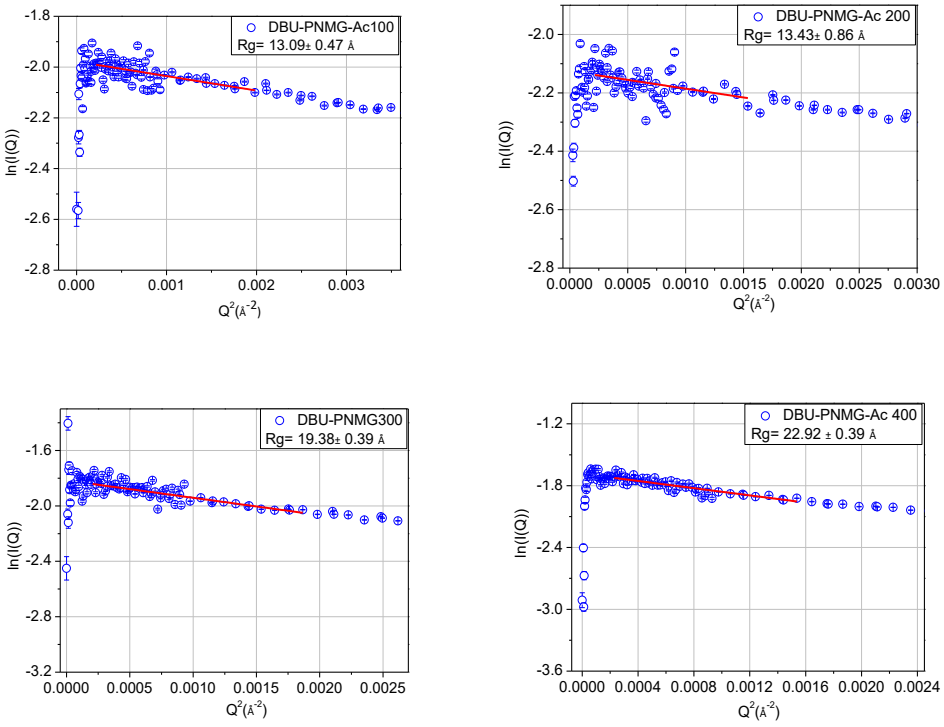

Figure S3.8. Guinier plots of linear analog 1 PNMGs with varying chain lengths.

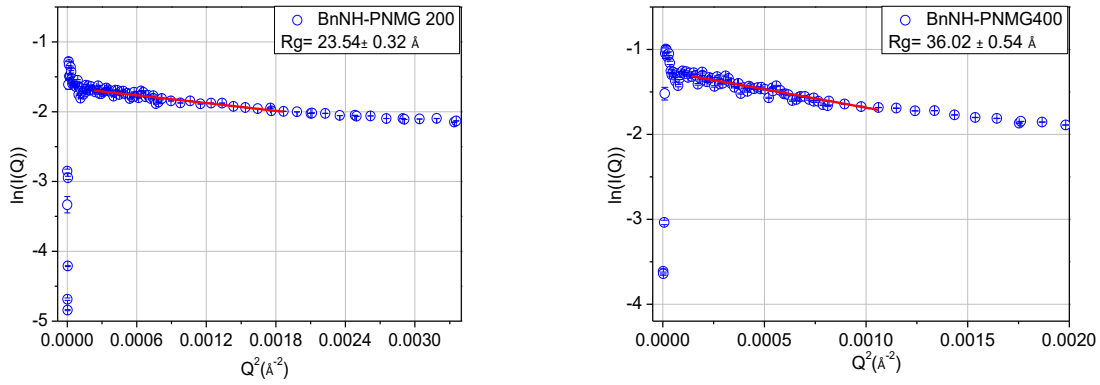

Figure S3.9. Guinier plots of linear analog 2 PNMGs with varying chain lengths.

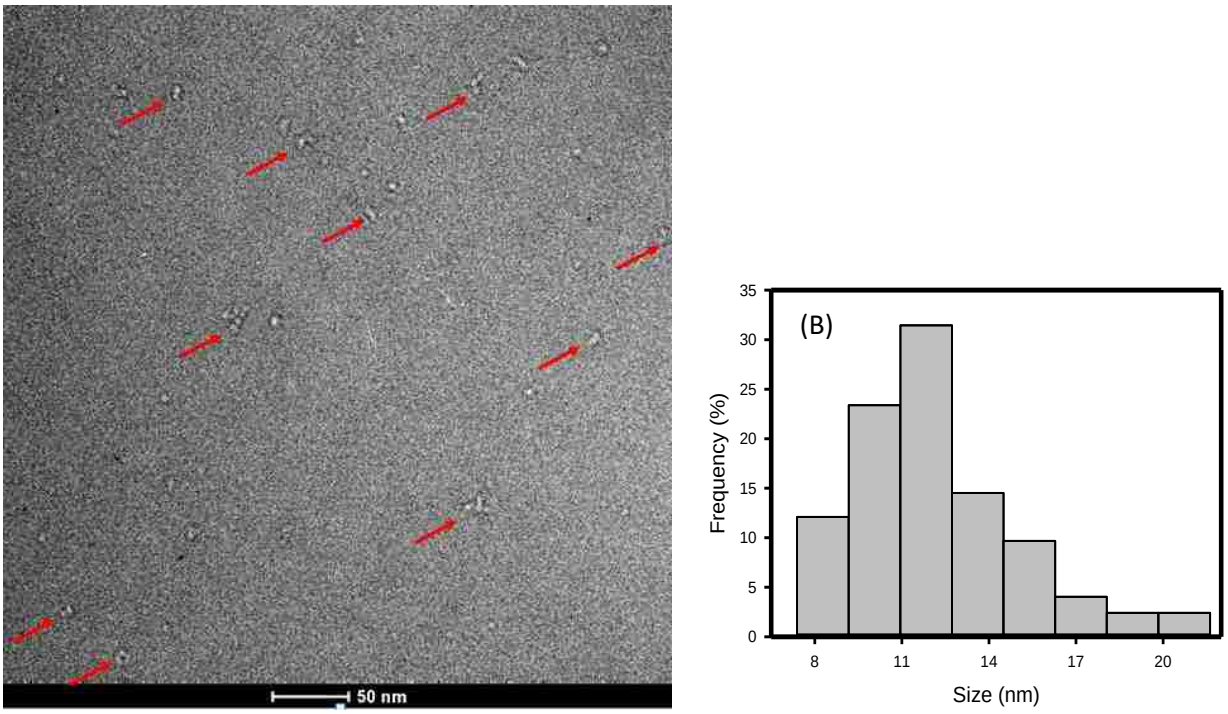

Figure S3.10. A representative cryo-TEM image of cyclic P(NBG-*r*-NPgG)-*g*-PEG bottlebrush copolymer (targeted DP= 400) in vitrified methanol. Dimers, trimers, and oligomers are indicated by the red arrows. (B) The histogram analysis of the aggregated particle sizes seen in the cryo-TEM micrograph. (Note: a total of 124 measurements of aggregated particle size are used in the analysis). The mean diameter of the aggregated particle is 12.2 ± 2.8 nm, consistent with the particle dimension determined from the SANS analysis (Figure 3.6 (B)).

Chapter 4. Synthesis and Characterization of Cleavable Core-Crosslinked Micelles Based on Amphiphilic Block Copolypeptoids as Smart Drug Carriers

4.1 Introduction

Polymeric micelles have been widely investigated as nanocarriers for drug delivery application due to their ability to enhance the water solubility of hydrophobic drugs, protect drugs against degrading enzymes, overcome multi-drug resistance (MRD),[96, 97] enhance accumulation of drugs selectively at the diseased sites and increase circulation time of drugs in human body.[98-100] Conventional polymeric micelles formed by self-assembly of amphiphilic polymers via hydrophobic interaction may spontaneously dissociate upon dilution, resulting in pre-leakage during drug delivery. To enhance the *in vivo* stability of the polymeric micelles, different strategies including chemical crosslinking of the micellar core or shell have been developed. The permanently cross-linked micelles, which cannot be disintegrated, may be difficult to remove through renal clearance.[105] In order to address the dilemma, stimuli-responsive core-crosslinked micelles (CCLMs) which can maintain their structures upon dilution and undergo dissociation in response to environmental cues, have been investigated in the last decade.[106, 107]

Nanocarriers based on polymeric micelles that are responsive to light,[108-111] temperature,[112-114] enzymes, pH, and a reductive environment have been developed for controlled drug delivery applications. In particular, redox responsive polymeric micelles have been judiciously designed by incorporating redox responsive units (*e.g.*, disulfide, diselenide[119], thio-ether[120] and acrylboronic ester[121]) either onto the polymer backbone, [122, 123] side chains[124, 125] or as cross-linkers.[126-128]

*This chapter previously appeared as [Ang Li and Donghui Zhang, Synthesis and Characterization of Cleavable Core-Cross-Linked Micelles Based on Amphiphilic Block Copolypeptoids as Smart Drug Carriers. *Biomacromolecules,* 2016, 17, 852–861.] It is reprinted by permission of American Chemical Society.

These micelles were shown to respond to oxidants (*e.g.*, H_2O_2) or reductants (*e.g.*, GSH) that are naturally present in the cellular environment by undergoing morphological changes. For *in vivo* drug delivery application, it is desirable that the building blocks of the nanocarriers are minimally cytotoxic and backbone degradable *in vivo*, allowing for systematic clearance of the materials. As a result, increasing attention has been focused on redox responsive micelles containing at least one hydrolytically degradable block such as polypeptide-*b*-poly(ethylene glycol) (PEG),[126] poly(ε-caprolactone)-*b*-PEG,[128] polylactide-*b*-PEG,[137] and poly(α-hydroxy acid)-*b*-PEG.[127, 138]. While poly (ethylene glycol) (PEG) is the most widely investigated polymer for various drug delivery systems with several PEGylated micellar or liposomal formulation in advanced clinical studies,[139-142] studies have shown that PEG can trigger complement activation,[143, 144] and PEGylated liposomes can be cleared rapidly upon repeated injections.[145-148] There is a clear and continued need to develop and investigate new micellar materials for drug delivery application.

Polypeptoids composed of poly (*N*-substituted glycine) backbones are a class of peptidomimetic polymers. Due to *N*-substitution, polypeptoids lack chirality and hydrogen bonding along the main chain, in contrast to polypeptides. This results in polypeptoids having enhanced proteolytic stability,[157, 212, 213] cell permeability,[214] thermal processability[15, 16, 69] and tunable conformation[7, 158, 215] by controlling the side chain structures, relative to polypeptides. Polypeptoids bearing neutral side groups have been found to be minimally cytotoxic[1, 19, 88, 151, 216] and can degrade in oxidative conditions that mimic inflammation *in vivo*,[165] suggesting their potential of systematic clearance desired for *in vivo* applications. Amphiphilic block copolymers comprised of hydrophilic poly(*N*-methyl glycine) (*a.k.a.* polysarcosine) in the forms of micelles, vesicles, nanoparticles or microparticles have been investigated as drug carriers.[150, 153, 164, 217-220] In some cases, pH responsive drug release has been demonstrated.[221, 222] Recent advances in the

synthetic method development have enabled the access to a wide range of well-defined polypeptoids with diverse side chain structures.[14, 26, 69, 75, 84, 223] Many of the fundamental physicochemical properties of polypeptoids have been benchmarked,[224] which set the stage for further development of functional polypeptoids for advanced applications.[28, 225]

In this work, we reported the synthesis and characterization of a new class of redox-active core-crosslinked polymeric micelles based on amphiphilic polypeptoid block copolymers. The polymers were synthesized by primary amine-initiated controlled polymerization of *N*-substituted *N*-carboxyanhydrides (R-NCAs). The solution self-assembly of block copolypeptoids were studied and the resultant polymeric micelles were core-crosslinked with disulfide linkages to confer redox responsive characteristics. The micellization and redox-triggered micellar dissociation have been characterized by a combination of analytical methods. Encapsulation of Doxorubicin (DOX), a blockbuster anti-cancer drug, with the micelles and the redox-triggered drug release behavior have also been investigated.

4.2 Materials and Methods

4.2.1 General considerations

DL-Dithiothreitol (DTT) (≥98%) and 1-anilinonaphthalene-8-sulfonic acid (1,8-ANS) (≥97%) were obtained from Sigma-Aldrich and used as received. Doxorubicin hydrochloride (DOX·HCl) (>99%) was purchased from LC Laboratories and used as received. All solvents used in this study were purchased from Sigma-Aldrich. Tetrahydrofuran (THF) was purified by passing through alumina columns under argon. The *N*-ethyl NCA (Et-NCA), *N*-propargyl NCA (Pg-NCA) and *N*-decyl NCA (De-NCA) were synthesized by adapting literature procedures.[69, 75, 165] 1-Azido-2-[(2-azidoethyl)disulfanyl]ethane cross-linker (CL1) and the 1,4-diazidobutane cross-linker (CL2) were synthesized by following a published procedure.[138]

4.2.2 Instrumentation

The ^{1}H NMR spectra were recorded on Bruker AV 400 and AV 500 spectrometers and the peaks were referenced in parts per million (ppm) relative to proton impurities of $CDCl_3$ or CD_2Cl_2, respectively. Size-exclusion chromatograms (SEC) were recorded on an Agilent 1200 system (Agilent 1200 series degasser, isocratic pump and auto sampler) equipped with three Phenomenex 5 μm, 300 x 7.8 mm columns [100 Å, 1000 Å and Linear (2)], Wyatt DAWN EOS multiangle light scattering (MALS) detector (GaAs 30 mW laser at λ= 690 nm) and Wyatt Optilab rEX differential refractive index (DRI) detector with a 690 nm light source. DMF containing 0.1 M LiBr was used as the eluent at a flow rate of 0.5 $mL \cdot min^{-1}$. The column temperature and the detector temperature were both kept at 25 ℃. All data analyses were performed using Wyatt Astra V 6.0 software. The polymer molecular weight (M_n) and the molecular weight distribution (PDI) were obtained by conventional SEC analyses with a standard calibration curve of polystyrene. High molecular weight (MW) shoulders were included in the peak analysis whenever they were present. The standard calibration curve was constructed with polystyrene standards (EasiCal PS-1 *M*W = 580 $g \cdot mol^{-1}$ to 7500 $kg \cdot mol^{-1}$,Varian) using Astra's column calibration template. Dynamic light scattering (DLS) was conducted on a Malvern Zetasizer Nano-ZS instrument and analyzed by the Zetasizer software version 7.03 using the cumulant method. Micelle samples were filtered through hydrophilic filters (pore size = 0.2 μm) before DLS measurement. Z-average diameters and the averaged size distributions were obtained from triplicate measurements. The UV-Vis absorption spectra were collected on HP 845x and processed on the software of HP 845x UV-Vis spectrometer. Fluorescence measurements were completed with the Perkin Elmer luminescence spectrometer LS 50B and the spectra were processed by the software of FL winlab. Transmission electron microscopic (TEM) samples were prepared by firstly drop-casting micellar solution onto a copper

grid, air-drying the solution at room temperature, and then negatively staining the sample with 1 wt% aqueous solution of uranyl acetate (UA). TEM analysis was conducted with JEM-1400 TEM at 80 kV.

4.2.3 Representative synthetic procedure for amphiphilic block copolypeptoids [PNEG-*b*-P(NPgG-*r*-NDG)]

N-Ethyl NCA (Et-NCA) (300 mg, 2.33 mmol) was dissolved in anhydrous THF (2.2 mL) to which a stock solution of benzylamine in THF (122 μL, 11.6 μmol, 95.2 mM) was added inside a glovebox under nitrogen atmosphere. The reaction mixture was allowed to react at 50 ℃ for 48 h to reach a complete conversion, as determined by ^{1}H NMR spectroscopic analysis of a reaction aliquot. *N*-propargyl NCA (Pg-NCA) (24 mg, 0.174 mmol) and *N*-decyl NCA (De-NCA) (42 mg, 0.174 mmol) were added to the above THF solution containing poly(*N*-ethyl glycine) polymer (PNEG). The reaction mixture was heated at 50 ℃ for additional 24 h to reach complete monomer conversion. An excess of hexane was added to the reaction mixture to precipitate the resulting block copolypeptoid polymer. The suspension was filtered through a Durapore membrane filter (0.45 μm, 47 mm, PVDF) and the precipitate were collected and dried under vacuum to afford a white solid (216 mg, 91%). ^{1}H NMR spectrum of poly(*N*-ethyl glycine)-*b*-poly[(*N*-propargyl glycine)-*r*-(*N*-decyl glycine)] δ (in CD_2Cl_2, ppm): 1.07 ($^{Et}CH_3CH_2$), 3.39 ($^{Et}CH_3CH_2$-), 4.00 (^{Et}-CH_2NCO-), 2.38 ($^{Pg}CHCCH_2$-), 4.28 ($^{Pg}CHCCH_2$-), 4.24 (^{Pg}–CH_2NCO-), 0.87 ($^{De}CH_3(CH_2)_7CH_2CH_2$-), 1.26 ($^{De}CH_3(CH_2)_7CH_2CH_2$-), 1.50 ($^{De}CH_3(CH_2)_7CH_2CH_2$-), 3.39 ($^{De}CH_3(CH_2)_7CH_2CH_2$-), 4.00 (^{De}–$CH_2$NCO-).

4.2.4 Determination of critical micelle concentration (CMC)

A stock solution of PNEG-*b*-P(NPgG-*r*-NDG) (0.2 mM) and 1,8-ANS (80 μM) was prepared by dissolving the PNEG-*b*-P(NPgG-*r*-NDG) diblock copolypeptoid (12 mg) in an aqueous solution of 1,8-ANS (3 mL, 80 μM). Aqueous solutions of different PNEG-*b*-P(NPgG-*r*-

NDG) concentration (0.14-22.7 μM) and a constant 1,8-ANS concentration (80 μM) were then prepared by transferring varying volumes of the stock solution (3-625 μL) into a 5 mL volumetric flask and diluted with the 1,8-ANS aqueous solution (80 μM). The fluorescence spectra were collected from 400-600 nm at λ_{ex} = 370 nm excitation wavelength. The fluorescence maximum, which shifts to lower wavelength in the range of 452-487 nm with increasing polymer concentration, was plotted against the polymer concentration. The concentration at the inflection point is defined as the critical micellation concentration.[226]

4.2.5 Preparation of core-crosslinked micelles (CCLMs) and irreversibly core-crosslinked micelles (ICCLMs) based on the amphiphilic block copolypeptoids.

A stock solution of the PNEG-*b*-P(NPgG-*r*-NDG) block copolypeptoid in DMF [660 μL, 14 μmol (propargyl group)] was mixed with a stock solution containing the 1-azido-2-[(2-azidoethyl)disulfanyl]ethane cross-linker (CL1) in DMF (40 μL, 5 μmol,) at room temperature. Distilled water (20 mL) was then added into the above solution dropwise with vigorous stirring for 24 h at room temperature. Aqueous solutions of $CuCl_2$ (50 μL, 3.5 μmol,) and sodium ascorbate (74 μL, 3.5 μmol) were then added into the above solution and stirred for an additional 24 h at room temperature. The mixture was transferred to a dialysis bag (MWCO = 3,500 Da) and dialyzed against deionized water for 36 h. The core-crosslinked micelles were obtained by lyophilization as a white solid (18 mg, 90%). The ICCLMs were prepared by the same procedure except for using the 1,4-diazidobutane as the crosslinker (CL2).

4.2.6 DTT-triggered CCLM dissociation.

An aqueous solution of CCLMs (0.9 mg·mL^{-1}, 8 mL) was purged by bubbling nitrogen through it for 15 min followed by addition of DTT (12.3 mg, 80 mmol). The reaction mixture was stirred for 36 h at room temperature and dried with a rotary evaporator. The resulting solid was dissolved in DCM and precipitated out by addition of an excess diethyl ether. Subsequent

centrifugation and filtration yielded a white solid (6.5 mg, 90%) which was subjected to further analysis by SEC, DLS and ^{1}H NMR methods.

4.2.7 DTT-triggered fluorophore release studies

1,8-ANS-loaded CCLMs was obtained by using 1,8-ANS aqueous solution (80 μM) and following the same procedure as that for the preparation of the blank CCLMs. After 1,8-ANS-loaded CCLMs were obtained, the solution was diluted below the CMC (0.05 mg/mL) by PBS buffer solution and allowed to reach equilibrium for overnight. Various amount of DTT was then added into the 1,8-ANS-loaded CCLMs solution (3 mL) to have the DTT concentration in the 0.045 μM-10 mM range. (Note: this concentration range approximately corresponds to 1 to more than 100 folds of the –S-S- content in the micellar solution by assuming 80% propargyl groups in the polymer micelles are crosslinked by disulfide linkages). The fluorescence intensity of the solution was monitored by the luminescence spectrometer in a time-driven mode.

4.2.8 Representative procedure of drug encapsulation

PNEG-*b*-P(NPgG-*r*-NDG) (10 mg, 6.8 μmol (propargyl group)) and CL1 (0.55 mg, 2.7 μmol) were dissolved in minimum DMF (50-150 μL). A THF solution of triethylamine (TEA) (10 μL, 5.2 μmol) was added into an aqueous solution of the DOX·HCl salt (10 mL, 3.2 mg, 5.5μmol) and stirred at room temperature for 1-2 h. The mixture was then added to the DMF solution containing the block copolypeptoid and the CL1 with vigorous stirring for 24 h, to which two aqueous solutions of $CuCl_2$ (25 μL, 1.7 μmol) and sodium ascorbate (37μL, 1.7 μmol) were then added. After stirring for an additional 24 h, the solution mixture was centrifuged first to remove any precipitated DOX and dialyzed against DI water for another 4 d to remove any non-encapsulated and soluble DOX in solution. Subsequent lyophilization yielded the DOX-loaded CCLMs as a red solid (9.6 mg, 87%).

4.2.9 DLC and DLE measurements

A DMF solution of DOX-loaded CCLMs (0.3 mg·mL^{-1}) was prepared by dissolving DOX-loaded CCLMs (3 mg) in DMF (10 mL) at room temperature. The encapsulated DOX concentration and the mass of the DOX in the CCLMs were determined by measuring the UV-Vis absorption of the solution at λ= 480 nm and comparing it to a standard curve that correlates the absorption and the DOX concentration in DMF. Drug loading capacity (DLC) and drug loading efficiency (DLE) were obtained by using equation 1 and 2. The averages of DLC and DLE were obtained based on triplicate experiments.

$$\mathrm{DLC\%} = \frac{\text{Encapsulated DOX Concentration}}{\text{CCLM Concentration}} \times 100\% \qquad \text{eq. 1}$$

$$\mathrm{DLE\%} = \frac{\text{Mass of Encapsulated DOX}}{\text{Mass of Initial Loaded DOX}} \times 100\% \qquad \text{eq. 2}$$

4.2.10 *In vitro* drug release study

DOX-loaded CCLMs (0.18 mg) were dissolved in PBS buffer (5 mL) containing DTT (10 mM). The solution was then placed into a dialysis bag (MWCO = 3,000 Da) and dialyzed against the PBS buffer containing DTT (20 mL, 10 mM) at 37 ℃ in the dark. Aliquots of the buffer solution (5 mL each time) outside the dialysis bag were collected every few hours. The buffer solution outside the dialysis bag was then replenished with the same amount of fresh PBS buffer containing DTT. The collected aliquots were then freeze-dried, re-dissolved in DMF (1 mL) and filtered through a syringe filter (pore size=0.2 μm). Fluorescence excitation intensity of the obtained DMF solutions was measured (λ_{em}= 560 nm) and converted into DOX concentration using a standard curve that correlates the fluorescence intensity and the DOX concentration in DMF. Drug release studies of DOX-loaded CCLMs and DOX-loaded non-crosslinked micelles

(NCLMs) without DTT were conducted by following the same procedure. The average of cumulative drug release percentage was obtained based on triplicate experiments.

4.2.11 Cell viability study

Human hepatoblastoma cells (HepG2) were plated in a 96-well plate (10000 cell/well) using MEMS medium and then incubated in an incubator containing 5% CO_2 at 37 °C for 24 h. Freeze-dried CCLMs and ICCLMs were re-dissolved in the MEMS medium (1 mg/mL), respectively. They were filtered through a sterile filter (pore size = 0.2 μm), diluted to different concentrations, added into cells, and then incubated with HepG2 cells in the incubator for another 48 h. Cell cytotoxicity was measured using Promega's CellTiter 96® Non-Radioactive Cell Proliferation Assay Kit with the manufacture's protocol. Cell viability was obtained by comparing the absorption of each well (λ= 570 nm) to a positive control, which contained only HepG2 cells. Each experimental group was repeated twice on two different days with 4 trials for each run.

4.2.12 Tumor cell inhibition study

Inhibition of tumor cell growth and proliferation in the presence of DOX or DOX-loaded micelles was investigated by a similar procedure as that for the cell viability study. Briefly, freeze-dried DOX-loaded CCLMs and DOX-loaded ICCLMs, and free DOX·HCl were dissolved in MEMS medium respectively at various initial DOX concentrations (0.1- 40 μg/mL). The solutions were filtered through a sterile syringe filter (pore size = 0.2 μm) and then added into HepG2 cells (a perpetual cell line consisting of human liver carcinoma), which had already been incubated in an incubator containing 5% CO_2 at 37 °C for 24 h. Cell viability was quantified after another 48-hour incubation using Promega's CellTiter 96® Non-Radioactive Cell Proliferation Assay Kit with the manufacture's protocol. Cell viability was obtained by comparing the absorption of each well (λ= 570 nm) to a positive control, which contained only HepG2 cells. The cell inhibition is

quantitatively defined as the percentage of cell death relative to the positive control (*i.e.*, HepG2 cells only), thus cell inhibition=1- cell viability. Time-dependent tumor cell inhibition study was conducted by the same procedure except that a constant initial DOX concentration (40 $\mu g \cdot ml^{-1}$) was used in the culturing of the HepG2 cells with the free DOX·HCl, the DOX-loaded CCLMs and DOX-loaded ICCLMs for 12 to 72 h. Each experimental group was repeated twice on two different days with 4 trials for each run.

4.3 Results and Discussion

Scheme 4.1. Synthesis of amphiphilic block copolypeptoids.

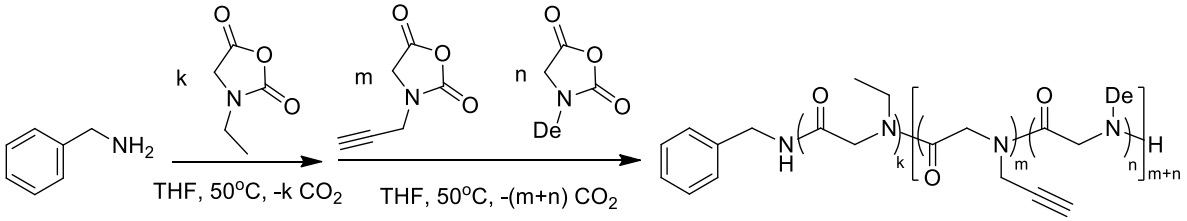

We have investigated the synthesis of amphiphilic diblock copolypeptoids consisting of a hydrophilic poly(*N*-ethyl glycine) (PNEG) block and a poly[(*N*-propargyl glycine)-*ran*-(*N*-decyl glycine)] [P(NPgG-*r*-NDG)] hydrophobic block. Previous studies have shown that PNEG homopolymer is readily soluble in water and a variety of organic solvents; both the poly(*N*-decyl glycine) (PNDG) and the poly(*N*-propargyl glycine) (PNPgG) homopolymers are hydrophobic and insoluble in water. As a result, we expect these amphiphilic diblock copolypeptoids to readily undergo micellization in aqueous solution. The presence of propargyl side groups in the hydrophobic blocks will allow for further functionalization or crosslinking post polymerization. Specifically, the block copolypeptoids with a targeted 230 total degree of polymerizations (DP) and varying composition were synthesized by sequential ring-opening polymerization of Et-NCA (M1) and then Pg-NCA (M2) and De-NCA (M3) together using benzyl amine initiators in varying initial monomers to initiator ratios in 50 ℃ THF. Each step of the polymerization was allowed to

reach complete conversion and the final block copolymers were isolated by precipitation into hexane and filtration and drying under vacuum.

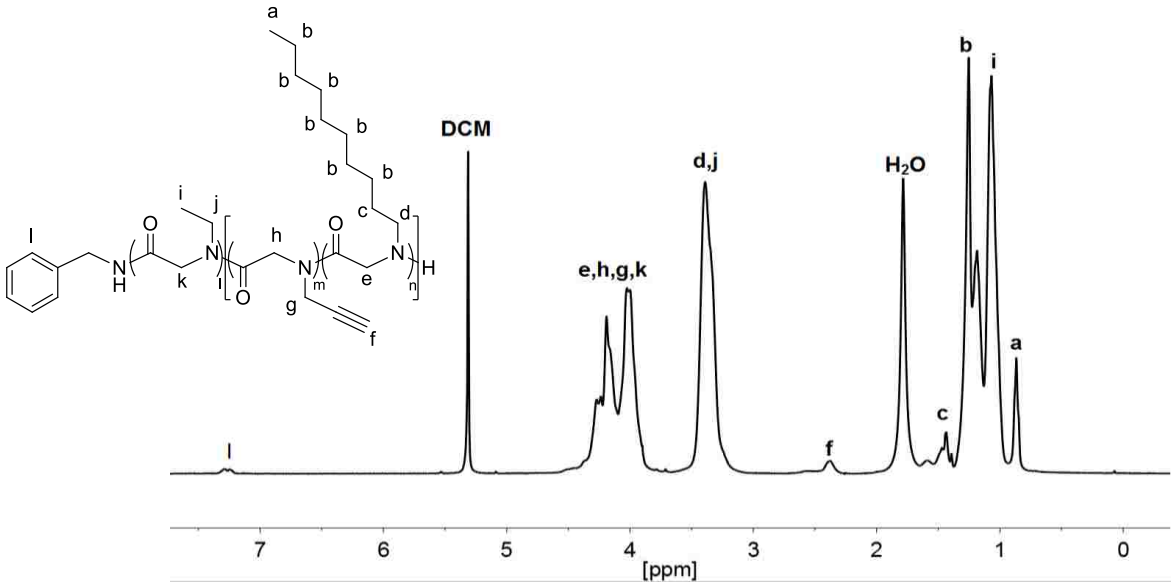

Figure 4.1. Representative ^{1}H NMR spectrum of PNEG$_{204}$-*b*-P(NPgG$_{13}$-*r*-NDG$_{15}$) polymer in CD_2Cl_2 (Entry 1, Table 4.1)

^{1}H NMR spectroscopic analysis of the resulting polymers confirms the formation of the PNEG-*b*-P(NPgG-*r*-NDG) block copolypeptoids abbreviated as EPgD (Figure 4.1). The polymer compositions (Table 4.1) were also determined by integrating the methyl protons of *N*-decyl glycine (D) segment at 0.87 ppm, propargyl proton of *N*-propargyl glycine (Pg) segments at 2.38 ppm and the methylene protons due to both *N*-propargyl glycine and *N*-ethyl glycine (E) segments at 3.39 ppm in relative to the benzyl end-group protons at 7.29 ppm in ^{1}H NMR spectra. All polymers exhibit approximately the same molecular weight in 20.0- 22.6 kg·mol^{-1} range.

Size-exclusion chromatographic (SEC) analysis of the polymers (in DMF/0.1 M LiBr solvent) revealed bimodal peaks with narrow molecular weight distribution (PDI< 1.10) (Figure S4.1). The minor shoulders present in several samples are tentatively attributed to the polymer aggregation. Despite the polymers have comparable molecular weights (M_n) as determined by ^{1}H

NMR analysis, they elute out the SEC column at different elution volumes, indicating that the E, Pg and D segments of the block copolypeptoids are solvated to varying extent in the DMF/0.1 M LiBr. This is consistent with our early observation of the relative solubility of the corresponding PNDG, PNPgG and PNEG homopolymers. In DMF/0.1 M LiBr at room temperature, PNDGs were found to have negligible solubility,[69] whereas PNPgGs readily dissolve albeit with a significant level of aggregates present[75] and PNEGs are highly soluble without any notable aggregation in the 5-10 mg/mL polymer concentration range typically used for SEC analysis.

Table 4.1. PNEG-*b*-P(NPgG-*r*-NDG) block copolypeptoid composition, M_n/PDI, critical micellar concentration (CMC) and micellar sizes

Entry	$[M1]_0$:$[M2]_0$:$[M3]_0$:$[I]_0$ [a]	Polymer composition [b]	M_n (NMR) [b] (kDa)	M_n (SEC) [c] (kDa)	CMC [d] ($\mu g \cdot mL^{-1}$)	Diameter [e] (nm)	PDI [e] (DLS)
1	200:15:15:1	$E_{204}Pg_{13}D_{15}$	21.6	36.8	113(24)	60.1 (0.9)	0.19
2	185:30:15:1	$E_{176}Pg_{34}D_{16}$	21.4	40.1	133(44)	25.5 (0.4)	0.28
3	155:60:15:1	$E_{144}Pg_{62}D_{18}$	21.8	40.8	123(25)	N/A [f]	N/A [f]
4	185:15:30:1	$E_{155}Pg_{13}D_{28}$	20.0	35.5	91(16)	N/A [f]	N/A [f]
5	155:15:60:1	$E_{134}Pg_{15}D_{49}$	22.6	30.3	93(18)	71.1 (0.9)	0.25

[a.] The initial monomer to initiator ratio; [b.] determined by ^{1}H NMR spectroscopy; [c.] determined by SEC using polystyrene standards (PDI of all entries < 1.10); [d.] determined by fluorescence spectroscopy; error bars are given in the parenthesis; [e.] Z-average diameter and polydispersity determined by DLS measurements; error bars are given in the parenthesis; [f.] multi-modal particle size distributions were observed for these samples by DLS analysis.

All polypeptoid block copolymers are readily dissolved in water at 1 $mg \cdot mL^{-1}$ polymer concentration. To characterize the critical micellar concentration (CMC), a series of aqueous solutions containing a constant concentration of 1-anilinonaphthalene-8-sulfonic acid (1,8-ANS) and varying concentrations of polypeptoids were prepared and measured by fluorescence spectroscopy in the 400-600 nm range with an excitation at λ= 370 nm (Figure 4.2). 1,8-ANS is a fluorophore that exhibits high fluorescence intensity in a hydrophobic environment but low

fluorescence intensity in a hydrophilic environment.[226] Plot of fluorescence maximum versus concentration revealed an inflection point where the fluorescence intensity increases sharply. The polymer concentration at the inflection point is defined as the CMC. The CMCs of all PNEG-*b*-P(NPgG-*r*-NDG) block copolypeptoids with varying compositions are not significantly different in the 91-133 $\mu g \cdot mL^{-1}$range, considering the error bars of the measured CMCs (Table 4.1).

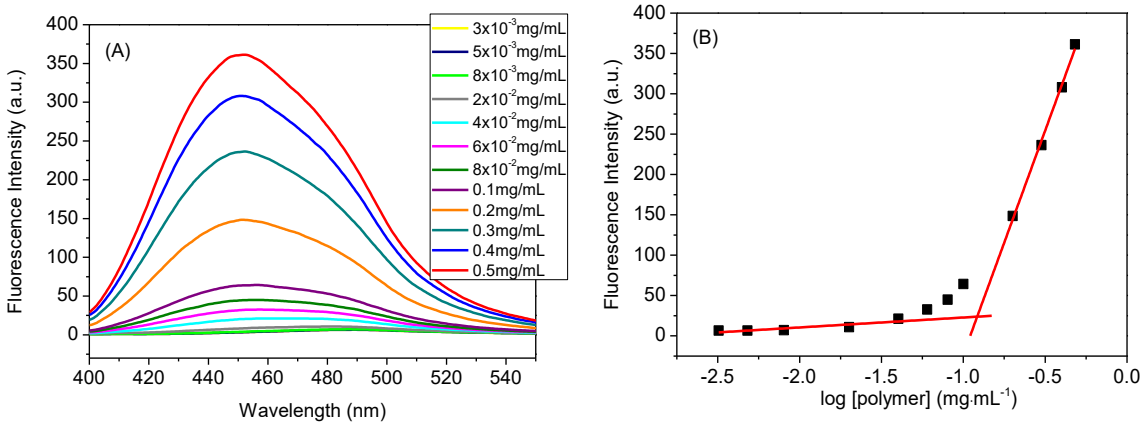

Figure 4.2. (A) Representative fluorescence spectra of 1,8-ANS (λ_{ex} =370 nm) in the aqueous solution of $E_{204}Pg_{13}D_{15}$ at varying concentrations; (B) a representative semi-log plot of the maximum fluorescence intensity (λ_{em} = 452- 487 nm) versus polymer concentrations.

The micellar size was characterized by dynamic light scattering (DLS) measurements of dilute aqueous solutions (0.5 $mg \cdot mL^{-1}$) containing the amphiphilic block copolypeptoids. DLS analysis revealed mono-modal particle size distributions for the $E_{204}Pg_{13}D_{15}$, $E_{176}Pg_{34}D_{16}$ and $E_{134}Pg_{15}D_{49}$ samples with moderate PDIs (0.19, 0.28 and 0.25 respectively) (Entry 1, 2 and 5, Table 4.1). The Z-average diameters of the particles are 25.5 ± 0.4, 60.1 ± 0.9 and 71.1 ± 0.9 nm respectively for these three polymer samples ($E_{176}Pg_{34}D_{16}$, $E_{204}Pg_{13}D_{15}$ and $E_{134}Pg_{15}D_{49}$), consistent with the formation of micelles. By contrast, samples $E_{144}Pg_{62}D_{18}$ and $E_{155}Pg_{13}D_{28}$ (Entry 3 and 4, Table 4.1) appear to form less defined aggregates, evidenced by multi-modal particle size distributions in DLS. Further experiments are required to fully understand the relationship between the polymer composition and micellar morphology and size distribution.

As the $E_{204}Pg_{13}D_{15}$ sample (Entry 1, Table 4.1) form relatively well-defined spherical micelles with moderate size distribution (PDI=0.19), it is used as the model system for the subsequent investigation of core-crosslinking of the micelles, stimuli-responsive dissociation, drug loading/release behavior and the cytotoxicity studies. Crosslinking of the $E_{204}Pg_{13}D_{15}$ micellar core was conducted with diazide crosslinkers by CuAAC chemistry in the presence of $CuCl_2$ and sodium ascorbate catalyst in water with a small amount of DMF (3.4 vol.%) which was used to facilitate the initial dissolution of the polymer. Two different diazide crosslinkers [*i.e.*, azido-2-[(2-azidoethyl) disulfanyl] ethane (CL1) and 1,4-diazidobutane (CL2)] were examined to produce reversible core-crosslinked micelles (CCLMs) bearing disulfide cross-linkages in the core and irreversible crosslinked micelles (ICCLMs). The resulting core-crosslinked micelles were purified by dialysis against deionized water for 36 h and were further characterized by a combination of ^{1}H NMR, SEC and DLS analysis. ^{1}H NMR analysis of the CCLMs in CD_2Cl_2, a non-selective solvent for both the hydrophilic and hydrophobic blocks of the block copolypeptoid ($E_{204}Pg_{13}D_{15}$) revealed the decreased intensity of decyl protons at 1.25 ppm and the disappearance of the characteristic propargyl proton at 2.38 ppm as compared to the ^{1}H NMR spectrum of the $E_{204}Pg_{13}D_{15}$ unimers (Figure S4.2). In addition, the triazole protons that typically appear at ~8 ppm after CuAAC chemistry are also absent. These results are consistent with the successful crosslinking of the $E_{204}Pg_{13}D_{15}$ micellar core by CuAAC chemistry, resulting in reduced solvation of the hydrophobic core segments where the decyl and triazole groups reside. SEC analysis of the CCLMs in 0.1M LiBr/DMF (a non-selective solvent for the $E_{204}Pg_{13}D_{15}$ polymer) revealed a prominent mono-modal peak at the low elution volume (18.4 mL) that has a much larger hydrodynamic size than the constituent $E_{204}Pg_{13}D_{15}$ unimers (Figure 4.3 (A)), indicating the formation of stabilized micelles. Two other small peaks at higher elution volumes were also observed in the SEC elugram

of the CCLMs and overlapped with the elugram peak for the $E_{204}Pg_{13}D_{15}$ unimers. They are attributed to the $E_{204}Pg_{13}D_{15}$ unimers and their small aggregates due to the incomplete core-crosslinking reaction (Figure 4.3 (A)). DLS analysis of the CCLMs in water (0.5 $mg{\cdot}mL^{-1}$) revealed that the micelles maintain a mono-modal size distribution and the hydrodynamic diameter is notably decreased to 42.4 ± 0.8 nm (PDI = 0.19) relative to the non-crosslinked micelle (NCLM) precursors (d = 60.1 ± 0.9 nm, PDI = 0.19) in water (Figure 4.3 (B)). In addition, the CCLMs exhibit very good micellar stability by maintaining the well-defined and swelled micellar structure (d = 59.2 ± 1.6 nm, PDI = 0.19) in diluted (0.05 $mg{\cdot}mL^{-1}$) DMF solution due to the covalent crosslinking in the micellar core. By contrast, the NCLMs become destabilized in dilute DMF solution, as evidenced by an increase of the hydrodynamic size, broadening of the size distribution (PDI = 0.41) and the appearance of unimers by DLS analysis (Figure 4.3 (B)). Further TEM analysis of both dried and uranyl acetate-stained CCLMs and NCLMs revealed the presence of mostly spherical micelles with occasionally short cylinders, suggesting that covalent crosslinking in the micellar core did not significantly alter the micellar morphology (Figure 4.4). The average diameter of the CCLMs (21.1 ± 2.3 nm) is comparable to that of the NCLM precursors (22.8 ± 2.9 nm) in the dry state.

To investigate whether the CCLMs can dissociate in reductive environment, an aqueous solution of CCLMs was treated with DTT (10 mM) at room temperature under a nitrogen atmosphere for 36 h. The reaction mixture was then dried under vacuum and further purified by re-dissolution in CH_2Cl_2 and precipitation with an excess diethyl ether. ^1H NMR analysis of the purified polymer product in CD_2Cl_2 revealed the increased intensity of decyl protons of *N*-decyl glycine (D) segments at 1.25 ppm relative to those of the CCLMs and the appearance of the characteristic triazole protons at 8.0 ppm after the DTT treatment (Figure S4.2). This is consistent

with the formation of new polymeric unimers bearing polar groups (*e.g.*, triazole and thiol) from the DTT-induced un-crosslinking of the CCLMs and the micellar dissociation (Scheme S4.1).

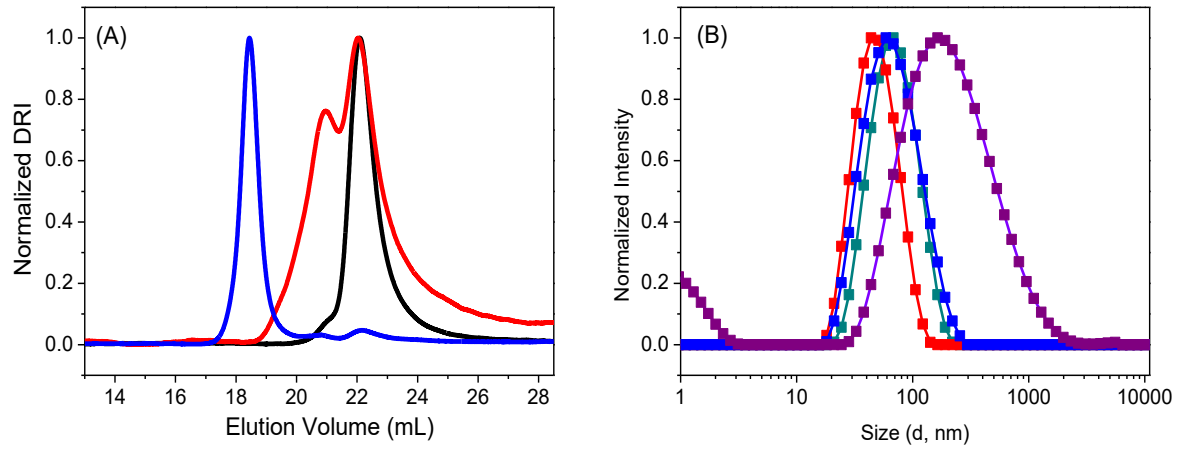

Figure 4.3. (A) Representative SEC chromatograms of the $E_{204}Pg_{13}D_{15}$ unimer (—) and the corresponding CCLMs before (—) and after DTT treatment (—) in DMF/ 0.1 M LiBr. (B) DLS size distribution of the $E_{204}Pg_{13}D_{15}$-based NCLMs in water (- ■ -) or DMF (- ■ -) and the corresponding CCLMs in water (- ■ -) or DMF (- ■ -). The micellar solutions in water or DMF are kept at 0.5 mg·mL^{-1} or 0.05 mg·mL^{-1} respectively in the DLS studies.

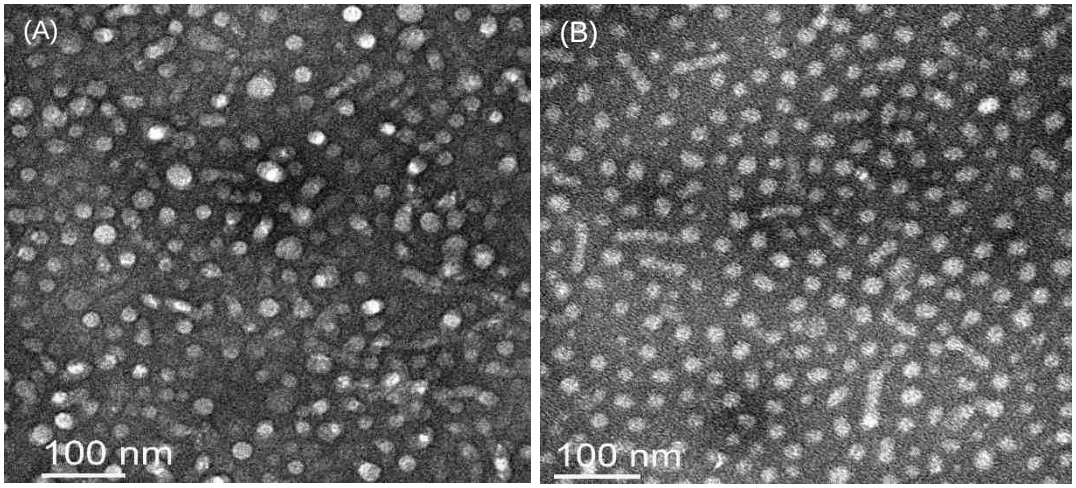

Figure 4.4. (A) TEM micrographs of the NCLMs and (B) CCLMs based on the $E_{204}Pg_{13}D_{15}$ block copolypeptoids. Samples were first stained with uranyl acetate prior to TEM imaging.

SEC analysis of the DTT-treated CCLMs in DMF revealed a broad bimodal peak with significantly reduced hydrodynamic sizes relative to the CCLMs, confirming the dissociation of the CCLMs upon DTT treatment (Figure 4.3 (A)). The peak at the higher elution volume is

attributed to the newly formed unimers from disintegration of the CCLMs and the shoulder peak at lower elution volume is presumably due to the unimer aggregation or incomplete micellar dissociation.

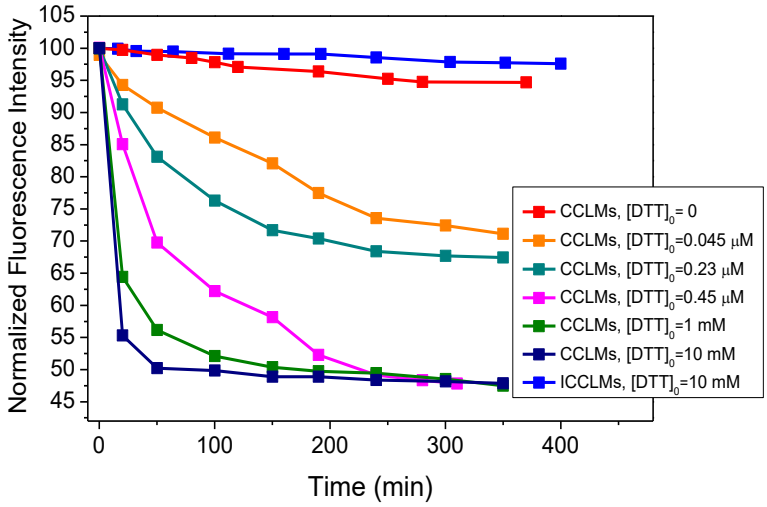

Figure 4.5. Plots of fluorescence intensity of 1,8-ANS-loaded core-crosslinked micelles (CCLMs) or irreversibly core-crosslinked micelles (ICCLMs) composed of $E_{204}Pg_{13}D_{15}$ in solution versus time after the addition of varying amount of DTT (0-10 mM).

The DTT-triggered dissociation of the CCLMs was also demonstrated by monitoring the release of encapsulated 1,8-ANS from the CCLMs in the presence of varying concentration of DTT in the 0.045 μM-10 mM range (Figure 4.5). An aqueous solution of ANS-loaded CCLMs was prepared and then diluted below the CMC of the non-crosslinked micellar analog (0.05 $mg \cdot mL^{-1}$, Entry 1, Table 4.1). The fluorescence intensity of the solution at λ= 470 nm was monitored at room temperature over a period of 350 min (Figure 4.5). The fluorescent intensity was shown to decrease over time and eventually flatten out to a constant non-zero value. Increasing the initial DTT concentration gives rise to accelerated fluorescence intensity decay and enhanced percentage fluorescent intensity reduction, suggesting faster and more 1,8-ANS release with higher DTT concentration in the solution. When the initial DTT concentration is 0.45 μM, 1 mM and 10

mM, the ultimate percentage reduction of the fluorescent intensity is approximately the same at 50%, indicating incomplete release of 1,8-ANS. This is tentatively attributed to the physical association of the 1,8-ANS with the resulting unimers after DTT treatment and the corresponding small aggregates (Figure 4. 3(A)). By contrast, 1,8-ANS-loaded CCLMs without DTT treatment and 1,8-ANS-laoded ICCLMs treated by 10 mM DTT only exhibited a minimal reduction of the fluorescence intensity by 5% and 2% respectively over a period of 350 min. These results clearly indicate that CCLMs can be used to encapsulate hydrophobic molecules and release them on demand under reductive conditions with DTT present.

To demonstrate the utility of the CCLMs for on demand drug release, we investigated the encapsulation and release of Doxorubicin (DOX), a hydrophobic cancer drug using the core-crosslinked diblock copolypeptoid micelles. DOX-loaded CCLMs were prepared by mixing DOX with the $E_{204}Pg_{13}D_{15}$ and the reductively active CL1 crosslinker in the presence of $CuCl_2$ and sodium ascorbate in H_2O and a small amount of DMF (0.5-1.5 vol.%). The reaction solution was centrifuged to remove any precipitated DOX and then dialyzed against DI water to yield the final DOX-loaded CCLMs. The initial DOX to polymer mass ratio (IDP) was systematically varied to assess the effect on the drug loading capacity (DLC) and drug loading efficiency (DLE).

The drug loading capacity (DLC) is the ratio of the mass of the encapsulated drug over the mass of the drug-loaded micelles, whereas the drug loading efficiency (DLE) is the ratio of the mass of the encapsulated drug in the micelles over the total mass of the drug used in the encapsulation process. We have found that core-crosslinking enhances the drug loading capacity and drug loading efficiency, as indicated by 2.8% and 4.8% DLC and 20% and 28% DLE for the DOX-loaded non-core-crosslinked micelles (NCLMs) and the corresponding core-crosslinked micellar counterpart (CCLMs) (Entry 1 and 2, Table 4.2). Inspired by an early report that drug

loading capacity can be enhanced by tuning the initial drug to polymer (IDP) ratio,[227] we systematically varied the IDP ratio from 15:100 to 60:100 during the preparation of the DOX-loaded CCLMs. It was found that the DLC of the DOX-loaded CCLMs increased from 4.8% to 20.3%. Further increase of the IDP ratio to 80:100 only enhanced the DLC by a modest percentage (2.8%) to 23.1%. The DLE also increases from 28% to 37% as the IDP is increased from 15:100 to 80:100; the dependence of DLE on IDP is more moderate relative to that of the DLC.

Table 4.2. DLC and DLE of the NCLMs and CCLMs based on the $E_{204}Pg_{13}D_{15}$ polymer (Entry 1, Table 4.1) with varying IDP ratios.

Entry	Sample	IDP ratio [a]	DLC (%) [b]	DLE (%) [c]
1	DOX-loaded NCLMs	15:100	2.8 (±0.3)	20 (±3)
2	DOX-loaded CCLMs	15:100	4.8 (±0.2)	28 (±2)
3	DOX-loaded CCLMs	30:100	9.6 (±1.7)	30 (±3)
4	DOX-loaded CCLMs	60:100	20.3 (±1.9)	36 (±2)
5	DOX-loaded CCLMs	80:100	23.1 (±1.5)	37 (±4)

[a.] The initial DOX and polymer mass ratio (IDP); [b.] drug loading capacity (DLC); [c.] drug loading efficiency (DLE).

Investigation of the drug release profile of the DOX-loaded CCLMs was conducted in PBS buffer with or without DTT (10 mM) present at 37 ℃ over the course of 30 h and compared to that of the DOX-loaded NCLMs without DTT (Figure 4.6). Specifically, the DOX-loaded CCLMs and DOX-loaded NCLMs were dissolved in the PBS buffer and then dialyzed against the buffer solution over time. It should be noted that the initial concentrations of DOX-loaded CCLMs and DOX-loaded NCLMs were diluted to be lower than the CMC of the NCLMs to induce the micellar dissociation. Aliquots of the outside buffer solution were taken, processed and analyzed by the fluorescence excitation spectroscopy with an emission wavelength at λ = 560 nm after every few hours. The DOX concentration from the aliquots was determined using a standard curve that

correlates the fluorescence excitation intensity at λ = 480 nm with the DOX concentration. The DOX-loaded CCLMs exhibited a gradual release profile with a 40 % DOX released from the micelles over a period of 30 h after DTT addition (Figure 4.6). By contrast, less than 5 % DOX was released over the same period of time without the DTT addition. Prolonged incubation time up to 50 h did not result in significant further increase of the DOX release (<5%). We tentatively attribute this to the association of the DOX with the unimers or small aggregates formed from the dissociation of the CCLMs (Figure 4.3 (A)), thus limiting the ultimate degree of DOX release. In comparison, the DOX-loaded NCLMs without DTT present exhibited a similar DOX release profile to that of the CCLMs with DTT present in the first 10 h (Figure 4.6). The maximum release of DOX (35%) from the NCLMs is slightly lower than that of the CCLMs with DTT (40%). This is probably due to the reduced stability of the CCLMs after un-crosslinking at the core relative to that of the NCLMs, considering that the un-crosslinked CCLMs bear more polar groups (*e.g.*, triazole and thiol) in the solvophobic blocks relative to the NCLMs and thus facilitating the dissociation of the formers (Scheme S4.1). The above results clearly indicate that the CCLMs based on the block copolypeptoids can efficiently encapsulate hydrophobic drugs with good to moderate DLC and DLE and the drugs can be gradually released on demand in the presence of DTT. We caution the extrapolation of the DOX release behavior of CCLMs or NCLMs shown here (Figure 4.6) to those with other bio-reductants (*e.g.*, GSH) or in cellular media (*vide infra*), as the rate of micellar dissociation due to cleavage of the disulfide crosslinkers may vary and the complex cellular environment can give rise to alternative degradation pathways for CCLMs or NCLMs.[53]

CCLMs and ICCLMs exhibit minimal cytotoxicity to HepG2 cells (a perpetual cell line consisting of human liver carcinoma), supported by the cell viability study using MTT assays.

More than 95% HepG2 cells remain alive after 48 h incubation with CCLMs or ICCLMs in the 0.01- 1 $mg \cdot mL^{-1}$ concentration range (Figure 4.7).

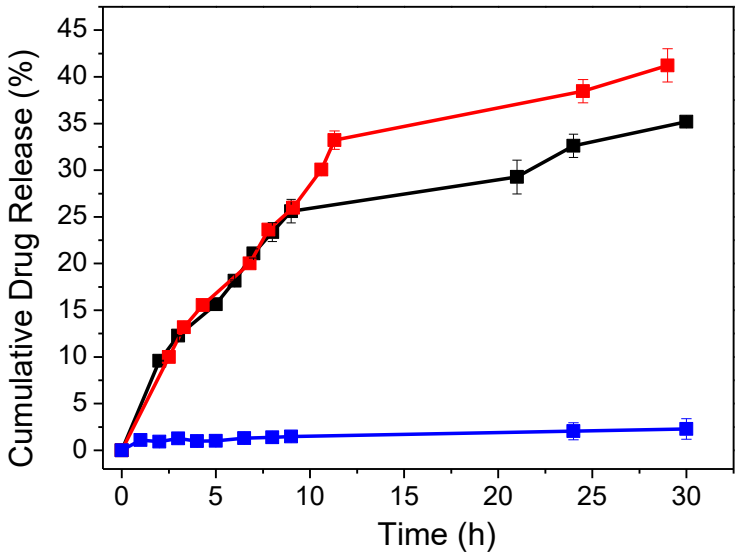

Figure 4.6. Plots of cumulative DOX release from the CCLMs (-■-) over time with the presence of DTT ($[DTT]_0$= 10 mM) and CCLMs (-■-) and NCLMs (-■-) without the presence of DTT. The CCLMS and NCLMs are both comprised of the $E_{204}Pg_{13}D_{15}$ polymer.

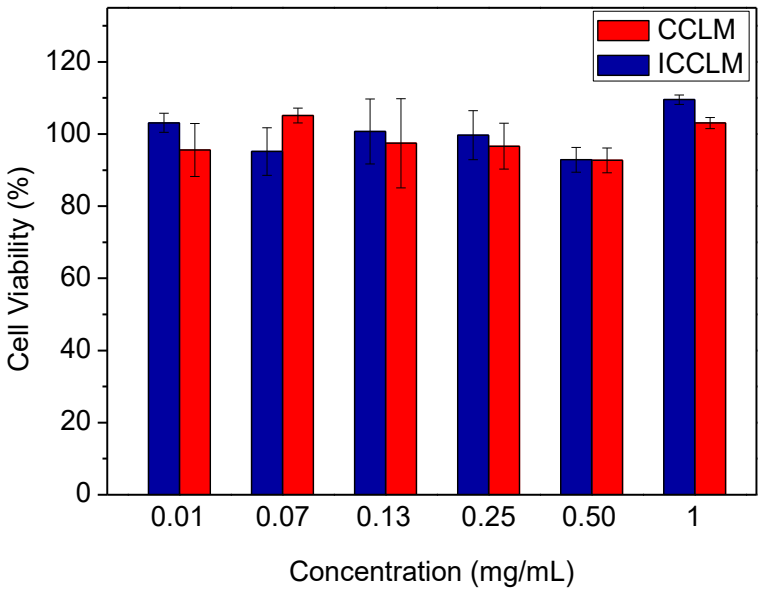

Figure 4.7. Percentage HepG2 cell viability after being cultured with CCLMs and ICCLMs both comprised of the $E_{204}Pg_{13}D_{15}$ block copolypeptoids for 48 h and characterized by MTT assays.

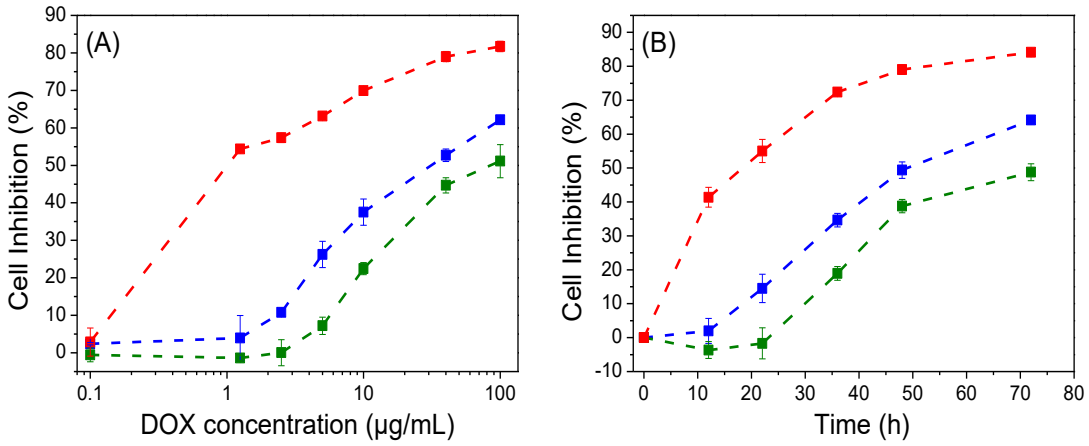

Figure 4.8. (A) The plots of percentage cell inhibition versus DOX concentration and (B) time-dependent cell inhibition studies at 40 μg·mL^{-1} equivalent DOX concentration for the DOX-loaded CCLMs (■), DOX-loaded ICCLMs (■) and free DOX·HCl (■). HepG2 cells were used in the study. The CCLMS and ICCLMs are both comprised of the $E_{204}Pg_{13}D_{15}$ polymer.

In addition, statistical T test was conducted for each concentration, and there was no significant difference (95% confidence interval) observed for the effect of CCLMs and ICCLMs on the percentage cell viability (Figure 4.7). Inhibition of tumor cell growth and proliferation was investigated by incubating DOX-loaded CCLMs, DOX-loaded ICCLMs, and free DOX·HCl with HepG2 cells for 48 h with varying DOX concentration (0.1 - 100 μg·mL^{-1}). Cell inhibition is quantitatively defined as the percentage of cell death at different conditions relative to the positive control (*i.e.*, cells only without any DOX). All three samples inhibited the growth and proliferation of HepG2 cells, as supported by increasing percentage cell inhibition with increasing DOX content in the solution (Figure 4.8 (A)). The cell inhibition by the DOX-loaded CCLMs is much lower than that of the free DOX·HCl in the entire DOX concentration range (0.1- 100 μg·mL^{-1}). For example, a 62% cell inhibition was observed for the DOX-loaded CCLM solution relative to the 82% in the free DOX·HCl solution. The DOX-loaded ICCLMs also inhibited the HepG2 cells' growth and proliferation but at a reduced level relative to the DOX-loaded CCLMs. This suggests that the release of DOX from ICCLMs may occur through polymer degradation by other

mechanisms (*e.g.*, oxidative degradation) in the cellular environment.[165] A time-dependent study of tumor cell inhibition activity over the course of 72 h was also conducted using the three samples at a constant DOX concentration (40 μg·mL^{-1}) (Figure 4.8 (B)). Notable tumor cell inhibition activities were observed with free DOX·HCl with 40% cell death after 12 h incubation. By contrast, DOX-loaded CCLMs and DOX-loaded ICCLMs exhibited delayed onset of tumor cell inhibition activities, evidenced by 15% and 19% cell inhibition at 22 h and 36 h for the former and the latter, respectively. After 72 h incubation, the DOX·HCl, DOX-loaded CCLMs and DOX-loaded ICCLMs exhibited a maximal cell inhibition of 84%, 64% and 49% respectively. Statistical T-tests revealed that the DOX-loaded CCLMs and DOX-loaded ICCLMs exhibited significantly different cell inhibition against HepG2 cells in the 5 to 100 μg·mL^{-1} concentration range (Figure 4.8 (A)) and over the 22 to 72 h time window (Figure 4.8 (B)) ($P < 0.05$). The higher tumor cell inhibition activities of DOX-loaded CCLMs relative to the DOX-loaded ICCLMs are tentatively attributed to the un-crosslinking of the CCLM micellar core under reductive environment in cancer cells, thereby enabling more efficient release of DOX and resulting in more HepG2 cell death from the CCLMs than the ICCLMs.

4.4 Conclusions

The first redox-responsive core-crosslinked micelles (CCLMs) based on amphiphilic block copolypeptoids were synthesized by combining primary amine-initiated ring-opening polymerization method with CuAAC click chemistry. The micellar structures (*i.e.*, size) can be tailored by adjusting the chemical composition of the constituting polymers. The polypeptoid-based CCLMs were shown to respond to reducing cues in solution (*e.g.*, DTT) by disintegrating into unimers or small aggregates. Both CCLMs and ICCLMs were minimally cytotoxic to HepG2 cells, evidenced by the cell viability study. Doxorubicin (DOX) can be efficiently encapsulated

within the polypeptoid-based CCLMs with maximally attainable 23% drug loading capacity and 34% drug loading efficiency. Accelerated drug release from the DOX-encapsulated CCLMs can be achieved by the addition of DTT in the micellar solution. *In vivo* cell culture studies revealed that the DOX-loaded CCLMs exhibited higher tumor cell inhibition activities against HepG2 cells than that of the DOX-loaded ICCLMs. This is attributed to the redox-triggered disintegration of the CCLMs in the cellular environment, resulting in more efficient release of the DOX from the CCLMs than the ICCLMs. However, the CCLMs have the drawbacks of incomplete drug release, resulting in lower tumor cell inhibition activity than the free DOX·HCl. This study suggests the potential use of polypeptoid-based CCLMs as redox-responsive nanocarriers for cancer therapy. Future efforts will focus on the new chemical designs of polypeptoid-based CCLMs (*i.e.*, crosslinkers and polymer structures) to improve total drug release efficiency.

4.5 Supplementary Data

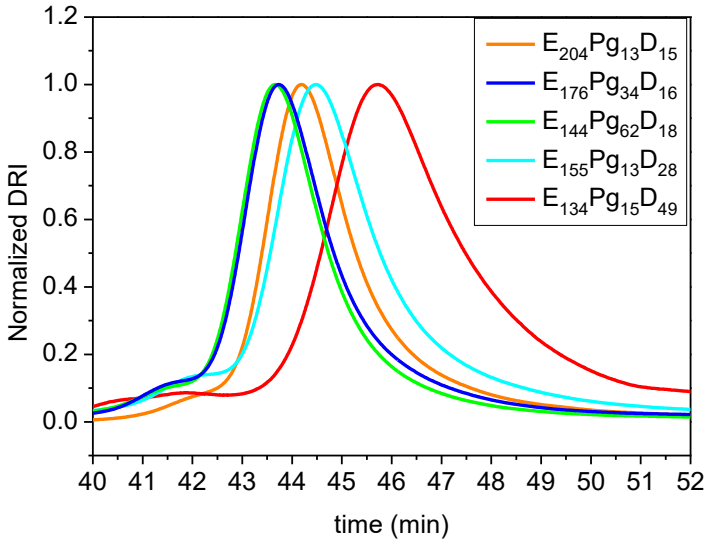

Figure S4.1. SEC chromatograms of PNEG-*b*-P(NPgG-*r*-NDG) with varying compositions (Entry 1-5, Table 4.1).

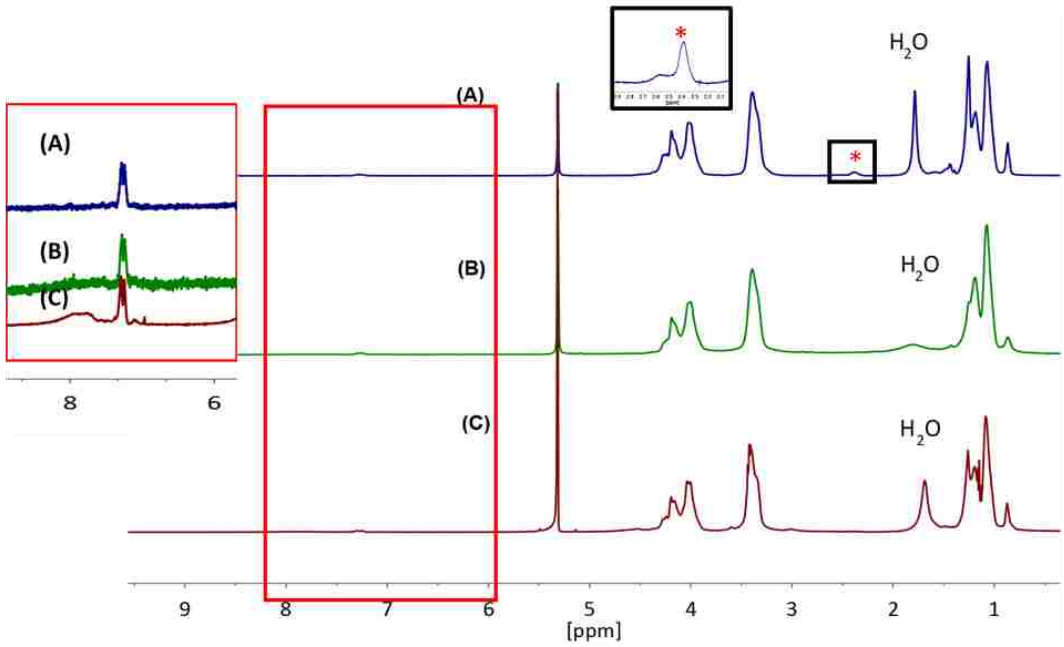

Figure S4.2. (A) ^{1}H NMR spectra of the $E_{204}Pg_{13}D_{15}$ unimer (Entry 1, Table 4.1), (B) the corresponding core-crosslinked micelles (CCLMs) and (C) the disintegrated micelles after DTT treatment in CD_2Cl_2.

Scheme S4.1. Synthesis of CCLMs and Cleavage of CCLMs using DTT.

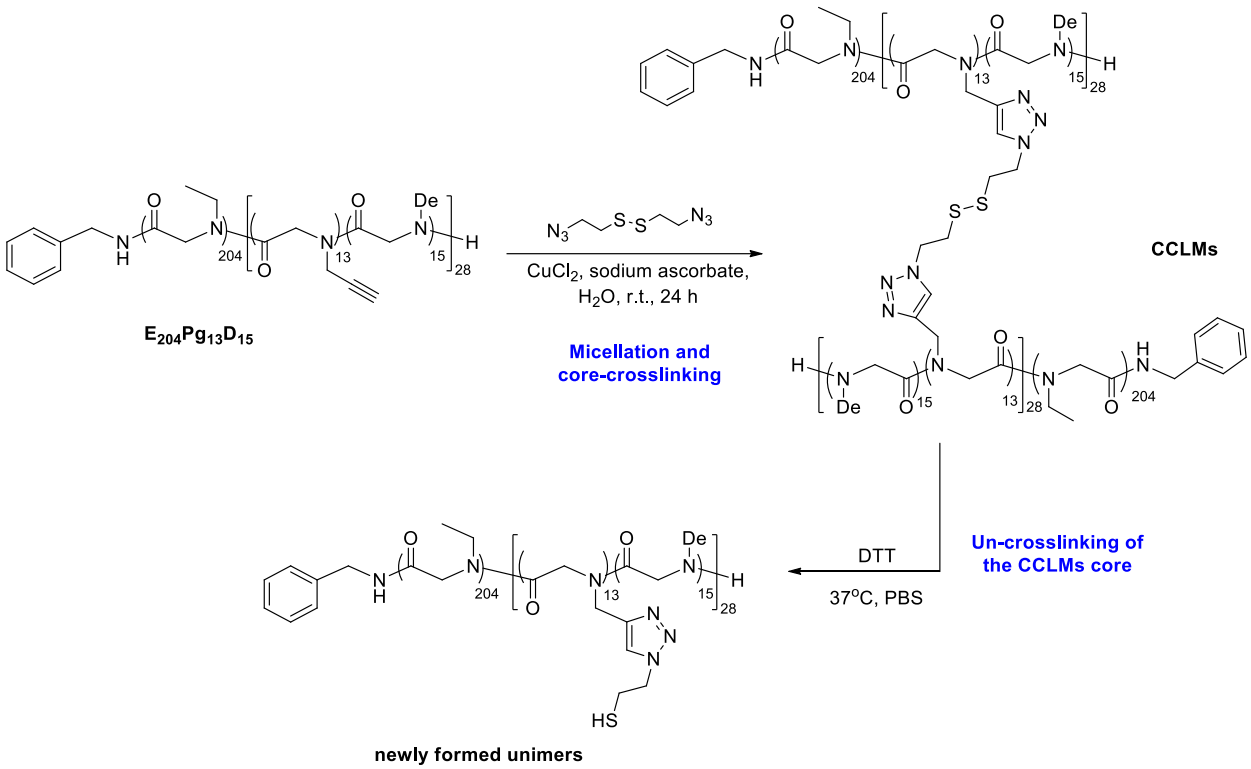

Chapter 5. Conclusions and Remarks

A big progress has been made by polymer chemists on the synthesis and characterization of diverse and functional polypeptoids in the past decade. In the next stage, how far a polypeptoid scientist can go in the biomedical application depends strongly on how easy and versatile the synthetic approaches can be. Pursuing facile polymerizations of polypeptoids never ends. It is a pleasure to work on this emerging but promising polymer in my graduate career. I could enrich the library of facile synthetic methods towards cyclic polypeptoids and push the polypeptoids in the biomedical research a little step further.

Amidine-mediated ring-opening polymerization (ROP) of *N*-butyl *N*-carboxyanhydrides (Bu-NCA) was investigated from four aspects, including the control over molecular weight (M_n) and molecular weight distribution (PDI), the identification of the polymerization, the kinetics of the polymerization, and the investigation of the polymer architecture. It was shown by this study that well-defined cyclic poly(*N*-butyl glycine)s (PNBGs) can be synthesized via this polymerization. The bicyclic amidine, DBU, is a good alternative of *N*-heterocyclic carbene (NHC) to mediate zwitterionic ring-opening polymerization (ZROP). However, the polymerization has slow initiation, and the M_ns of high molecular weight PNBGs are deviated from theoretical values. Seeking better alternatives among other organo-catalysts (*e.g.* pyridines, tertiary amine, and bicyclic guanidines) is still necessary.

By following the lately developed synthetic pathway, the cyclic bottlebrush polypeptoids which may possess unique properties were synthesized. The cyclic bottlebrush polypeptoids adopt a toroid structure in dry state and a cyclic architecture in methanol. In contrast, the linear bottlebrush polypeptoid analogs form rod-like aggregates in dry state. Out of expectation, zwitterionic cyclic polypeptoids have a strong tendency to form clusters in methanol. This

observation was further supported by the DLS analysis and the cryo-TEM image of cyclic bottlebrush polypeptoids (targeted DP= 400). The interplay of dipole-dipole interaction and solvophobic interaction is the driving force for the cluster formation, which cannot be prevented by the brush-like side chains of cyclic bottlebrush polypeptoids. This is the first time for us to perceive the effect of dipole-dipole interaction on the aggregation behaviors of zwitterionic cyclic polypeptoids in methanol.

The first smart drug carriers based on amphiphilic diblock copolypeptoids were synthesized via click chemistry. Our study demonstrated that the synthesized core-crosslinked micelles (CCLMs) are mono-disperse spherical micelles in both water and DMF. High drug loading capacity (DLC) (up to 23.1%) can be obtained by increasing the initial drug to polymer ratios (IDP). The CCLMs were shown to exhibit good biocompatibility and cancer cell inhibition activity. Polypeptoid-based micelles can be further assessed in the next stage of biomedical research. Fast cleavage of the disulfide crosslinking sites of the CCLMs upon treatment of dithothreitol (DTT) was indicated by the study of micellar dissociation (Chapter 4, Figure 4.5), but incomplete dissociation of and limited drug release efficiency of the CCLMs were observed. One possible reason for the problems is that the hydrophobic poly(*N*-butyl glycine) (PNDG) segments form crystallization after crosslinking, which prevents the disulfide cleavage deeper inside the hydrophobic core. The next-generation redox-responsive CCLMs composed of polypeptoids with the potential to undergo complete dissociation under a reducing environment can be prepared by using hydrophobic polypeptoids without side chain crystallization (*e.g.* poly(*N*-2-ethyl-1-hexyl glycine)).

References

1. Lahasky, S. H.; Hu, X.; Zhang, D., Thermoresponsive poly (α-peptoid) s: tuning the cloud point temperatures by composition and architecture. *ACS Macro Lett.* **2012**, *1*, 580-584.

2. Murphy, J. E.; Uno, T.; Hamer, J. D.; Cohen, F. E.; Dwarki, V.; Zuckermann, R. N., A combinatorial approach to the discovery of efficient cationic peptoid reagents for gene delivery. *Proceedings of the National Academy of Sciences* **1998**, *95*, 1517-1522.

3. Kirshenbaum, K.; Barron, A. E.; Goldsmith, R. A.; Armand, P.; Bradley, E. K.; Truong, K. T.; Dill, K. A.; Cohen, F. E.; Zuckermann, R. N., Sequence-specific polypeptoids: a diverse family of heteropolymers with stable secondary structure. *Proceedings of the National Academy of Sciences* **1998**, *95*, 4303-4308.

4. Armand, P.; Kirshenbaum, K.; Goldsmith, R. A.; Farr-Jones, S.; Barron, A. E.; Truong, K. T.; Dill, K. A.; Mierke, D. F.; Cohen, F. E.; Zuckermann, R. N., NMR determination of the major solution conformation of a peptoid pentamer with chiral side chains. *Proceedings of the National Academy of Sciences* **1998**, *95*, 4309-4314.

5. Wu, C. W.; Sanborn, T. J.; Zuckermann, R. N.; Barron, A. E., Peptoid oligomers with α-chiral, aromatic side chains: effects of chain length on secondary structure. *J. Am. Chem. Soc.* **2001**, *123*, 2958-2963.

6. Wu, C. W.; Sanborn, T. J.; Huang, K.; Zuckermann, R. N.; Barron, A. E., Peptoid oligomers with α-chiral, aromatic side chains: sequence requirements for the formation of stable peptoid helices. *J. Am. Chem. Soc.* **2001**, *123*, 6778-6784.

7. Guo, L.; Li, J.; Brown, Z.; Ghale, K.; Zhang, D., Synthesis and characterization of cyclic and linear helical poly (α-peptoid) s by N-heterocyclic carbene-mediated ring-opening polymerizations of N-substituted N-carboxyanhydrides. *Pept. Sci.* **2011**, *96*, 596-603.

8. Guo, L.; Zhang, D. *Non-Conventional Functional Block Copolymers*, American Chemical Society, **2011**.

9. Sanii, B.; Kudirka, R.; Cho, A.; Venkateswaran, N.; Olivier, G. K.; Olson, A. M.; Tran, H.; Harada, R. M.; Tan, L.; Zuckermann, R. N., Shaken, not stirred: Collapsing a peptoid monolayer to produce free-floating, stable nanosheets. *J. Am. Chem. Soc.* **2011**, *133*, 20808-20815.

10. Robertson, E. J.; Battigelli, A.; Proulx, C.; Mannige, R. V.; Haxton, T. K.; Yun, L.; Whitelam, S.; Zuckermann, R. N., Design, Synthesis, Assembly, and Engineering of Peptoid Nanosheets. *Acc. Chem. Res.* **2016**, *49*, 379-389.

11. Mannige, R. V.; Haxton, T. K.; Proulx, C.; Robertson, E. J.; Battigelli, A.; Butterfoss, G. L.; Zuckermann, R. N.; Whitelam, S., Peptoid nanosheets exhibit a new secondary-structure motif. *Nature* **2015**.

12. Zuckermann, R. N., Peptoid origins. *Pept. Sci.* **2011**, *96*, 545-555.

13. Szwarc, M. *Fortschritte der Hochpolymeren-Forschung*, Springer, **1965**.

14. Lee, C.-U.; Li, A.; Ghale, K.; Zhang, D., Crystallization and Melting Behaviors of Cyclic and Linear Polypeptoids with Alkyl Side Chains. *Macromolecules* **2013**, *46*, 8213-8223.

15. Fetsch, C.; Luxenhofer, R., Thermal Properties of Aliphatic Polypeptoids. *Polymers* **2013**, *5*, 112-127.

16. Rosales, A. M.; Murnen, H. K.; Zuckermann, R. N.; Segalman, R. A., Control of crystallization and melting behavior in sequence specific polypeptoids. *Macromolecules* **2010**, *43*, 5627-5636.

17. Sun, J.; Teran, A. A.; Liao, X.; Balsara, N. P.; Zuckermann, R. N., Crystallization in sequence-defined peptoid diblock copolymers induced by microphase separation. *J. Am. Chem. Soc.* **2014**, *136*, 2070-2077.

18. Gangloff, N.; Ulbricht, J.; Lorson, T.; Schlaad, H.; Luxenhofer, R., Peptoids and polypeptoids at the frontier of supra-and macromolecular engineering. *Chem. Rev.* **2015**, *116*, 1753-1802.

19. Fetsch, C.; Flecks, S.; Gieseler, D.; Marschelke, C.; Ulbricht, J.; van Pée, K. H.; Luxenhofer, R., Self-Assembly of Amphiphilic Block Copolypeptoids with C2-C5 Side Chains in Aqueous Solution. *Macromol. Chem. Phys.* **2015**, *216*, 547-560.

20. Murnen, H. K.; Rosales, A. M.; Dobrynin, A. V.; Zuckermann, R. N.; Segalman, R. A., Persistence length of polyelectrolytes with precisely located charges. *Soft Matter* **2013**, *9*, 90-98.

21. Robinson, J. W.; Secker, C.; Weidner, S.; Schlaad, H., Thermoresponsive Poly (N-C3 glycine) s. *Macromolecules* **2013**, *46*, 580-587.

22. Patch, J. A.; Barron, A. E., Mimicry of bioactive peptides via non-natural, sequence-specific peptidomimetic oligomers. *Curr. Opin. Chem. Biol.* **2002**, *6*, 872-877.

23. Zuckermann, R. N.; Kerr, J. M.; Kent, S. B.; Moos, W. H., Efficient method for the preparation of peptoids [oligo (N-substituted glycines)] by submonomer solid-phase synthesis. *J. Am. Chem. Soc.* **1992**, *114*, 10646-10647.

24. Hadjichristidis, N.; Iatrou, H.; Pitsikalis, M.; Sakellariou, G., Synthesis of well-defined polypeptide-based materials via the ring-opening polymerization of α-amino acid N-carboxyanhydrides. *Chem. Rev.* **2009**, *109*, 5528-5578.

25. Gibbs, T. J.; Boomhoff, M.; Tomkinson, N. C., A mild and efficient method for the one-pot monocarboxymethylation of primary amines. *Synlett* **2007**, *2007*, 1573-1576.

26. Fetsch, C.; Grossmann, A.; Holz, L.; Nawroth, J. F.; Luxenhofer, R., Polypeptoids from N-substituted glycine N-carboxyanhydrides: hydrophilic, hydrophobic, and amphiphilic polymers with poisson distribution. *Macromolecules* **2011**, *44*, 6746-6758.

27. Akssira, M.; Boumzebra, M.; Kasmi, H.; Dahdouh, A.; Roumestant, M.-L.; Viallefont, P., New Routes to 1, 4-benzodiazepin-2, 5-diones. *Tetrahedron* **1994**, *50*, 9051-9060.

28. Zhang, D.; Lahasky, S. H.; Guo, L.; Lee, C.-U.; Lavan, M., Polypeptoid materials: current status and future perspectives. *Macromolecules* **2012**, *45*, 5833-5841.

29. Xuan, S.; Lee, C.-U.; Chen, C.; Doyle, A. B.; Zhang, Y.; Guo, L.; John, V. T.; Hayes, D.; Zhang, D., Thermoreversible and Injectable ABC Polypeptoid Hydrogels: Controlling the Hydrogel Properties through Molecular Design. *Chem. Mater.* **2016**, *28*, 727-737.

30. Tao, X.; Deng, Y.; Shen, Z.; Ling, J., Controlled Polymerization of N-Substituted Glycine N-Thiocarboxyanhydrides Initiated by Rare Earth Borohydrides toward Hydrophilic and Hydrophobic Polypeptoids. *Macromolecules* **2014**, *47*, 6173-6180.

31. Tao, X.; Deng, C.; Ling, J., PEG-Amine-Initiated Polymerization of Sarcosine N-Thiocarboxyanhydrides Toward Novel Double-Hydrophilic PEG-b-Polysarcosine Diblock Copolymers. *Macromol. Rapid Commun.* **2014**, *35*, 875-881.

32. Kricheldorf, H. R.; von Lossow, C.; Schwarz, G., Primary Amine-Initiated Polymerizations of Alanine-NCA and Sarcosine-NCA. *Macromol. Chem. Phys.* **2004**, *205*, 918-924.

33. Sisido, M.; Imanishi, Y.; Higashimura, T., Molecular weight distribution of polysarcosine obtained by NCA polymerization. *Die Makromolekulare Chemie* **1977**, *178*, 3107-3114.

34. Chan, B. A.; Xuan, S.; Horton, M.; Zhang, D., 1, 1, 3, 3-Tetramethylguanidine-Promoted Ring-Opening Polymerization of N-Butyl N-Carboxyanhydride Using Alcohol Initiators. *Macromolecules* **2016**, *49*, 2002-2012.

35. Clarson, S.; Semlyen, J., Cyclic polysiloxanes: 1. Preparation and characterization of poly (phenylmethylsiloxane). *Polymer* **1986**, *27*, 1633-1636.

36. Bielawski, C. W.; Benitez, D.; Grubbs, R. H., An" endless" route to cyclic polymers. *Science* **2002**, *297*, 2041-2044.

37. Kricheldorf, H. R., Cyclic polymers: Synthetic strategies and physical properties. *J. Polym. Sci., Part A: Polym. Chem.* **2010**, *48*, 251-284.

38. Shin, E. J.; Jeong, W.; Brown, H. A.; Koo, B. J.; Hedrick, J. L.; Waymouth, R. M., Crystallization of cyclic polymers: synthesis and crystallization behavior of high molecular weight cyclic poly (ε-caprolactone) s. *Macromolecules* **2011**, *44*, 2773-2779.

39. Pérez, R.; Córdova, M.; López, J.; Hoskins, J.; Zhang, B.; Grayson, S.; Müller, A., Nucleation, crystallization, self-nucleation and thermal fractionation of cyclic and linear poly (ε-caprolactone) s. *React. Funct. Polym.* **2014**, *80*, 71-82.

40. Qiu, X.-P.; Tanaka, F.; Winnik, F. M., Temperature-induced phase transition of well-defined cyclic poly (N-isopropylacrylamide) s in aqueous solution. *Macromolecules* **2007**, *40*, 7069-7071.

41. Heo, K.; Kim, Y. Y.; Kitazawa, Y.; Kim, M.; Jin, K. S.; Yamamoto, T.; Ree, M., Structural characteristics of amphiphilic cyclic and linear block copolymer micelles in aqueous solutions. *ACS Macro Lett.* **2014**, *3*, 233-239.

42. Honda, S.; Yamamoto, T.; Tezuka, Y., Tuneable enhancement of the salt and thermal stability of polymeric micelles by cyclized amphiphiles. *Nature communications* **2013**, *4*, 1574.

43. Lecommandoux, S.; Borsali, R.; Schappacher, M.; Deffieux, A.; Narayanan, T.; Rochas, C., Microphase separation of linear and cyclic block copolymers poly (styrene-b-isoprene): SAXS experiments. *Macromolecules* **2004**, *37*, 1843-1848.

44. Zhu, Y.; Gido, S. P.; Iatrou, H.; Hadjichristidis, N.; Mays, J. W., Microphase separation of cyclic block copolymers of styrene and butadiene and of their corresponding linear triblock copolymers. *Macromolecules* **2003**, *36*, 148-152.

45. Poelma, J. E.; Ono, K.; Miyajima, D.; Aida, T.; Satoh, K.; Hawker, C. J., Cyclic Block Copolymers for Controlling Feature Sizes in Block Copolymer Lithography. *ACS Nano* **2012**, *6*, 10845-10854.

46. Zhang, K.; Lackey, M. A.; Cui, J.; Tew, G. N., Gels based on cyclic polymers. *J. Am. Chem. Soc.* **2011**, *133*, 4140-4148.

47. Cortez, M. A.; Godbey, W. T.; Fang, Y.; Payne, M. E.; Cafferty, B. J.; Kosakowska, K. A.; Grayson, S. M., The Synthesis of Cyclic Poly (ethylene imine) and Exact Linear Analogues: An Evaluation of Gene Delivery Comparing Polymer Architectures. *J. Am. Chem. Soc.* **2015**, *137*, 6541-6549.

48. Ishizu, K.; Ichimura, A., Synthesis of cyclic diblock copolymers by interfacial condensation. *Polymer* **1998**, *39*, 6555-6558.

49. Laurent, B. A.; Grayson, S. M., An efficient route to well-defined macrocyclic polymers via "click" cyclization. *J. Am. Chem. Soc.* **2006**, *128*, 4238-4239.

50. Xu, J.; Ye, J.; Liu, S., Synthesis of well-defined cyclic poly (N-isopropylacrylamide) via click chemistry and its unique thermal phase transition behavior. *Macromolecules* **2007**, *40*, 9103-9110.

51. Hoskins, J. N.; Grayson, S. M., Synthesis and degradation behavior of cyclic poly (ε-caprolactone). *Macromolecules* **2009**, *42*, 6406-6413.

52. Jia, Z.; Monteiro, M. J., Cyclic polymers: methods and strategies. *J. Polym. Sci., Part A: Polym. Chem.* **2012**, *50*, 2085-2097.

53. Kricheldorf, H. R.; Lee, S.-R., Polylactones. 35. Macrocyclic and Stereoselective Polymerization of. beta.-D, L-Butyrolactone with Cyclic Dibutyltin Initiators. *Macromolecules* **1995**, *28*, 6718-6725.

54. Xia, Y.; Boydston, A. J.; Yao, Y.; Kornfield, J. A.; Gorodetskaya, I. A.; Spiess, H. W.; Grubbs, R. H., Ring-expansion metathesis polymerization: catalyst-dependent polymerization profiles. *J. Am. Chem. Soc.* **2009**, *131*, 2670-2677.

55. Fan, X.; Huang, B.; Wang, G.; Huang, J., Synthesis of Amphiphilic Heteroeight-Shaped Polymer Cyclic-[Poly(ethylene oxide)-b-polystyrene]2 via "Click" Chemistry. *Macromolecules* **2012**, *45*, 3779-3786.

56. Hossain, M. D.; Jia, Z.; Monteiro, M. J., Complex Polymer Topologies Built from Tailored Multifunctional Cyclic Polymers. *Macromolecules* **2014**, *47*, 4955-4970.

57. Yamamoto, T., Synthesis of cyclic polymers and topology effects on their diffusion and thermal properties. *Polym. J.* **2013**, *45*, 711-717.

58. Ren, J. M.; Satoh, K.; Goh, T. K.; Blencowe, A.; Nagai, K.; Ishitake, K.; Christofferson, A. J.; Yiapanis, G.; Yarovsky, I.; Kamigaito, M., Stereospecific Cyclic Poly (methyl methacrylate) and Its Topology-Guided Hierarchically Controlled Supramolecular Assemblies. *Angew. Chem. Int. Ed.* **2014**, *53*, 459-464.

59. Brown, H. A.; Waymouth, R. M., Zwitterionic Ring-Opening Polymerization for the Synthesis of High Molecular Weight Cyclic Polymers. *Acc. Chem. Res.* **2013**, *46*, 2585-2596.

60. Culkin, D. A.; Jeong, W.; Csihony, S.; Gomez, E. D.; Balsara, N. P.; Hedrick, J. L.; Waymouth, R. M., Zwitterionic polymerization of lactide to cyclic poly(lactide) by using N-heterocyclic carbene organocatalysts. *Angew. Chem. Int. Ed.* **2007**, *46*, 2627-2630.

61. Jeong, W.; Shin, E. J.; Culkin, D. A.; Hedrick, J. L.; Waymouth, R. M., Zwitterionic polymerization: a kinetic strategy for the controlled synthesis of cyclic polylactide. *J. Am. Chem. Soc.* **2009**, *131*, 4884-4891.

62. Brown, H. A.; Xiong, S.; Medvedev, G. A.; Chang, Y. A.; Abu-Omar, M. M.; Caruthers, J. M.; Waymouth, R. M., Zwitterionic Ring-Opening Polymerization: Models for Kinetics of Cyclic Poly(caprolactone) Synthesis. *Macromolecules* **2014**, *47*, 2955-2963.

63. Acharya, A. K.; Chang, Y. A.; Jones, G. O.; Rice, J. E.; Hedrick, J. L.; Horn, H. W.; Waymouth, R. M., Experimental and Computational Studies on the Mechanism of Zwitterionic Ring-Opening Polymerization of Δ-Valerolactone with N-Heterocyclic Carbenes. *The Journal of Physical Chemistry B* **2014**, *118*, 6553-6560.

64. Guo, L.; Zhang, D., Cyclic poly (α-peptoid) s and their block copolymers from N-heterocyclic carbene-mediated ring-opening polymerizations of N-substituted N-carboxylanhydrides. *J. Am. Chem. Soc.* **2009**, *131*, 18072-18074.

65. Zhang, X.; Waymouth, R. M., Zwitterionic Ring Opening Polymerization with Isothioureas. *ACS Macro Lett.* **2014**, *3*, 1024-1028.

66. Asenjo-Sanz, I.; Veloso, A.; Miranda, J. I.; Pomposo, J. A.; Barroso-Bujans, F., Zwitterionic polymerization of glycidyl monomers to cyclic polyethers with B (C6F5) 3. *Polym. Chem.* **2014**, *5*, 6905-6908.

67. Brown, H. A.; Chang, Y. A.; Waymouth, R. M., Zwitterionic polymerization to generate high molecular weight cyclic poly(carbosiloxane)s. *J. Am. Chem. Soc.* **2013**, *135*, 18738-18741.

68. Shin, E. J.; Brown, H. A.; Gonzalez, S.; Jeong, W.; Hedrick, J. L.; Waymouth, R. M., Zwitterionic copolymerization: Synthesis of cyclic gradient copolymers. *Angew. Chem. Int. Ed.* **2011**, *50*, 6388-6391.

69. Lee, C.-U.; Smart, T. P.; Guo, L.; Epps III, T. H.; Zhang, D., Synthesis and characterization of amphiphilic cyclic diblock copolypeptoids from n-heterocyclic carbene-mediated zwitterionic polymerization of n-substituted n-carboxyanhydride. *Macromolecules* **2011**, *44*, 9574-9585.

70. Guo, L.; Lahasky, S. H.; Ghale, K.; Zhang, D., N-Heterocyclic Carbene-Mediated Zwitterionic Polymerization of N-Substituted N-Carboxyanhydrides toward Poly (α-peptoid) s: Kinetic, Mechanism, and Architectural Control. *J. Am. Chem. Soc.* **2012**, *134*, 9163-9171.

71. Kricheldorf, H. R.; Bösinger, K., Mechanismus der NCA-Polymerisation, 3. Über die Amin katalysierte Polymerisation von Sarkosin-NCA und-NTA. *Makromol. Chem.* **1976**, *177*, 1243-1258.

72. Kricheldorf, H. R.; Von Lossow, C.; Schwarz, G., Tertiary amine catalyzed polymerizations of α-amino acid N-carboxyanhydrides: The role of cyclization. *J. Polym. Sci., Part A: Polym. Chem.* **2006**, *44*, 4680-4695.

73. Kricheldorf, H. R.; von Lossow, C.; Schwarz, G., Cyclic polypeptides by solvent-induced polymerizations of α-amino acid N-carboxyanhydrides. *Macromolecules* **2005**, *38*, 5513-5518.

74. Kricheldorf, H. R.; Lossow, C. V.; Lomadze, N.; Schwarz, G., Cyclic polypeptides by thermal polymerization of α-amino acid N-carboxyanhydrides. *J. Polym. Sci., Part A: Polym. Chem.* **2008**, *46*, 4012-4020.

75. Lahasky, S. H.; Serem, W. K.; Guo, L.; Garno, J. C.; Zhang, D., Synthesis and characterization of cyclic brush-like polymers by N-heterocyclic carbene-mediated zwitterionic polymerization of N-propargyl N-carboxyanhydride and the grafting-to approach. *Macromolecules* **2011**, *44*, 9063-9074.

76. Xia, Y.; Boydston, A. J.; Grubbs, R. H., Synthesis and direct imaging of ultrahigh molecular weight cyclic brush polymers. *Angew. Chem. Int. Ed.* **2011**, *50*, 5882-5885.

77. Boydston, A. J.; Holcombe, T. W.; Unruh, D. A.; Fréchet, J. M.; Grubbs, R. H., A direct route to cyclic organic nanostructures via ring-expansion metathesis polymerization of a dendronized macromonomer. *J. Am. Chem. Soc.* **2009**, *131*, 5388-5389.

78. Schappacher, M.; Deffieux, A., Atomic force microscopy imaging and dilute solution properties of cyclic and linear polystyrene combs. *J. Am. Chem. Soc.* **2008**, *130*, 14684-14689.

79. Schappacher, M.; Deffieux, A., Imaging of Catenated, Figure-of-Eight, and Trefoil Knot Polymer Rings. *Angew. Chem. Int. Ed.* **2009**, *121*, 6044-6047.

80. Schappacher, M.; Deffieux, A., Synthesis of macrocyclic copolymer brushes and their self-assembly into supramolecular tubes. *Science* **2008**, *319*, 1512-1515.

81. Asano, N.; Kitamura, S.; Terao, K., Local conformation and intermolecular interaction of rigid ring polymers are not always the same as the linear analogue: cyclic amylose tris (phenylcarbamate) in Θ solvents. *The Journal of Physical Chemistry B* **2013**, *117*, 9576-9583.

82. Wang, Y.; Qin, W.; Qiu, D., Small-Angle Neutron Scattering Study of Cyclic Poly (ethylene glycol) Adsorption on Colloidal Particles. *Langmuir* **2014**, *30*, 5170-5175.

83. Lu, H.; Bai, Y.; Wang, J.; Gabrielson, N. P.; Wang, F.; Lin, Y.; Cheng, J., Ring-opening polymerization of γ-(4-vinylbenzyl)-L-glutamate N-carboxyanhydride for the synthesis of functional polypeptides. *Macromolecules* **2011**, *44*, 6237-6240.

84. Robinson, J. W.; Schlaad, H., A versatile polypeptoid platform based on N-allyl glycine. *Chem. Commun.* **2012**, *48*, 7835-7837.

85. Secker, C.; Robinson, J. W.; Schlaad, H., Alkyne-X modification of polypeptoids. *Eur. Polym. J.* **2015**, *62*, 394-399.

86. Lu, L.; Lahasky, S. H.; Zhang, D.; Garno, J. C., Directed Growth of Polymer Nanorods using Surface-Initiated Ring-Opening Polymerization of N-Allyl N-Carboxyanhydride. *ACS applied materials & interfaces* **2016**, *8*, 4014-4022.

87. Schneider, M.; Tang, Z.; Richter, M.; Marschelke, C.; Förster, P.; Wegener, E.; Amin, I.; Zimmermann, H.; Scharnweber, D.; Braun, H. G., Patterned Polypeptoid Brushes. *Macromol. Biosci.* **2016**, *16*, 75-81.

88. Tao, X.; Du, J.; Wang, Y.; Ling, J., Polypeptoids with tunable cloud point temperatures synthesized from N-substituted glycine N-thiocarboxyanhydrides. *Polym. Chem.* **2015**, *6*, 3164-3174.

89. Cowie, J.; Sirianni, A., The solution properties of some polyoxyethylene-polyoxypropylene surfactants in nonaqueous solvents. *J. Am. Oil Chem. Soc.* **1966**, *43*, 572-575.

90. Enyiegbulam, M.; Hourston, D., Formation of ABA poly (styrene-b-butadiene) copolymer micelles in methyl ethyl ketone and other solvents. *Polymer* **1978**, *19*, 727-729.

91. Kotaka, T.; Tanaka, T.; Hattori, M.; Inagaki, H., Block copolymer micelles in dilute solution. *Macromolecules* **1978**, *11*, 138-145.

92. Dawkins, J. V.; Taylor, G., Micelle formation by AB block copolymers of polystyrene and poly (dimethylsiloxane) in n-alkanes. *Die Makromolekulare Chemie* **1979**, *180*, 1737-1741.

93. Bednář, B.; Devátý, J.; Koupalova, B.; Králíček, J.; Tuzar, Z., Micellization of three-block copolymer poly [styrene-b-(ethene-co-butene)-b-styrene] in mixed solvents of tetrahydrofuran/ethanol. *Polymer* **1984**, *25*, 1178-1184.

94. Yokoyama, M.; Miyauchi, M.; Yamada, N.; Okano, T.; Sakurai, Y.; Kataoka, K.; Inoue, S., Characterization and anticancer activity of the micelle-forming polymeric anticancer drug adriamycin-conjugated poly (ethylene glycol)-poly (aspartic acid) block copolymer. *Cancer Res.* **1990**, *50*, 1693-1700.

95. Yokoyama, M.; Okano, T.; Sakurai, Y.; Ekimoto, H.; Shibazaki, C.; Kataoka, K., Toxicity and antitumor activity against solid tumors of micelle-forming polymeric anticancer drug and its extremely long circulation in blood. *Cancer Res.* **1991**, *51*, 3229-3236.

96. Kim, D.; Lee, E. S.; Oh, K. T.; Gao, Z. G.; Bae, Y. H., Doxorubicin-Loaded Polymeric Micelle Overcomes Multidrug Resistance of Cancer by Double-Targeting Folate Receptor and Early Endosomal pH. *Small* **2008**, *4*, 2043-2050.

97. Yan, Y.; Ochs, C. J.; Such, G. K.; Heath, J. K.; Nice, E. C.; Caruso, F., Bypassing multidrug resistance in cancer cells with biodegradable polymer capsules. *Adv. Mater.* **2010**, *22*, 5398-5403.

98. Matsumura, Y.; Maeda, H., A new concept for macromolecular therapeutics in cancer chemotherapy: mechanism of tumoritropic accumulation of proteins and the antitumor agent smancs. *Cancer Res.* **1986**, *46*, 6387-6392.

99. Maeda, H., SMANCS and polymer-conjugated macromolecular drugs: advantages in cancer chemotherapy. *Adv. Drug Del. Rev.* **2001**, *46*, 169-185.

100. Stolnik, S.; Illum, L.; Davis, S., Long circulating microparticulate drug carriers. *Adv. Drug Del. Rev.* **2012**, *64*, 290-301.

101. Liu, J.; Zeng, F.; Allen, C., In vivo fate of unimers and micelles of a poly (ethylene glycol)-block-poly (caprolactone) copolymer in mice following intravenous administration. *European Journal of Pharmaceutics and Biopharmaceutics* **2007**, *65*, 309-319.

102. Henselwood, F.; Liu, G., Water-soluble nanospheres of poly (2-cinnamoylethyl methacrylate)-block-poly (acrylic acid). *Macromolecules* **1997**, *30*, 488-493.

103. Thurmond, K. B.; Kowalewski, T.; Wooley, K. L., Water-soluble knedel-like structures: the preparation of shell-cross-linked small particles. *J. Am. Chem. Soc.* **1996**, *118*, 7239-7240.

104. Zhang, Q.; Remsen, E. E.; Wooley, K. L., Shell cross-linked nanoparticles containing hydrolytically degradable, crystalline core domains. *J. Am. Chem. Soc.* **2000**, *122*, 3642-3651.

105. Wei, H.; Zhuo, R.-X.; Zhang, X.-Z., Design and development of polymeric micelles with cleavable links for intracellular drug delivery. *Prog. Polym. Sci.* **2013**, *38*, 503-535.

106. Gil, E. S.; Hudson, S. M., Stimuli-reponsive polymers and their bioconjugates. *Prog. Polym. Sci.* **2004**, *29*, 1173-1222.

107. Talelli, M.; Barz, M.; Rijcken, C. J.; Kiessling, F.; Hennink, W. E.; Lammers, T., Core-Crosslinked Polymeric Micelles: Principles, Preparation, Biomedical Applications and Clinical Translation. *Nano Today* **2015**, *10*, 93-117.

108. Lee, H.-i.; Wu, W.; Oh, J. K.; Mueller, L.; Sherwood, G.; Peteanu, L.; Kowalewski, T.; Matyjaszewski, K., Light-Induced Reversible Formation of Polymeric Micelles. *Angew. Chem. Int. Ed.* **2007**, *119*, 2505-2509.

109. Jiang, X.; Lavender, C. A.; Woodcock, J. W.; Zhao, B., Multiple micellization and dissociation transitions of thermo-and light-sensitive poly (ethylene oxide)-b-poly (ethoxytri (ethylene glycol) acrylate-co-o-nitrobenzyl acrylate) in water. *Macromolecules* **2008**, *41*, 2632-2643.

110. Kumar, S.; Allard, J.-F.; Morris, D.; Dory, Y. L.; Lepage, M.; Zhao, Y., Near-infrared light sensitive polypeptide block copolymer micelles for drug delivery. *J. Mater. Chem.* **2012**, *22*, 7252-7257.

111. Liu, G.-Y.; Chen, C.-J.; Li, D.-D.; Wang, S.-S.; Ji, J., Near-infrared light-sensitive micelles for enhanced intracellular drug delivery. *J. Mater. Chem.* **2012**, *22*, 16865-16871.

112. Neradovic, D.; Van Nostrum, C.; Hennink, W., Thermoresponsive polymeric micelles with controlled instability based on hydrolytically sensitive N-isopropylacrylamide copolymers. *Macromolecules* **2001**, *34*, 7589-7591.

113. Liu, S. Q.; Tong, Y. W.; Yang, Y. Y., Incorporation and in vitro release of doxorubicin in thermally sensitive micelles made from poly(N-isopropylacrylamide-co-N,N-dimethylacrylamide)-b-poly(D,L-lactide-co-glyco lide) with varying compositions. *Biomaterials* **2005**, *26*, 5064-5074.

114. Jiang, X.; Liu, S.; Narain, R., Degradable thermoresponsive core cross-linked micelles: fabrication, surface functionalization, and biorecognition. *Langmuir* **2009**, *25*, 13344-13350.

115. Gerweck, L. E.; Seetharaman, K., Cellular pH gradient in tumor versus normal tissue: potential exploitation for the treatment of cancer. *Cancer Res.* **1996**, *56*, 1194-1198.

116. Kuppusamy, P.; Li, H.; Ilangovan, G.; Cardounel, A. J.; Zweier, J. L.; Yamada, K.; Krishna, M. C.; Mitchell, J. B., Noninvasive imaging of tumor redox status and its modification by tissue glutathione levels. *Cancer Res.* **2002**, *62*, 307-312.

117. Fan, J.; Zeng, F.; Wu, S.; Wang, X., Polymer micelle with pH-triggered hydrophobic–hydrophilic transition and de-cross-linking process in the core and its application for targeted anticancer drug delivery. *Biomacromolecules* **2012**, *13*, 4126-4137.

118. Kakizawa, Y.; Harada, A.; Kataoka, K., Glutathione-sensitive stabilization of block copolymer micelles composed of antisense DNA and thiolated poly (ethylene glycol)-b lock-poly

(l-lysine): a potential carrier for systemic delivery of antisense DNA. *Biomacromolecules* **2001**, *2*, 491-497.

119. Ma, N.; Li, Y.; Xu, H.; Wang, Z.; Zhang, X., Dual redox responsive assemblies formed from diselenide block copolymers. *J. Am. Chem. Soc.* **2009**, *132*, 442-443.

120. Napoli, A.; Valentini, M.; Tirelli, N.; Müller, M.; Hubbell, J. A., Oxidation-responsive polymeric vesicles. *Nature materials* **2004**, *3*, 183-189.

121. Broaders, K. E.; Grandhe, S.; Fréchet, J. M., A biocompatible oxidation-triggered carrier polymer with potential in therapeutics. *J. Am. Chem. Soc.* **2010**, *133*, 756-758.

122. Ding, J.; Chen, J.; Li, D.; Xiao, C.; Zhang, J.; He, C.; Zhuang, X.; Chen, X., Biocompatible reduction-responsive polypeptide micelles as nanocarriers for enhanced chemotherapy efficacy in vitro. *J. Mater. Chem. B* **2013**, *1*, 69-81.

123. Zhong, Y.; Yang, W.; Sun, H.; Cheng, R.; Meng, F.; Deng, C.; Zhong, Z., Ligand-directed reduction-sensitive shell-sheddable biodegradable micelles actively deliver doxorubicin into the nuclei of target cancer cells. *Biomacromolecules* **2013**, *14*, 3723-3730.

124. Li, Y.; Xiao, K.; Luo, J.; Xiao, W.; Lee, J. S.; Gonik, A. M.; Kato, J.; Dong, T. A.; Lam, K. S., Well-defined, reversible disulfide cross-linked micelles for on-demand paclitaxel delivery. *Biomaterials* **2011**, *32*, 6633-6645.

125. Wei, R.; Cheng, L.; Zheng, M.; Cheng, R.; Meng, F.; Deng, C.; Zhong, Z., Reduction-responsive disassemblable core-cross-linked micelles based on poly(ethylene glycol)-b-poly(N-2-hydroxypropyl methacrylamide)-lipoic acid conjugates for triggered intracellular anticancer drug release. *Biomacromolecules* **2012**, *13*, 2429-2438.

126. Cheng, Y.; He, C.; Xiao, C.; Ding, J.; Ren, K.; Yu, S.; Zhuang, X.; Chen, X., Reduction-responsive cross-linked micelles based on PEGylated polypeptides prepared via click chemistry. *Polym. Chem.* **2013**, *4*, 3851-3858.

127. Wang, H.; Tang, L.; Tu, C.; Song, Z.; Yin, Q.; Yin, L.; Zhang, Z.; Cheng, J., Redox-responsive, core-cross-linked micelles capable of on-demand, concurrent drug release and structure disassembly. *Biomacromolecules* **2013**, *14*, 3706-3712.

128. Cajot, S.; Lautram, N.; Passirani, C.; Jérôme, C., Design of reversibly core cross-linked micelles sensitive to reductive environment. *J. Controlled Release* **2011**, *152*, 30-36.

129. Qin, A.; Tian, M.; Ramireddy, C.; Webber, S. E.; Munk, P.; Tuzar, Z., Polystyrene-poly (methacrylic acid) block copolymer micelles. *Macromolecules* **1994**, *27*, 120-126.

130. Bluhm, T.; Malhotra, S., Poly (styrene-b-isoprene) micelles. Effect of molecular weight on micelle size. *Eur. Polym. J.* **1986**, *22*, 249-251.

131. Brown, D. S.; Dawkins, J. V.; Farnell, A. S.; Taylor, G., Study of micelle formation by the diblock copolymer poly (styrene-b-dimethyl siloxane) in n-dodecane by small angle X-ray scattering. *Eur. Polym. J.* **1987**, *23*, 463-467.

132. Linse, P., Micellization of poly (ethylene oxide)-poly (propylene oxide) block copolymers in aqueous solution. *Macromolecules* **1993,** *26*, 4437-4449.

133. Kabanov, A. V.; Batrakova, E. V.; Melik-Nubarov, N. S.; Fedoseev, N. A.; Dorodnich, T. Y.; Alakhov, V. Y.; Chekhonin, V. P.; Nazarova, I. R.; Kabanov, V. A., A new class of drug carriers: micelles of poly (oxyethylene)-poly (oxypropylene) block copolymers as microcontainers for drug targeting from blood in brain. *J. Controlled Release* **1992**, *22*, 141-157.

134. Zhou, Z.; Chu, B., Phase behavior and association properties of poly (oxypropylene)-poly (oxyethylene)-poly (oxypropylene) triblock copolymer in aqueous solution. *Macromolecules* **1994**, *27*, 2025-2033.

135. Prud'homme, R. K.; Wu, G.; Schneider, D. K., Structure and rheology studies of poly (oxyethylene-oxypropylene-oxyethylene) aqueous solution. *Langmuir* **1996**, *12*, 4651-4659.

136. Alexandridis, P.; Holzwarth, J. F.; Hatton, T. A., Micellization of poly (ethylene oxide)-poly (propylene oxide)-poly (ethylene oxide) triblock copolymers in aqueous solutions: thermodynamics of copolymer association. *Macromolecules* **1994**, *27*, 2414-2425.

137. Lee, S. Y.; Tyler, J. Y.; Kim, S.; Park, K.; Cheng, J. X., FRET imaging reveals different cellular entry routes of self-assembled and disulfide bonded polymeric micelles. *Mol. Pharm.* **2013**, *10*, 3497-3506.

138. Zhang, Z.; Yin, L.; Tu, C.; Song, Z.; Zhang, Y.; Xu, Y.; Tong, R.; Zhou, Q.; Ren, J.; Cheng, J., Redox-Responsive, Core Cross-Linked Polyester Micelles. *ACS Macro Lett* **2013**, *2*, 40-44.

139. Hamaguchi, T.; Matsumura, Y.; Suzuki, M.; Shimizu, K.; Goda, R.; Nakamura, I.; Nakatomi, I.; Yokoyama, M.; Kataoka, K.; Kakizoe, T., NK105, a paclitaxel-incorporating micellar nanoparticle formulation, can extend in vivo antitumour activity and reduce the neurotoxicity of paclitaxel. *Br. J. Cancer* **2005**, *92*, 1240-1246.

140. Kim, S. C.; Kim, D. W.; Shim, Y. H.; Bang, J. S.; Oh, H. S.; Kim, S. W.; Seo, M. H., In vivo evaluation of polymeric micellar paclitaxel formulation: toxicity and efficacy. *J. Controlled Release* **2001**, *72*, 191-202.

141. Yang, T.; Cui, F. D.; Choi, M. K.; Cho, J. W.; Chung, S. J.; Shim, C. K.; Kim, D. D., Enhanced solubility and stability of PEGylated liposomal paclitaxel: in vitro and in vivo evaluation. *Int. J. Pharm.* **2007**, *338*, 317-326.

142. Harrington, K.; Lewanski, C.; Northcote, A.; Whittaker, J.; Wellbank, H.; Vile, R.; Peters, A.; Stewart, J., Phase I-II study of pegylated liposomal cisplatin (SPI-077 TM) in patients with inoperable head and neck cancer. *Ann. Oncol.* **2001**, *12*, 493-496.

143. Hamad, I.; Hunter, A. C.; Szebeni, J.; Moghimi, S. M., Poly(ethylene glycol)s generate complement activation products in human serum through increased alternative pathway turnover and a MASP-2-dependent process. *Mol. Immunol.* **2008**, *46*, 225-232.

144. Moghimi, S. M.; Hunter, A. C.; Dadswell, C. M.; Savay, S.; Alving, C. R.; Szebeni, J., Causative factors behind poloxamer 188 (Pluronic F68, Flocor)-induced complement activation in human sera. A protective role against poloxamer-mediated complement activation by elevated serum lipoprotein levels. *Biochim. Biophys. Acta* **2004**, *1689*, 103-113.

145. Ishida, T.; Kiwada, H., Accelerated blood clearance (ABC) phenomenon upon repeated injection of PEGylated liposomes. *Int. J. Pharm.* **2008**, *354*, 56-62.

146. Ishida, T.; Harada, M.; Wang, X. Y.; Ichihara, M.; Irimura, K.; Kiwada, H., Accelerated blood clearance of PEGylated liposomes following preceding liposome injection: effects of lipid dose and PEG surface-density and chain length of the first-dose liposomes. *J. Controlled Release* **2005**, *105*, 305-317.

147. Wang, X.; Ishida, T.; Kiwada, H., Anti-PEG IgM elicited by injection of liposomes is involved in the enhanced blood clearance of a subsequent dose of PEGylated liposomes. *J. Controlled Release* **2007**, *119*, 236-244.

148. Ishida, T.; Kashima, S.; Kiwada, H., The contribution of phagocytic activity of liver macrophages to the accelerated blood clearance (ABC) phenomenon of PEGylated liposomes in rats. *J. Controlled Release* **2008**, *126*, 162-165.

149. Sun, J.; Jiang, X.; Lund, R.; Downing, K. H.; Balsara, N. P.; Zuckermann, R. N., Self-assembly of crystalline nanotubes from monodisperse amphiphilic diblock copolypeptoid tiles. *Proceedings of the National Academy of Sciences* **2016**, *113*, 3954-3959.

150. Birke, A.; Huesmann, D.; Kelsch, A.; Weilbächer, M.; Xie, J.; Bros, M.; Bopp, T.; Becker, C.; Landfester, K.; Barz, M., Polypeptoid-block-polypeptide copolymers: Synthesis, characterization, and application of amphiphilic block copolypept (o) ides in drug formulations and miniemulsion techniques. *Biomacromolecules* **2014**, *15*, 548-557.

151. Heller, P.; Mohr, N.; Birke, A.; Weber, B.; Reske-Kunz, A.; Bros, M.; Barz, M., Directed Interactions of Block Copolypept (o) ides with Mannose-binding Receptors: PeptoMicelles Targeted to Cells of the Innate Immune System. *Macromol. Biosci.* **2015**, *15*, 63-73.

152. Heller, P.; Birke, A.; Huesmann, D.; Weber, B.; Fischer, K.; Reske-Kunz, A.; Bros, M.; Barz, M., Introducing PeptoPlexes: Polylysine-block-Polysarcosine Based Polyplexes for Transfection of HEK 293T Cells. *Macromol. Biosci.* **2014**, *14*, 1380-1395.

153. Holm, R.; Klinker, K.; Weber, B.; Barz, M., Synthesis of Amphiphilic Block Copolypept (o) ides by Bifunctional Initiators: Making PeptoMicelles Redox Sensitive. *Macromol. Rapid Commun.* **2015**, *36*, 2083-2091.

154. Hara, E.; Makino, A.; Kurihara, K.; Yamamoto, F.; Ozeki, E.; Kimura, S., Pharmacokinetic change of nanoparticulate formulation "Lactosome" on multiple administrations. *Int. Immunopharmacol.* **2012**, *14*, 261-266.

155. Hara, E.; Ueda, M.; Makino, A.; Hara, I.; Ozeki, E.; Kimura, S., Factors influencing in vivo disposition of polymeric micelles on multiple administrations. *ACS medicinal chemistry letters* **2014**, *5*, 873-877.

156. Hara, E.; Ueda, M.; Kim, C. J.; Makino, A.; Hara, I.; Ozeki, E.; Kimura, S., Suppressive immune response of poly-(sarcosine) chains in peptide-nanosheets in contrast to polymeric micelles. *J. Pept. Sci.* **2014**, *20*, 570-577.

157. Simon, R. J.; Kani, R. S.; Zuckerman, R. N.; Huebner, V. D.; Jewell, D. A.; Banville, S.; Ng, S.; Wang, L.; Rosenberg, S.; Marlowe, C. K.; Spellmeyer, D. C.; Tan, R.; Frankel, A. D.; Santi, D. V.; Cohen, F. E.; Bartlett, P. A. *Proc. Natl. Acad. Sci. USA* **1992**, *89*, 9367-9371.

158. Kirshenbaum, K.; Barron, A. E.; Goldsmith, R. A.; Armand, P.; Bradley, E. K.; Truong, K. T.; Dill, K. A.; Cohen, F. E.; Zuckermann, R. N., Sequence-specific polypeptoids: a diverse family of heteropolymers with stable secondary structure. *Proc. Natl. Acad. Sci. USA* **1998**, *95*, 4303-4308.

159. Lee, B.-C.; Zuckermann, R. N.; Dill, K. A., Folding a nonbiological polymer into a compact multihelical structure. *J. Am. Chem. Soc.* **2005**, *127*, 10999-11009.

160. Rosales, A. M.; Murnen, H. K.; Kline, S. R.; Zuckermann, R. N.; Segalman, R. A., Determination of the persistence length of helical and non-helical polypeptoids in solution. *Soft Matter* **2012**, *8*, 3673-3680.

161. Baldauf, C.; Gunther, R.; Hofmann, H. J., Helices in peptoids of alpha- and beta-peptides. *Phys. Biol.* **2006**, *3*, 1-9.

162. Guo, L.; Li, J.; Brown, Z.; Ghale, K.; Zhang, D., Synthesis and characterization of cyclic and linear helical poly(α-peptoid)s by N-heterocyclic carbene-mediated ring-opening polymerizations of N-substituted N-carboxyanhydrides. *Biopolymers* **2011**, *96*, 596-603.

163. Tanisaka, H.; Kizaka-Kondoh, S.; Makino, A.; Tanaka, S.; Hiraoka, M.; Kimura, S., Near-infrared fluorescent labeled peptosome for application to cancer imaging. *Bioconjug. Chem.* **2007**, *19*, 109-117.

164. Makino, A.; Kizaka-Kondoh, S.; Yamahara, R.; Hara, I.; Kanzaki, T.; Ozeki, E.; Hiraoka, M.; Kimura, S., Near-infrared fluorescence tumor imaging using nanocarrier composed of poly (L-lactic acid)-block-poly (sarcosine) amphiphilic polydepsipeptide. *Biomaterials* **2009**, *30*, 5156-5160.

165. Ulbricht, J.; Jordan, R.; Luxenhofer, R., On the biodegradability of polyethylene glycol, polypeptoids and poly(2-oxazoline)s. *Biomaterials* **2014**, *35*, 4848-4861.

166. Shin, E. J.; Jeong, W.; Brown, H. A.; Koo, B. J.; Hedrick, J. L.; Waymouth, R. M., Crystallization of Cyclic Polymers: Synthesis and Crystallization Behavior of High Molecular Weight Cyclic Poly(ε-caprolactone)s. *Macromolecules* **2011**, *44*, 2773-2779.

167. Yamamoto, T.; Tezuka, Y., Topological polymer chemistry: a cyclic approach toward novel polymer properties and functions. *Polym. Chem.* **2011**, *2*, 1930-1941.

168. Ono, N.; Yamada, T.; Saito, T.; Tanaka, K.; Kaji, A., A convenient procedure for esterification of carboxylic acids. *Bull. Chem. Soc. Jpn.* **1978**, *51*, 2401-2404.

169. Lohmeijer, B. G.; Pratt, R. C.; Leibfarth, F.; Logan, J. W.; Long, D. A.; Dove, A. P.; Nederberg, F.; Choi, J.; Wade, C.; Waymouth, R. M., Guanidine and amidine organocatalysts for ring-opening polymerization of cyclic esters. *Macromolecules* **2006**, *39*, 8574-8583.

170. Coady, D. J.; Fukushima, K.; Horn, H. W.; Rice, J. E.; Hedrick, J. L., Catalytic insights into acid/base conjugates: highly selective bifunctional catalysts for the ring-opening polymerization of lactide. *Chem. Commun.* **2011**, *47*, 3105-3107.

171. Iwasaki, Y.; Yamaguchi, E., Synthesis of Well-Defined Thermoresponsive Polyphosphoester Macroinitiators Using Organocatalysts. *Macromolecules* **2010**, *43*, 2664-2666.

172. Todd, R.; Tempelaar, S.; Lo Re, G.; Spinella, S.; McCallum, S. A.; Gross, R. A.; Raquez, J.-M.; Dubois, P., Poly (ω-pentadecalactone)-b-poly (l-lactide) Block Copolymers via Organic-Catalyzed Ring Opening Polymerization and Potential Applications. *ACS Macro Lett.* **2015**, *4*, 408-411.

173. De Rycke, N.; Couty, F.; David, O. R., Increasing the reactivity of nitrogen catalysts. *Chemistry* **2011**, *17*, 12852-12871.

174. Baidya, M.; Mayr, H., Nucleophilicities and carbon basicities of DBU and DBN. *Chem. Commun.* **2008**, 1792-1794.

175. Carafa, M.; Mesto, E.; Quaranta, E., DBU-Promoted Nucleophilic Activation of Carbonic Acid Diesters. *Eur. J. Org. Chem.* **2011**, *2011*, 2458-2465.

176. Shieh, W.-C.; Dell, S.; Repic, O., Nucleophilic catalysis with 1, 8-diazabicyclo [5.4. 0] undec-7-ene (DBU) for the esterification of carboxylic acids with dimethyl carbonate. *J. Org. Chem.* **2002**, *67*, 2188-2191.

177. Brown, H. A.; De Crisci, A. G.; Hedrick, J. L.; Waymouth, R. M., Amidine-Mediated Zwitterionic Polymerization of Lactide. *ACS Macro Lett.* **2012**, *1*, 1113-1115.

178. Nečas, D.; Klapetek, P., Gwyddion: an open-source software for SPM data analysis. *Open Phys.* **2012**, *10*, 181-188.

179. Li, X.; Guo, L.; Casiano-Maldonado, M.; Zhang, D.; Wesdemiotis, C., Top-down multidimensional mass spectrometry methods for synthetic polymer analysis. *Macromolecules* **2011**, *44*, 4555-4564.

180. Wang, L.; Bochmann, M.; Cannon, R. D.; Carpentier, J.-F.; Roisnel, T.; Sarazin, Y., Kinetic Analysis of the Living Ring-Opening Polymerisation ofL-Lactide with Tin(II) Initiators. *Eur. J. Inorg. Chem.* **2013**, *2013*, 5896-5905.

181. Guo, L.; Lahasky, S. H.; Ghale, K.; Zhang, D., N-Heterocyclic carbene-mediated zwitterionic polymerization of N-substituted N-carboxyanhydrides toward poly(alpha-peptoid)s: kinetic, mechanism, and architectural control. *J. Am. Chem. Soc.* **2012**, *134*, 9163-71.

182. Choi, B. G.; Kim, G. H.; Yi, K. B.; Kim, J.-N.; Hong, W. H., Influence of operating temperature on CO2-NH3 reaction in an aqueous solution. *Korean J. Chem. Eng.* **2012**, *29*, 478-482.

183. Qi, G.; Wang, Y.; Estevez, L.; Duan, X.; Anako, N.; Park, A.-H. A.; Li, W.; Jones, C. W.; Giannelis, E. P., High efficiency nanocomposite sorbents for CO2 capture based on amine-functionalized mesoporous capsules. *Energy. Environ. Sci.* **2011**, *4*, 444-452.

184. Galezowski, W.; Jarczewski, A.; Stanczyk, M.; Brzezinski, B.; Bartl, F.; Zundel, G., Homoconjugated hydrogen bonds with amidine and guanidine bases Osmometric, potentiometric and FTIR studies. *J. Chem. Soc., Faraday Trans.* **1997**, *93*, 2515-2518.

185. Ferri, D.; Bürgi, T.; Baiker, A., FTIR study of chiral modifier–reactant interactions. The cinchonidine–alkenoic acid system. *J. Chem. Soc., Perkin Trans. 2.* **2002**, 437-441.

186. Rawlinson, D. J.; Humke, B. M., Peroxyester reaction of dimethylformamide. *Tetrahedron Lett.* **1972**, *13*, 4395-4398.

187. Dell'Amico, D. B.; Calderazzo, F.; Giurlani, U., Metal-assisted electrophilic reactions on carbon dioxide: synthesis of mixed carboxylato–carbamato anhydrides. *J. Chem. Soc., Chem. Commun.* **1986**, 1000-1001.

188. Lee, S.; Spencer, N. D., Sweet, hairy, soft, and slippery. *SCIENCE-NEW YORK THEN WASHINGTON-* **2008**, *319*, 575.

189. Johnson, J. A.; Lu, Y. Y.; Burts, A. O.; Xia, Y.; Durrell, A. C.; Tirrell, D. A.; Grubbs, R. H., Drug-loaded, bivalent-bottle-brush polymers by graft-through ROMP. *Macromolecules* **2010**, *43*, 10326-10335.

190. Huang, K.; Rzayev, J., Well-defined organic nanotubes from multicomponent bottlebrush copolymers. *J. Am. Chem. Soc.* **2009**, *131*, 6880-6885.

191. Heinrich, C. D.; Thelakkat, M., Poly-(3-hexylthiophene) bottlebrush copolymers with tailored side-chain lengths and high charge carrier mobilities. *Journal of Materials Chemistry C* **2016**, *4*, 5370-5378.

192. Hutter, N. A.; Reitinger, A.; Zhang, N.; Steenackers, M.; Williams, O. A.; Garrido, J. A.; Jordan, R., Microstructured poly (2-oxazoline) bottle-brush brushes on nanocrystalline diamond. *PCCP* **2010**, *12*, 4360-4366.

193. Shieh, W.-C.; Dell, S.; Repic, O., Nucleophilic catalysis with 1, 8-diazabicyclo [5.4. 0] undec-7-ene (DBU) for the esterification of carboxylic acids with dimethyl carbonate. *J. Org. Chem.* **2002**, *67*, 2188-2191.

194. Endo, K. *New Frontiers in Polymer Synthesis*, Springer, **2008**.

195. Guo, L.; Lahasky, S. H.; Ghale, K.; Zhang, D., N-Heterocyclic Carbene-Mediated Zwitterionic Polymerization of N-Substituted N-Carboxyanhydrides toward Poly(α-peptoid)s: Kinetic, Mechanism, and Architectural Control. *J. Am. Chem. Soc.* **2012**, *134*, 9163-9171.

196. Guo, L.; Zhang, D., Cyclic Poly(α-peptoid)s and Their Block Copolymers from N-Heterocyclic Carbene-Mediated Ring-Opening Polymerizations of N-Substituted N-Carboxylanhydrides. *J. Am. Chem. Soc.* **2009**, *131*, 18072-18074.

197. Li, A.; Lu, L.; Li, X.; He, L.; Do, C.; Garno, J. C.; Zhang, D., Amidine-Mediated Zwitterionic Ring-Opening Polymerization of N-Alkyl N-Carboxyanhydride: Mechanism, Kinetics, and Architecture Elucidation. *Macromolecules* **2016**, *49*, 1163-1171.

198. Wignall, G. D.; Littrell, K. C.; Heller, W. T.; Melnichenko, Y. B.; Bailey, K. M.; Lynn, G. W.; Myles, D. A.; Urban, V. S.; Buchanan, M. V.; Selby, D. L., The 40 m general purpose small-angle neutron scattering instrument at Oak Ridge National Laboratory. *J. Appl. Crystallogr.* **2012**, *45*, 990-998.

199. Zhao, J.; Gao, C. Y.; Liu, D., The extended Q-range small-angle neutron scattering diffractometer at the SNS. *J. Appl. Crystallogr.* **2010**, *43*, 1068-1077.

200. Jorgensen, W. L.; Tirado-Rives, J., The OPLS [optimized potentials for liquid simulations] potential functions for proteins, energy minimizations for crystals of cyclic peptides and crambin. *J. Am. Chem. Soc.* **1988**, *110*, 1657-1666.

201. Jorgensen, W. L.; Maxwell, D. S.; Tirado-Rives, J., Development and Testing of the OPLS All-Atom Force Field on Conformational Energetics and Properties of Organic Liquids. *J. Am. Chem. Soc.* **1996**, *118*, 11225-11236.

202. Park, S. H.; Szleifer, I., Structural and Dynamical Characteristics of Peptoid Oligomers with Achiral Aliphatic Side Chains Studied by Molecular Dynamics Simulation. *J. Phys. Chem. B* **2011**, *115*, 10967-10975.

203. Mart ńez, L.; Andrade, R.; Birgin, E. G.; Mart ńez, J. M., PACKMOL: A package for building initial configurations for molecular dynamics simulations. *J. Comput. Chem.* **2009**, *30*, 2157-2164.

204. Roux, B., The Calculation of the Potential of Mean Force Using Computer-Simulations. *Comput. Phys. Commun.* **1995**, *91*, 275-282.

205. Souaille, M.; Roux, B., Extension to the weighted histogram analysis method: combining umbrella sampling with free energy calculations. *Comput. Phys. Commun.* **2001**, *135*, 40-57.

206. Plimpton, S., Fast Parallel Algorithms for Short-Range Molecular Dynamics. *J. Comput. Phys.* **1995**, *117*, 1-19.

207. Villarrubia, J., Algorithm for scanned probe microscope image simulation, surface reconstruction, and tip estimation. *J. Res. Natl. Inst. Stand. Technol.* **1997**, *102*, 425-454.

208. Gagliardi, S.; Arrighi, V.; Ferguson, R.; Dagger, A. C.; Semlyen, J. A.; Higgins, J. S., On the difference in scattering behavior of cyclic and linear polymers in bulk. *J. Chem. Phys.* **2005**, *122*, 64-904.

209. Jang, S. S.; Çağin, T.; Goddard III, W. A., Effect of cyclic chain architecture on properties of dilute solutions of polyethylene from molecular dynamics simulations. *J. Chem. Phys.* **2003**, *119*, 1843-1854.

210. Hammouda, B. *Polymer Characteristics*, Springer, **1993**.

211. Brewer, A. K.; Striegel, A. M., Characterizing the size, shape, and compactness of a polydisperse prolate ellipsoidal particle via quadruple-detector hydrodynamic chromatography. *Analyst* **2011**, *136*, 515-519.

212. Miller, S. M.; Simon, R. J.; Ng, S.; Zuckermann, R. N.; Kerr, J. M.; Moos, W. H., Proteolytic studies of homologous peptide and N-substituted glycine peptoid oligomers. *Bioorg. Med. Chem. Lett.* **1994**, *4*, 2657-2662.

213. Miller, S. M.; Simon, R. J.; Ng, S.; Zuckermann, R. N.; Kerr, J. M.; Moos, W. H., Comparison of the proteolytic susceptibilities of homologous L-amino acid, D-amino acid, and N-substituted glycine peptide and peptoid oligomers. *Drug Dev. Res.* **1995**, *35*, 20-32.

214. Kwon, Y.-U.; Kodadek, T., Quantitative evaluation of the relative cell permeability of peptoids and peptides. *J. Am. Chem. Soc.* **2007**, *129*, 1508-1509.

215. Mannige, R. V.; Haxton, T. K.; Proulx, C.; Robertson, E. J.; Battigelli, A.; Butterfoss, G. L.; Zuckermann, R. N.; Whitelam, S., Peptoid nanosheets exhibit a new secondary-structure motif. *Nature* **2015**, *526*, 415-420.

216. Xuan, S.; Lee, C.-U.; Chen, C.; Doyle, A. B.; Zhang, Y.; Guo, L.; John, V. T.; Hayes, D.; Zhang, D., Thermoreversible and Injectable ABC Polypeptoid Hydrogels: Controlling the Hydrogel Properties through Molecular Design. *Chem. Mater.* **2015**, 10.1021/acs.chemmater.5b03528.

217. Tanisaka, H.; Kizaka-Kondoh, S.; Makino, A.; Tanaka, S.; Hiraoka, M.; Kimura, S., Near-infrared fluorescent labeled peptosome for application to cancer imaging. *Bioconjugate Chem.* **2008**, *19*, 109-117.

218. Yamamoto, F.; Yamahara, R.; Makino, A.; Kurihara, K.; Tsukada, H.; Hara, E.; Hara, I.; Kizaka-Kondoh, S.; Ohkubo, Y.; Ozeki, E., Radiosynthesis and initial evaluation of 18 F labeled nanocarrier composed of poly (L-lactic acid)-block-poly (sarcosine) amphiphilic polydepsipeptide. *Nuclear medicine and biology* **2013**, *40*, 387-394.

219. Makino, A.; Hara, E.; Hara, I.; Yamahara, R.; Kurihara, K.; Ozeki, E.; Yamamoto, F.; Kimura, S., Control of in vivo blood clearance time of polymeric micelle by stereochemistry of amphiphilic polydepsipeptides. *J. Controlled Release* **2012**, *161*, 821-825.

220. Kidchob, T.; Kimura, S.; Imanishi, Y., Preparation, structure and release profile of polypeptide microcapsules. *J. Controlled Release* **1996**, *40*, 285-291.

221. Kidchob, T.; Kimura, S.; Imanishi, Y., pH-responsive release from polypeptide microcapsules. *J. Appl. Polym. Sci.* **1997**, *63*, 453-458.

222. Kimura, S.; Kidchob, T.; Imanishi, Y., Controlled release from amphiphilic polymer aggregates. *Polym. Adv. Technol.* **2001**, *12*, 85-95.

223. Robinson, J. W.; Secker, C.; Weidner, S.; Schlaad, H., Thermoresponsive Poly(N-C3 glycine)s. *Macromolecules* **2013**, *46*, 580-587.

224. Gangloff, N.; Ulbricht, J.; Lorson, T.; Schlaad, H.; Luxenhofer, R., Peptoids and Polypeptoids at the Frontier of Supra-and Macromolecular Engineering. *Chem. Rev.* **2015**.

225. Luxenhofer, R.; Fetsch, C.; Grossmann, A., Polypeptoids: A perfect match for molecular definition and macromolecular engineering *J. Polym. Sci., Part A: Polym. Chem.* **2013**, *51*, 2731-2752.

226. Kim, W.; Thévenot, J.; Ibarboure, E.; Lecommandoux, S.; Chaikof, E. L., Self-Assembly of Thermally Responsive Amphiphilic Diblock Copolypeptides into Spherical Micellar Nanoparticles. *Angew. Chem. Int. Ed.* **2010**, *49*, 4257-4260.

227. Sanson, C.; Schatz, C.; Le Meins, J.-F.; Soum, A.; Thévenot, J.; Garanger, E.; Lecommandoux, S., A simple method to achieve high doxorubicin loading in biodegradable polymersomes. *J. Controlled Release* **2010**, *147*, 428-435.

Appendix: Copyright Release

RightsLink®

Home | Create Account | Help

Title: 1,1,3,3-Tetramethylguanidine-Promoted Ring-Opening Polymerization of N-Butyl N-Carboxyanhydride Using Alcohol Initiators

Author: Brandon A. Chan, Sunting Xuan, Matthew Horton, et al

Publication: Macromolecules

Publisher: American Chemical Society

Date: Mar 1, 2016

LOGIN

If you're a copyright.com user, you can login to RightsLink using your copyright.com credentials. Already **a RightsLink user** or want to learn more?

PERMISSION/LICENSE IS GRANTED FOR YOUR ORDER AT NO CHARGE

This type of permission/license, instead of the standard Terms & Conditions, is sent to you because no fee is being charged for your order. Please note the following:

- Permission is granted for your request in both print and electronic formats, and translations.
- If figures and/or tables were requested, they may be adapted or used in part.
- Please print this page for your records and send a copy of it to your publisher/graduate school.
- Appropriate credit for the requested material should be given as follows: "Reprinted (adapted) with permission from (COMPLETE REFERENCE CITATION). Copyright (YEAR) American Chemical Society." Insert appropriate information in place of the capitalized words.
- One-time permission is granted only for the use specified in your request. No additional uses are granted (such as derivative works or other editions). For any other uses, please submit a new request.

If credit is given to another source for the material you requested, permission must be obtained from that source.

BACK | CLOSE WINDOW

Title: Amidine-Mediated Zwitterionic Ring-Opening Polymerization of N-Alkyl N-Carboxyanhydride: Mechanism, Kinetics, and Architecture Elucidation

Author: Ang Li, Lu Lu, Xin Li, et al

Publication: Macromolecules

Publisher: American Chemical Society

Date: Feb 1, 2016

PERMISSION/LICENSE IS GRANTED FOR YOUR ORDER AT NO CHARGE

This type of permission/license, instead of the standard Terms & Conditions, is sent to you because no fee is being charged for your order. Please note the following:

- Permission is granted for your request in both print and electronic formats, and translations.
- If figures and/or tables were requested, they may be adapted or used in part.
- Please print this page for your records and send a copy of it to your publisher/graduate school.
- Appropriate credit for the requested material should be given as follows: "Reprinted (adapted) with permission from (COMPLETE REFERENCE CITATION). Copyright (YEAR) American Chemical Society." Insert appropriate information in place of the capitalized words.
- One-time permission is granted only for the use specified in your request. No additional uses are granted (such as derivative works or other editions). For any other uses, please submit a new request.

BACK CLOSE WINDOW

Title: Synthesis and Characterization of Cleavable Core-Cross-Linked Micelles Based on Amphiphilic Block Copolypeptoids as Smart Drug Carriers

Author: Ang Li, Donghui Zhang

Publication: Biomacromolecules

Publisher: American Chemical Society

Date: Mar 1, 2016

PERMISSION/LICENSE IS GRANTED FOR YOUR ORDER AT NO CHARGE

This type of permission/license, instead of the standard Terms & Conditions, is sent to you because no fee is being charged for your order. Please note the following:

- Permission is granted for your request in both print and electronic formats, and translations.
- If figures and/or tables were requested, they may be adapted or used in part.
- Please print this page for your records and send a copy of it to your publisher/graduate school.
- Appropriate credit for the requested material should be given as follows: "Reprinted (adapted) with permission from (COMPLETE REFERENCE CITATION). Copyright (YEAR) American Chemical Society." Insert appropriate information in place of the capitalized words.
- One-time permission is granted only for the use specified in your request. No additional uses are granted (such as derivative works or other editions). For any other uses, please submit a new request.

Vita

Ang Li was born in Qingdao, Shandong Province, China. He received his bachelor degree in polymer science and engineering from Beijing Technology and Business University in 2011. He joined Professor Donghui Zhang's group at Louisiana State University in 2011 and started his graduate research of synthesis and development of polypeptoids. Ang anticipates to graduate with his PhD degree of chemistry in December 2016.